DESIGN AND REALIZATION A QUASI YAGI ANTENNA ARRAY AND ITS FEED SYSTEM PRINTED ON A CERAMIC SUBSTRATE FOR X-BAND RADAR APPLICATIONS

A THESIS SUBMITTED TO
THE GRADUATE SCHOOL OF NATURAL AND APPLIED SCIENCES
OF
MIDDLE EAST TECHNICAL UNIVERSITY

BY

BERKAY ATABAY

IN PARTIAL FULFILLMENT OF THE REQUIREMENTS
FOR
THE DEGREE OF MASTER OF SCIENCE
IN
ELECTRİCAL AND ELECTRONİCS ENGİNEERİNG

DECEMBER 2019

Approval of the thesis:

DESIGN AND REALIZATION A QUASI YAGI ANTENNA ARRAY AND ITS FEED SYSTEM PRINTED ON A CERAMIC SUBSTRATE FOR X-BAND RADAR APPLICATIONS

submitted by **BERKAY ATABAY** in partial fulfillment of the requirements for the degree of **Master of Scıence in Electrical and Electronics Engineering Department, Middle East Technical University** by,

Prof. Dr. Halil Kalıpçılar
Dean, Graduate School of **Natural and Applied Sciences** _____

Prof. Dr. İlkay Ulusoy
Head of Department, **Electrical and Electronics Eng.** _____

Prof. Dr. Gülbin Dural Ünver
Supervisor, **Electrical and Electronics Eng., METU** _____

Examining Committee Members:

Prof. Dr. Sencer Koç
Electrical and Electronics Eng. Dept. METU _____

Prof. Dr. Gülbin Dural Ünver
Electrical and Electronics Eng., METU _____

Prof. Dr. Mustafa Kuzuoğlu
Electrical and Electronics Eng. Dept. METU _____

Prof. Dr. Özlem Aydın Çivi
Electrical and Electronics Eng. Dept. METU _____

Assoc. Prof. Dr. Nursel Akçam
Electrical and Electronics Eng. Dept. GAZİ University _____

Date: 11.12.2019

I hereby declare that all information in this document has been obtained and presented in accordance with academic rules and ethical conduct. I also declare that, as required by these rules and conduct, I have fully cited and referenced all material and results that are not original to this work.

Name, Surname: Berkay Atabay

Signature:

ABSTRACT

DESIGN AND REALIZATION A QUASI YAGI ANTENNA ARRAY AND ITS FEED SYSTEM PRINTED ON A CERAMIC SUBSTRATE FOR X-BAND RADAR APPLICATIONS

Atabay, Berkay
Master of Scıence, Electrical and Electronics Engineering
Supervisor: Prof. Dr. Gülbin Dural Ünver

December 2019, 95 pages

This thesis includes design, simulation, realization and measurement of a four-element quasi- Yagi antenna array printed on a ceramic substrate for X-band radar applications. The microstrip array antenna is designed using four quasi-Yagi antennas in a linear configuration and is printed on Alumina 99.6% substrate made by Coorstek Corporation. The antenna can fit into small areas because of compact structure due to the use of high dielectric constant substrates. In addition, the use of alumina ceramic substrates provide resistance in heating stroke which may be critical in many applications. These properties make this design an appealing choice as a radiating element. Especially in radar applications antenna parameters such as gain, return loss, impedance bandwidth (BW) are investigated in the single element as well as the array environment. Mutual coupling between the array elements is also predicted.

The quasi-Yagi radiator employed as radiating element in the array measured an exceptional impedance bandwidth of 52% for a S11< -10 dB from 7.5 GHz to 12 GHz, with 3 dB to 5 dB of absolute gain in the same frequency range. The antenna consisting of a microstrip line feed and microstrip to coplanar stripline transition (Balun). The microstrip array antenna is designed and simulated using Ansys HFSS, a high frequency electromagnetic field simulation program. Then to investigate the effects of

all parameters a parametric study is performed using HFSS. The four coplanar strip dipole antennas and feeding mechanisms are designed and simulated with appropriate power divider structure. This equal power divider can operate at X-Band and designed with AWR program. Finally, the antenna element and four-element uniform linear array antenna are manufactured with thin film technology, measured, and their performances are compared with simulation results.

Keywords: Quasi Yagi Antenna, Antenna Array, Wilkinson Power Divider, Ceramic

ÖZ

X-BANT RADAR UYGULAMALARI İÇİN SERAMİK TABAN MALZEME ÜZERİNE BASILMIŞ QUASİ YAGİ ANTEN DİZİSİ VE BESLEME SİSTEM TASARIMI VE GERÇEKLENMESİ

Atabay, Berkay
Yüksek Lisans, Elektrik ve Elektronik Mühendisliği
Tez Danışmanı: Prof. Dr. Gülbin Dural Ünver

Aralık 2019, 95 sayfa

Bu tez X-bant radar uygulamaları için dört elemanlı quasi yagi anten dizisinin tasarımını, simulasyonunu, gerçeklenmesini ve ölçümlerini içermektedir. Mikroşerit anten dizisi doğrusal konfigürasyonda dizilmiş dört quasi yagi anten elemanı ile tasarlanmıştır ve Coorstek firmasından alınan 99.6 yoğunlukta alumina üzerine basılmıştır. Yüksek dielektrik katsayısına sahip taban malzeme seçildiği için çok küçük alanlara sığabilen bir anten tasarımıdır. Buna ek olarak, alumina seramik taban malzeme seçildiği için ısı atımı gerektiren kritik birçok uygulamada kullanılabilir. Bu gibi özellikleri sebebiyle yayınım elemanlarında iyi bir seçenektir. Antenin çevresel eleman olarak kullanılması için özellikle radar uygulamalarında kazanç, geri dönüş kaybı, empedans bant genişliği parametreleri araştırılmıştır. Dizi antende herbir elaman arasındaki etkilenebilirlik izlenmiştir.

Quasi Yagi yayınım elemanının 7.5 GHz -12 GHz bandında %52 bant genişliği 10 dB ve altında geri dönüş kaybı bunlarla birlikte 3 ile 5 dB arasında kazancı ölçülmüştür. Bu anten mikroşerit hat beslemesinden ve mikroşeritten eş düzlemsel şerit hatta geçiş yapısından oluşmaktadır. Mikroşerit dizi anten tasarımı yapılmış, yüksek frekans elektromanyetik dalga simulasyon programı olan HFSS programı kullanılarak simulasyonları yapılmıştır. İlk olarak, mikroşerit besleme hattını ve mikroşerit hattan

eş düzlemsel şerit hatta geçişini içeren Mikroşerit anten yapısı tasarlanırken yüksek frekanslı elektromanyetik alan benzeşim programı Ansys HFSS kullanılarak tasarlanmış ve benzeşimi yapılmıştır. Sonraki aşamada bütün parametrelerin etkilerinin incelenmesi amacıyla Ansys HFSS kullanılarak parametrik analizler gerçekleştirilmiştir. Dört düzlemsel şerit dipol anten elemanlarından oluşan doğrusal bir anten dizisi ve bu diziyi besleyecek uygun bir güç bölücü yapısı tasarlanmıştır. Bu eşit güç bölücü X bantta çalışabilmektedir ve AWR programı kullanılarak tasarlanmıştır. Son olarak, tekil anten elemanı ve dört elamanlı doğrusal anten dizisi ince film teknolojisi ile üretilmiş ölçümleri alınmış ve bu antenlerin performansları benzeşim programı sonuçları ile karşılaştırılmıştır.

Anahtar Kelimeler: Quasi Yagi Anten, Anten Dizisi, Wilkinson Güç Bölücü, Seramik

To my family, Şule and my little daughter Elis

ACKNOWLEDGEMENTS

I would like to express my sincere gratitude to my advisor, Prof. Dr. Gülbin Dural Ünver, for her valuable guidance, support and technical suggestions throughout the study.

I would also like to thank Prof. Dr. Sencer Koç, Prof. Dr. Mustafa Kuzuoğlu, Prof. Dr. Özlem Aydın Çivi, Assoc. Prof. Dr. Nursel Akçam for being in my jury and sharing their opinions.

I would like to express my gratitude to Dr. Taylan Eker for proposing this topic to me and Kadir İşeri for their invaluable help and guidance in the design and manufacturing process.

I am grateful to ASELSAN INC. for the financial and technical opportunities provided for the completion of this thesis. I would also like to express my sincere appreciation for Kenan Çapraz and Kadir İşeri for their valuable friendship, motivation and help.

For their understanding my spending lots of time on this work ,my sincere thanks to my parents.

Lastly, for her great support, understanding and love, I am also grateful to my wife, Şule and my little daughter Elis.

TABLE OF CONTENTS

LIST OF TABLES

TABLES

LIST OF FIGURES

FIGURES

LIST OF SYMBOLS

SYMBOLS

ACE	Acetone
AiP	Antenna in Package
Au	Gold
Al_2O_3	Aluminum Oxide
BW	Bandwidth
CPS	Coplanar Stripline
CPW	Coplanar Waveguide
CTE	Coefficient of Thermal Expansion
IC	Integrated Circuit
IPA	Isopropyl Alcohol
LTSA	Linearly Tapered Slot Antenna
MMICs	Monolithic Microwave Integrated Circuit
MoM	Method of Moment
MWO	Microwave Office
MCM	Multi-Chip Module
MS	Microstrip
PCB	Printed Circuit Board
PCAAD	Personal Computer Aided Antenna Design

SiP	Session Initiation Protocol
SMA	Subminiature version A
TiW	Titanium Tungsten
UHF	Ultra High Frequency

CHAPTER 1

INTRODUCTION

1.1. Preface

Antenna is one of the most critical elements in all wireless communication systems. Antenna design requires careful design and concepts. The choice of an antenna normally depends on many factors such as gain, bandwidth, directivity, etc. In many applications as spacecraft, aircraft and radar applications, where size, weight, performance and the costs are constraints, with the appropriate radiation characteristics are required. Due to fabrication simplicity feeding networks with substrates, printed array is commonly used solutions. The main aim of this thesis is to design quasi-Yagi antenna array to operate in X band at frequency range of 7.5 GHz to 12 GHz printed onto a ceramic substrate to place inside a radom to be used in the front part of an aircraft. Radomes placed in front of the aircrafts that include antennas and radar systems. If the design area is limited with the technical specs and it has to be put into in-package electronic system, choosing the design method is very significant. Gain has to be 8-10 dbi belong to operating bandwidth. The thesis work can be improved with adding phase shifters for scanning all phase angles in the future. The main aim is improving the single antenna gain with designing an array structure onto the ceramic substrate.

The requirements of these antennas that many companies dedicated to this particular type of antenna were created and exist today [1]. High heating dissipation characteristics are also necessary requirement for the final design. There are many feeding techniques, but the most common feeding techniques used for printed dipoles involve the coaxial feed, CPS feed and the coupled-line feed. Considering the facts, microstrip antenna type is selected to go on since it can carry out the desired antenna specifications. A microstrip antenna consists of a dielectric substrate, a radiating on one side of this dielectric and a ground plane on the other side. Regular shapes (rectangular, circular, square dipoles)

are generally chosen for simplicity to clearly analyze the performance of the antenna. The radiation caused by the electric field can be increased or decreased by varying the parameters like the dielectric constant and the substrate thickness [4].

Printed antennas have not only advantages but also disadvantages. To start with output power level relatively is lower [3,4]. Generally, they have narrow bandwidths. Alternatively, Vivaldi and tapered slot antennas provide broad bandwidth by using the travelling waves (LTSA-Linearly Tapered Slot Antenna) [5].

Computer aided techniques have become helpful in the design, analysis, optimization and fabrication of microstrip antennas and arrays. Electromagnetic modelling was performed making extensive use of simulation softwares such as HFSS®, CST®, MWO® and many others.

There exists a requirement in radar applications to develop a lightweight, low profile and compact phased array antenna capable of scanning its main beam through the E-plane as with in package radar systems. The second important aim is to select the best heating dissipation for in package system.

Antenna in Package (or AiP) is a new trend in packaging that is suitable for smaller and high integrated ICs (Integrated Circuit) which consists of ICs and antennas inside a package. Antenna in Package allows integration of all the components, the system integrator no longer needs to design complex RF circuits at the application PCB (Printed Circuit Board) level and the overall size of the complete application is reduced. However, the system integrator still needs to ensure that the RF signal is connected to a suitable antenna that is placed within the application. The connection between RF signals and the antenna must ensure low insertion loss and good impedance matching and also antenna placement needs to be controlled for optimum radiation performance. The integration of the antenna within the same package as the RF SiP (Session Initiation Protocol) greatly reduces the difficulty at the system level. This approach coupled to aggressive miniaturization of antenna itself, using the same substrate technologies. Final design can be used in Antenna in Package systems as shown in Figure 1.1.

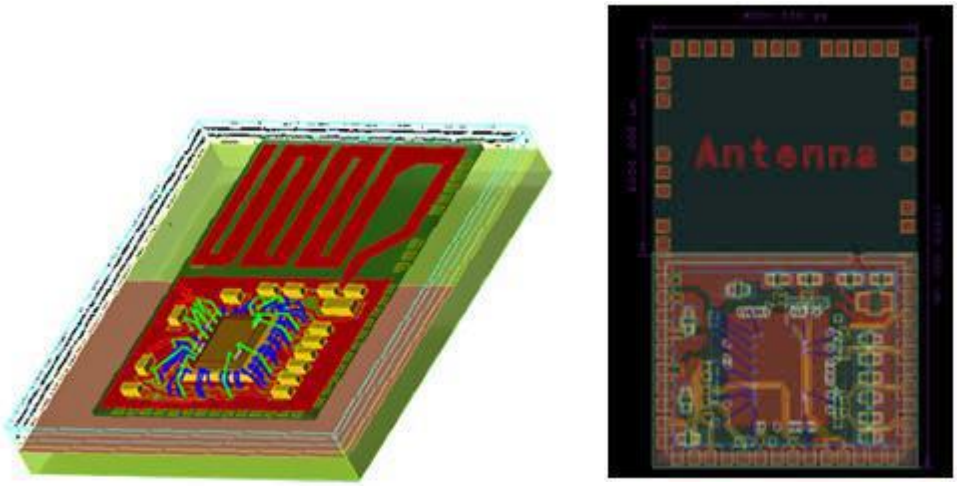

Figure 1.1. The sample 3-D view of Antenna in Package structures

1.2. Organization of the Thesis

Chapter 1 summerizes the importance of microstrip antennas in the communications industry. Both the significance and the applications of the active microstrip antennas are discussed. Moreover, the aim of the thesis is also listed. A summary of research on antenna elements employed in planar microstrip array antennas are compared. It will review the background information and theory of microstrip antenna. The historical development of the microstrip antenna, including its advantages and disadvantages, are presented.

Chapter 2 provides a literature review related to the design of the microstrip antenna. The design formulas for calculating the effective dielectric constant, free space wavelength and characteristic impedance are all listed accordingly. After giving an explanation of the equations developed by Wheeler, the microstrip relationship plots for the characteristic impedance and effective dielectric constant versus substrate

width and height ratio (w/h) are given. This chapter ends with an analysis of microstrip discontinuities, listing of all the various common discontinuities found in microstrip antenna designs. The individual characteristics of the quasi-Yagi antenna will be presented, including the advantages and disadvantages of this type of antenna structures.

Chapter 3 concentrates on the design and development of the quasi-Yagi antenna. The design procedures involved in obtaining the dimensions for both the antennas will be shown in detail. The aim of the design is to obtain wider bandwidth and better radiation patterns for both the antennas. In addition, other design considerations such as design configuration and the material selected for the antenna are also presented. All simulated results related to the quasi-Yagi antenna are provided. A sensitivity analysis of the quasi-Yagi antenna with respect to five design parameters; the length of the director, distance between the director and the driver, distance between the coupled microstrip lines, length of the driver and distance from the driver to the reflector, are presented. The effects of these parameters on its operational frequency and impedance bandwidth are investigated and the parameters most affecting the performance of the antenna are identified.

Chapter 4 presents the design and simulation of the uniform beamforming network. The main purpose is increasing the gain and directivity of the array antenna therefore equal power divider design and simulation results are also presented.

The elements and beamforming networks are combined in Chapter 5 to form the microstrip array. The elements and beamforming network are combined with fabrication steps, measurement results are presented in this chapter.

Chapter 6 concludes with a summary of the work carried out for this thesis and the future prospects for both the quasi-Yagi antenna. Subsequently, the future prospects of microstrip antennas, especially broadband planar antennas, will be addressed. Also, it consists of the findings, concluding remarks and recommendations made.

CHAPTER 2

QUASI YAGI ANTENNA REWIEV

2.1. Introduction

A typical quasi-Yagi antenna consists of three main components, a dipole driver, parasitic director and reflector elements. The ground plane acts as a reflector to achieve a directive radiation pattern. Also to improve the directivity, two parasitic directors are designed and optimized at the operating frequency of 10 GHz. This antenna has advantages of small size and simple structure for fabrication.

The principle of operation of the uniplanar quasi-Yagi antenna is reported in this chapter. It utilizes a similar principle like a traditional Yagi-uda dipole antenna array. In this design the ground plane is used as a reflector element. The director and driver of the antenna are placed on the same plane of the high dielectric substrate so that the surface waves generated by the antenna is directed to the end fire direction. The truncated ground plane on the bottom side of the substrate acts as a reflector element. Coplanar strips are uniplanar transmission lines and a balun is usually desired to provide efficient transition between the coplanar strip line and the microstrip lines [6]. The general appearance of quasi-Yagi is shown in Figure 2.1.

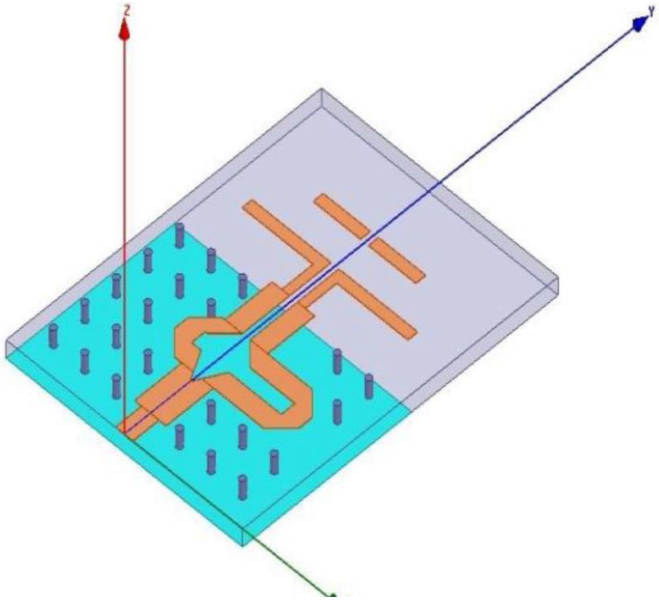

Figure 2.1. Uniplanar Quasi-Yagi Antenna

2.2. Printed Dipoles

When implementing planar dipoles, two general approaches exist. The first is to print the dipole on one side of a dielectric substrate. The second method is by printing each arm on each side of a dielectric substrate and feeding the dipole from the one side of the substrate. The two printed dipole implementations are shown in Figure 2.2.

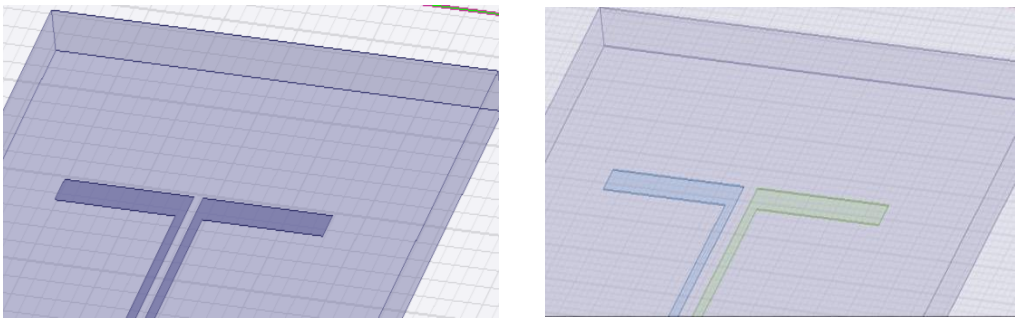

(a) Dipole is on one side (b) Each arm on each side of a substrate

Figure 2.2. Two method of Printed dipoles

Baluns are used when feeding microstrip dipoles and play two major roles, first as a converter from an unbalanced transmission line to a balanced transmission line and then as an impedance transformer. Feeding microstrip dipoles involves ingenuity and many authors have utilized different techniques to accomplish a balanced feed for these antennas with a differential angled dipole fed by a single-ended microstrip line. The feed used in this antenna is a truncated ground plane, yielding excellent BW(Bandwidth) performance from 8 GHz to 12 GHz. An equally successful topology involved a balun which makes the transition between the microstrip line and CPS (Coplanar Stripline) lines by feeding the dipole with equal magnitude but 180 out of phase. This is accomplished by making the feed line feeding the one arm λ/2 longer than the line feeding the other arm, as seen in Figure 2.1. An alternative to this method is to gradually transform the electric field distribution of the microstrip line to that of the CPS by optimally tapering the ground conductor trace to provide impedance as well as field matching.

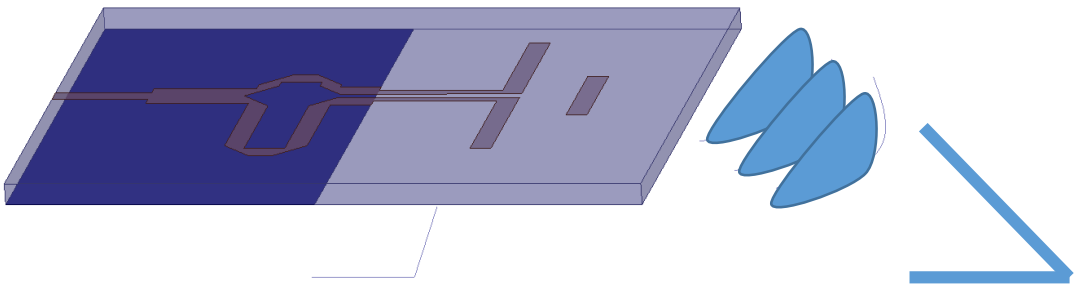

Figure 2.3. End-Fire Radiation Direction of Quasi-Yagi Antenna

2.3. Antenna Performance

By using a high-permittivity substrate, the antenna will be extremely compact in terms of freespace wavelength, and thus an array with tide spacing requirements. Itoh et al. published works on a quasi-Yagi antenna printed on a high-permittivity substrate fed

by a microstrip line and also by a coplanar waveguide (CPW) [6]. Other works on planar Yagi-Uda antennas with simplified feeding structures are and Neculoiu et al. proposed membrane-supported Yagi-Uda antenna structures on silicon and gallium arsenide semiconductors in the V- and W-band. However, as the semiconductors are generally poor antenna substrates, micromachining technology has to be used to gain sufficient antenna efficiency. This, in fact, enlarges the antenna dimensions since antennas on a thin membrane have to be designed considering the free-space wavelength. As we designed the antenna for the mere purpose of proving our concept, we adopted a basic design. We chose Alumina as antenna substrate because of its properties as a high-permittivity and low-loss substrate and its ability to be processed in thin film technology. The antenna is a planar structure that uses only one metal layer. To allow measurement with a coplanar microwave probe, the antenna has been combined with a CPW to CPS balun that could be omitted in a differential circuit. The substrate thickness was chosen 0.635 mm and gold coating thickness is 5um. Yet, this substrate thickness already posed quite a challenge regarding substrate waves. Compared to the works mentioned, the substrate is thicker in terms of wavelengths. We noticed an improved antenna performance using a finite reflector length compared to a truncated ground plane that is used in the works mentioned. All dimensions were optimized to get a suitable pattern and a maximum front-to-back ratio. The distance of the director to the substrate edge was a crucial point in the design, as substrate waves are generated in some cases that causes a back radiation.

The reported performance of the antenna measures a 52% BW for a VSWR < 2.5, 5dB of gain, and an end-fire beam with a cross polarization level below -12 dB across the entire X-band. Mutual coupling is measured below -22 dB for two elements spaced $\lambda/2$ at the center frequency of 10 GHz.

Various other researchers pursued this antenna design with slight modifications, with the intention of optimized gain and presented a coplanar waveguide (CPW) fed quasi-Yagi antenna with broad BW covering the X-band. The antenna utilized two directors, a driven element and a suspended ground plane acting as a reflector element. The

antenna measures a 44% BW for VSWR < 2.5, efficiency of 95% and a gain of 7.4 dBi. The increased gain is attributed to the addition of an extra director. The quasi-Yagi antenna was also successfully down scaled in frequency and implemented by various other researchers.

A quasi-Yagi antenna is fed with a balun, which provides symmetry and matching of a feeding microstrip line to balanced CPS. Some researchers investigated the dimensional parameters of the quasi-Yagi antenna and the effects of the balun on the input return loss [10]. The effects of the balun on the radiation performance were also studied.

Due to the favorable radiation performance and impedance BW depicted by the quasi-Yagi antenna it was decided to employ this antenna as the radiating element in a four-element linear phased antenna array. To ensure power is distributed correctly to all elements and over the entire X band, a uniform beamforming network using multi-section 3-dB power dividers was developed. In the future the beam of this array will be scanned in the E-plane by the addition of a phase delay circuit.

Study will concern the study of quasi Yagi antennas with alumina (Al_2O_3) dielectric substrate whose specification are presented in Appendix A. Compactness of microstrip antennas has made them very attractive for applications in communication systems. As the need for the antenna miniaturization continues, a possible solution is offered by utilization of alumina dielectric materials as substrate. The main requirement for miniaturization of the components is a high value of the dielectric permittivity of the material. It also necessary a low dielectric loss to assure a better efficiency of the device in our case of the yagi antenna and a good stability with the temperature to assure a better frequency stability of the antenna or array. The performance of the quasi-Yagi radiator makes this antenna an appropriate candidate for phased array antenna design.

CHAPTER 3

ANALYSIS AND DESIGN OF QUASI YAGI ANTENNA

3.1. Design Requirements

The radiating characteristics of a single antenna are not adequate for many applications since it either does not supply high enough values of gain, or the radiation pattern does not fulfil the requirements. To increase the gain, the dimensions of a single element can be enlarged, which directly impacts on the manufacturing cost and mechanical constraints associated with a bigger structure. The other option for increasing the gain is by forming an array of radiating elements in an electrical and geometrical configuration. Radiating elements are often chosen to be identical for simplicity and practically. Four quasi-Yagi radiators are modelled in a linear array topology in HFSS and analyzed to investigate the radiation performance, gain and mutual coupling.

In our design, dielectric constant is chosen to be high, so that the working area is small and line and space widths are small also. Special production methods are really necessary according to these substrates and widths such as thin film, semiconductor methods. This report on the scaling of the X-band quasi-Yagi antenna to produce a broad bandwidth antenna operating near 10 GHz. HFSS simulation is used to calculate the return loss input impedance and the radiation pattern, every small change may affect the whole results so all the critical parameters should be examined. The design can be used in a sample package as shown in Figure 3.1.

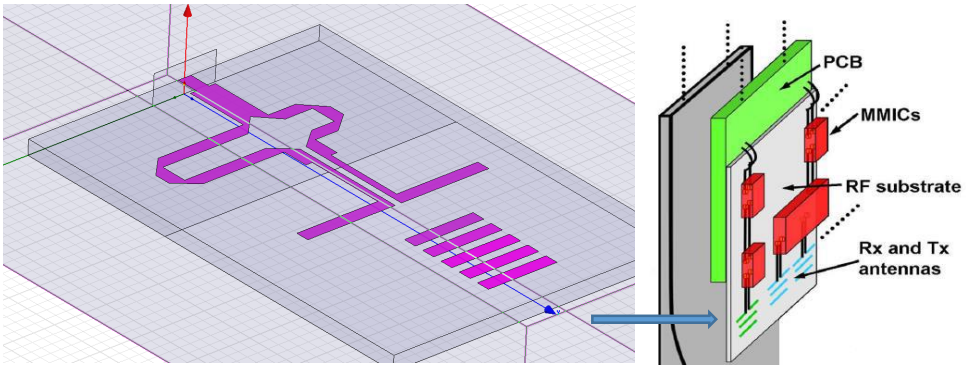

Figure 3.1. Sample view of project in using stage

The second part of the thesis is concerned with design procedures and considerations for both the antenna element and the array. Our design aimed obtaining wider bandwidth and better radiation patterns. In addition, a sensitivity analysis of the Quasi-Yagi antenna with respect to five design parameters is demonstrated in chapter 4 of this thesis. The simulation results showed that the quasi-Yagi antenna is able to achieve a simulated 50% frequency bandwidth for voltage standing-wave ratio (VSWR) < 2.5 at the center frequency of 10 GHz. During the sensitivity analysis, it has been found that the most sensitive parameters are the length of the driver, director and the distance from the driver to the reflector. Variations to these three parameters will affect the antenna's performance in terms of return loss and operational frequency.

3.2. Quasi-Yagi Radiator Simulation Results

Quasi-Yagi antenna design parameters such as driver, director and ground parameters are significant for the proper design. These are element spacing between directors, length and width. Generally quasi-Yagi antenna shows broadband (40-50% for VSWR<2) characteristics with modest gains (≥ 4dB) or narrower bandwidth (40-50% for VSWR<2) with higher gains (≥ 6dB). The broad pattern, low mutual coupling and wide bandwidth allow this antenna to be incorporated into multi-frequency phased arrays with very large scanning capability.

These antennas are to be fabricated with a high dielectric constant substrate material (Alumina Al_2O_3 with dielectric constant $\varepsilon_r = 9.9$), substrate thickness of 0.635 mm and design frequency of 10 GHz with metallization on both sides. The top metallization consists of a microstrip feed, a broadband microstrip to coplanar stripline, balun and two dipole elements, one of which is the driver element fed by CPS, and the second dipole being the parasitic director. The metallization on the bottom plane is a truncated microstrip ground, which serves as the reflector element for the antenna and cancels using reflector dipole. The parasitic director element acts as an impedance matching element and the second feature is directing the antenna propagation toward the endfire direction.

In this section, the theoretical development and the design details for every parts of the balun structure that includes microstrip to coplanar stripline transitions are explained.

There are many substrates available that can be used for the design of microstrip antennas, usually with their dielectric constants in the range of 2.2 to 12. The low dielectric constant ε_r is about 2.2 to 3, the medium around 6.15 and the high dielectric constant is approximately above 10.5. Normally, lower dielectric constants are usually used for providing better efficiency and larger bandwidth. However, it would also have a larger antenna size. On the other hand, for smaller antenna sizes need for higher dielectric constants. The drawbacks are that it is less efficient and has relatively smaller bandwidths. Therefore, there must be a design trade-off between the antenna size and good antenna performance [9].

Table 3.1. *Substrates properties[9]*

Material	Relative Dielectric Constant	Loss Tangent at 10 GHz	Thermal Conductivity	Dielectric Strength
Sapphire	11.7	0.0001	0.4	4000
Alumina	9.9	0.0001	0.2	4000
Quartz(fused)	3.8	0.0001	0.01	10000
GaAs	12.3	0.0016	0.3	350
RT Duroid 6010	10.5	0.0015	0.004	160
Air	1	0	0.000024	30
Beryllium oxide	6.6	0.0001	2.5	-
Si	11.7	0.005	0.9	300

The value of the effective dielectric constant ε_{eff} is needed in order to obtain the value of the guide wavelength. In Table 3.1, the formulas for calculating effective dielectric constants are given. It can be seen from the section that there are two sets of equation for calculating the effective dielectric constant. For calculating the effective dielectric constant as shown in Equation 3.2. using the effective dielectric constant ε_{eff} design frequency of 10 GHz, speed of light c, the calculations for the free-space wavelength, effective dielectric constant and guide wavelength is shown below.

Free-space wavelength (λ_0) = c / f (3.1)

= 3 x 10^8 / 10 x 10^9

= 30 mm

$$\varepsilon_r = \frac{\varepsilon+1}{2}\frac{\varepsilon-1}{2}\left[\left(1+\frac{12}{w/h}\right)+\left(0.04\left(1-\frac{w}{h}\right)\right)\right] \quad (3.2)$$

=6.8

Guide wavelength (λG) = $\lambda o / \varepsilon_r$ (3.3)

= 30 x 10^{-3} / 6.8

= 10.27 mm

Note that the simulated value of the effective dielectric constant is very close to the calculated value that is 6.8. Hence, for accuracy purposes, the calculated effective dielectric constant is used for the initial design.

Looking at the schematic diagram of the quasi-Yagi antenna shown in Figure 3.2., it can be seen that there are a lot of dimensions that need to be determined. The width W_{ml} is supposed to be connected to the microstrip feed and to the power amplifier for spatial power combining. The value of W_{ml} has to be designed so that the characteristic impedance of the microstrip (50Ω) to the balanced microstrip could be matched.

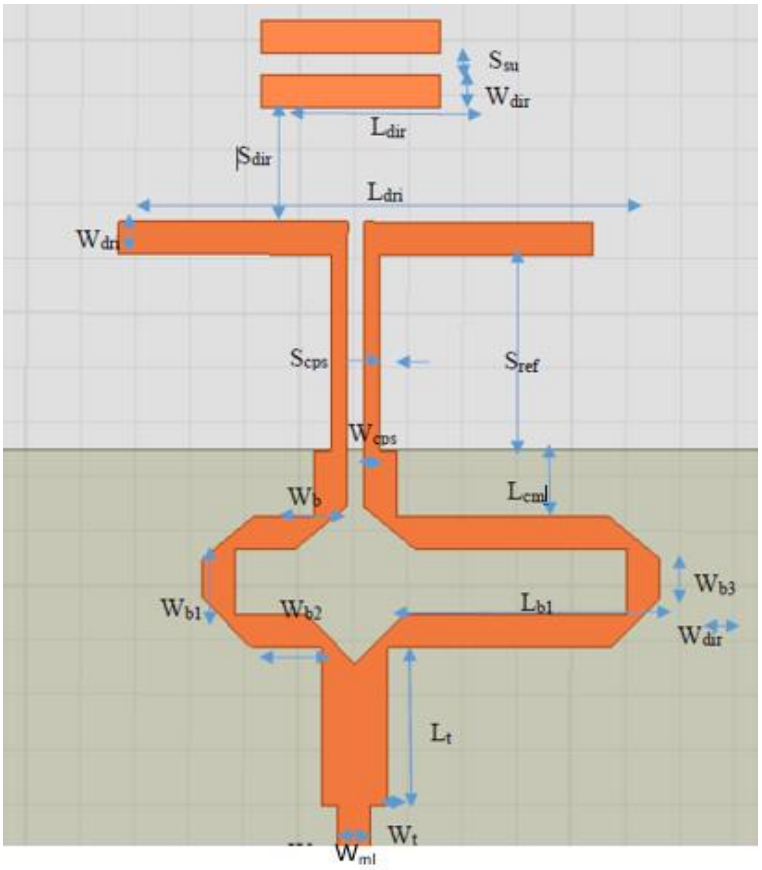

Figure 3.2. Part of antenna lengths

Table 3.2. *Final antenna dimensions based on mm*

W_{ml}	0.6	S_{ref}	3.6
W_{dir}	0.6	L_{dri}	8.7
L_t	2.9	W_{dri}	0.6
L_{b1}	4.1	L_{dir}	3.3
W_{b1}	1.2	W_t	0.3
W_{b4}	1.1	W_{b2}	1.1
L_{cml}	1.5	W_{b3}	0.71
S_{cps}	0.3	W_{cps}	0.3

There are a number of ways to determine the width of the microstrip, but the way which was done for this design is using the synthesis formula. Before using this method, the characteristic impedance Z_0 and the dielectric constant ε_r have to be given.

In addition, this method is only applicable to narrow microstrip lines. The calculations for the microstrip width-to-substrate thickness ratio *w/h* is shown below:

$$\frac{w}{h} = \frac{8\,expH}{exp(2H)-2} = \frac{8\exp(x)}{\exp(2xx)-2} \tag{3.4}$$

Where

$$H = \frac{Zo\sqrt{2(\varepsilon r+1)}}{120} + \frac{1}{2}\left(\frac{\varepsilon r-1}{\varepsilon r+1}\right)\left(\ln\frac{\pi}{2} + \frac{1}{\varepsilon r}\ln\frac{4}{\pi}\right) = \tag{3.5}$$

$$= \frac{50\sqrt{2(9.9+1)}}{120} + \frac{1}{2}\left(\frac{9.9-1}{9.9+1}\right)\left(\ln\frac{\pi}{2} + \frac{1}{9.9}\ln\frac{4}{\pi}\right)$$

$$= 2.1$$

After inserting the value of $Z_0 = 50\Omega$ and dielectric constant $\varepsilon r = 9.9$, the microstrip line width-to-substrate thickness ratio w/h is obtained. In order to find out the microstrip width required to match a 50Ω line, it is necessary to multiply the w/h ratio with the substrate thickness of 0.635mm. The resulting width obtained would be approximately 0.6mm. Alternatively, the microstrip width can also be found by using the software PCAAD®. This software allows the user to obtain the microstrip width value easily by just entering the required values for the antenna design. The result obtained from PCCAD® is similar to the calculated results shown above. After obtaining the value of W_{ml}, it can be seen from the Table 3.2 that the value of W_{ml} is similar to W_{dri} and W_{dir}. Hence, all these three dimensions are set to 0.6 mm. As for the values of W_{b1}, it is chosen to be 1.2 mm respectively as shown in Figure 3.2.

$$Z_0=\frac{60}{\sqrt{\varepsilon r}}\ln\left(\frac{8}{w/h}+0.25\frac{w}{h}\right) \quad (3.6)$$

$$= \frac{60}{\sqrt{6.8}}\ln\left(\frac{8}{0.9}+0.25(0.9)\right) = 50\Omega$$

The resulting characteristic impedance obtained is shown to be 50Ω, which proved that the *w/h* ratio used is effective in matching characteristic impedance of the conventional microstrip (50Ω) to the balanced microstrip.

Next, the length of the driver and director of the antenna is to be determined. Parametric study of a broadband uniplanar Quasi-Yagi antenna showed that the most sensitive parameters are the length of the driver L_{dri} and the distance from the driver to the reflector S_{ref}. The antenna's design frequency and its operational bandwidth will be affected by these two parameters. Thus, all the papers stated that the length of the driver would be optimum when it is about a guide wavelength and the distance between the driver and the reflector is about a quarter guide wavelength. Therefore, the calculations are done and shown below.

$L_{dri} = \lambda_G = 9.17$ mm

$S_{ref} = \lambda_G/4 = 2.2925$ mm

In addition, In [12] also states that a change in the length of the director L_{dir} and the distance between the director and the driver S_{dir} does not affect the design frequency and operational bandwidth. Moreover, the length of the gap between the coupled microstrip lines S_6 only affects the bandwidth moderately. Thus, the value of L_{dir} is set to be 4.8 mm, $S_{dir} = 2.5$ mm. However, further analysis on the effects of the length of the driver L_{dri} and the distance from the driver to the reflector will be investigated in the next chapter, where five parameters of the quasi-Yagi antenna are analyzed with respect to the S_{11} return loss. In [12] and [13], it is stated that by designing impedance matched T-junction and delaying one side of the microstrip line by half wavelength at the desired frequency, it will result in a predominantly odd mode in the coupled

microstrips. This means that the propagation mode in the coupled microstrips the odd mode propagates in the coupled microstrips, which can be easily transferred into the coplanar after the ground plane is truncated.

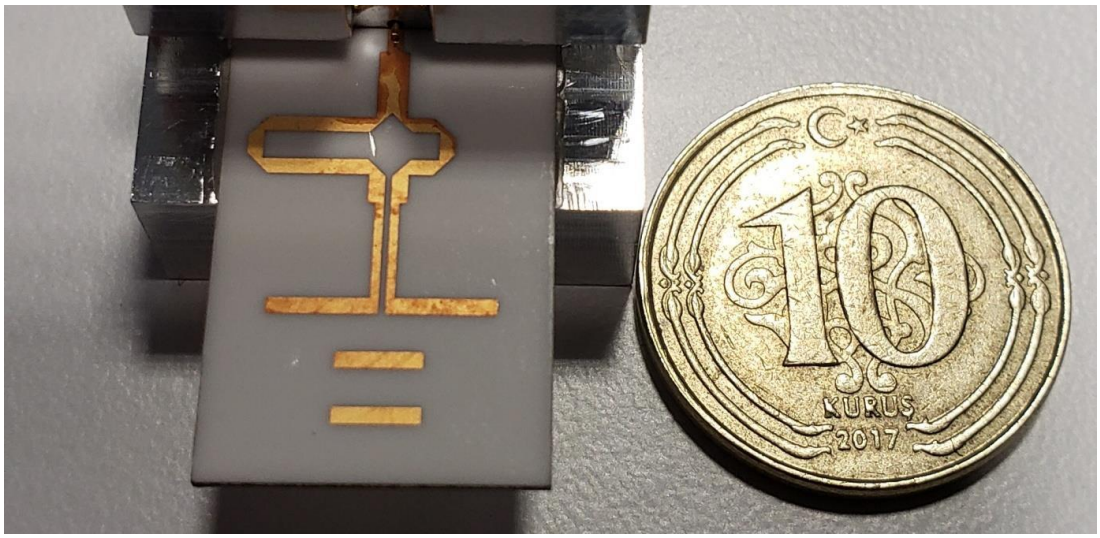

Figure 3.3. Fabricated single element antenna

The actual size of the Quasi-Yagi antenna after fabrication is shown in Figure 3.3. and Figure 3.3. The compactness of the antenna is seen when it is compared with the size of a coin.

The thickness of Alumina is 0.635 mm and dielectric constant is 9.9 are given in Appendix A. The antenna dimensions are (unit mm) $W_{ml} = W_{dri} = W_{dir} = 0.6$, $W_{b1} = 1.2$, $W_{cps} = S_{cps} = 0.3$, $L_{dir} = 3.3$, $L_{cml} = 1.5$, $L_{b1} = 4.1$, $L_{cml} = 1.5$, $S_{ref} = 3.6$ and $L_{dri} = 8.7$. The total area of the substrate is approximately $\lambda_0/2$ by $\lambda_0/2$ at the center frequency. All the sections of single element antenna is shown in Figure 3.4.

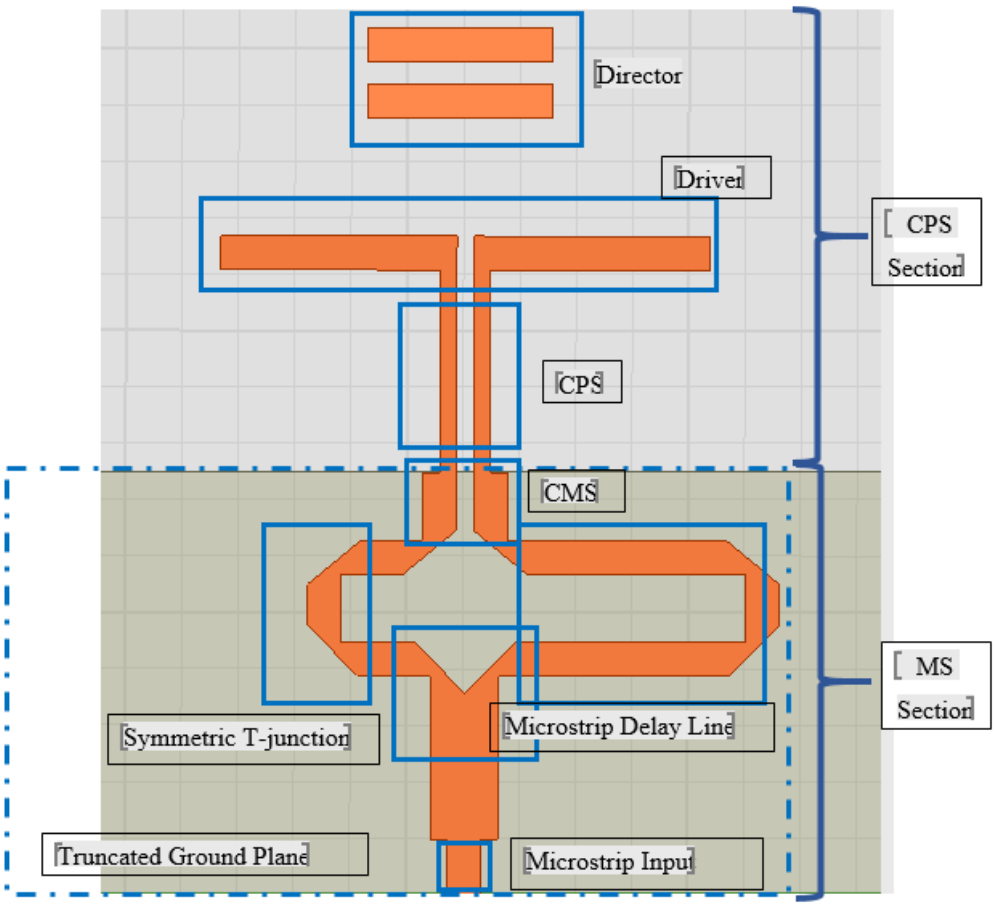

Figure 3.4. Sections of quasi-Yagi antenna

In order to reduce interferences coming from other systems, the use of printed dipole antenna is recommended as well as the distance of communications can be increased. Microstrip feeding has this advantage that is virtually a mechanical protective.

In order to convert microstrip to coplanar stripline for feeding antenna is required transmitted power from 50Ω line divide between two 50Ω lines. Therefore, we need an impedance transformer, is shown in Figure 3.5.

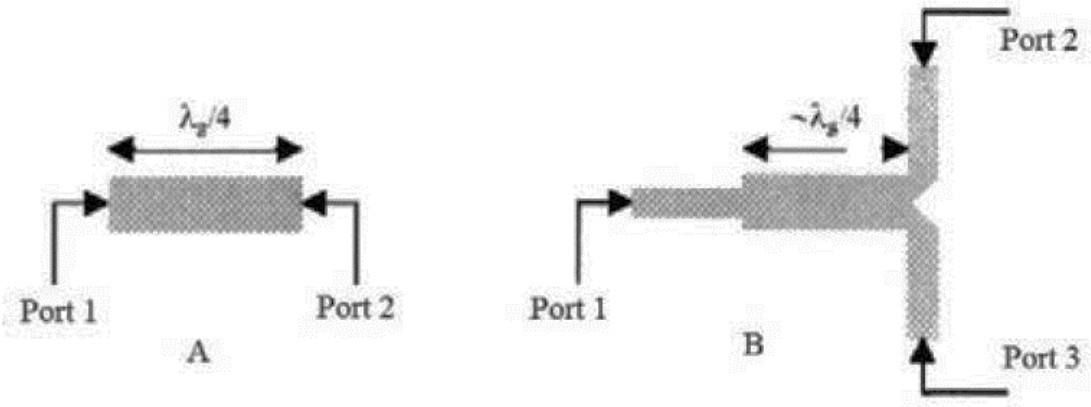

Figure 3.5. Matching on Microstrip inputs[13]

Balun phase shifter to generate a 180 phase difference between the coupled microstrip lines at working frequency, the correct excitation to the antenna is provided [13].

Selecting proper length for each arm in Figure 3.2. such that λg/4. This cause odd mode as a dominant mode in coupled microstrip line therefore feeding for CPS will be balanced. In order to the least effect on the phase and amplitude of the signal in 90^0 bends, we used mitered bends as shown in Figure 3.6. The distances between corners as shown in Figure 3.6. are calculated with formula 3.7.

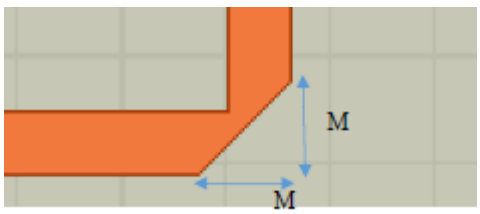

Figure 3.6. Mitered bends

The whole formulas and proofs are presented in reference [21]

Since CPS line does not accept even mode, behaves as open circuit for even mode of coupled microstrip line and allows us to negate unintended excited even mode in couple line. W and L are calculated for 100 Ω line.

Main part of antenna, reflector, which located on back of the board as a finite ground plane, driver feeding by CPS and director are designed in HFSS. Initial value of dimensions is chosen such as ordinary yagi antenna mentioned in the introduction. For a 100 Ω input impedance, the best response for much bandwidth will be obtained with these dimensions as shown in Table 3.2

With connecting the feeding part to radiator elements Figure 3.4. will be obtained. Since this step is the last one in this simulation and need more accuracy, the type of solution in HFSS is chosen Driven Mode and the antenna will be located in an air box that really makes radiation boundary. The input port is lumped port type with 50 Ω characteristic impedance and also integration line is drawn from MS line to ground. Solution frequency is considered 9 GHz for better accuracy. Other parameters are same as previous part.

After the latest optimization on all of dimensions specially dimensions of antenna and CPS line to achieve the lowest return loss, the following results for antenna dimensions is obtained that its details are given in Table 3.2.

There have several methods to improve gain, return loss and operational bandwidth. In next section these methods and simulation results will be explained.

All quasi-yagi designs, driver, director elements are similar but the most critical distinction is the feeding mechanism employed. Microstrip feed or coplanar waveguide (CPW) feed each requiring a balun to transform the transmission line mode at the input port of the antenna to the coplanar stripline. Each of these has its own merits. In no balun structure; one side of driver element is connected to the feed while the other side of driver is connected to the ground connected via a coplanar stripline.

Although this feeding technique and driver configuration do not require a balun, its necessities for two side of substrate to be etched so this is the disadvantage of the structure.

The antenna utilizes a simple CPW feed, so alleviating the complicated feeding network commonly required for the design of quasi-Yagi antenna. Proposed antenna is on a single layer and is very compact.

3.2.1. Number of Directors Effect

Start point of designing, the length of driven element should be $0.5\lambda_{eff}$, the length of the directors should be in the order of $0.45\lambda_{eff}$ according to Yagi design principles.

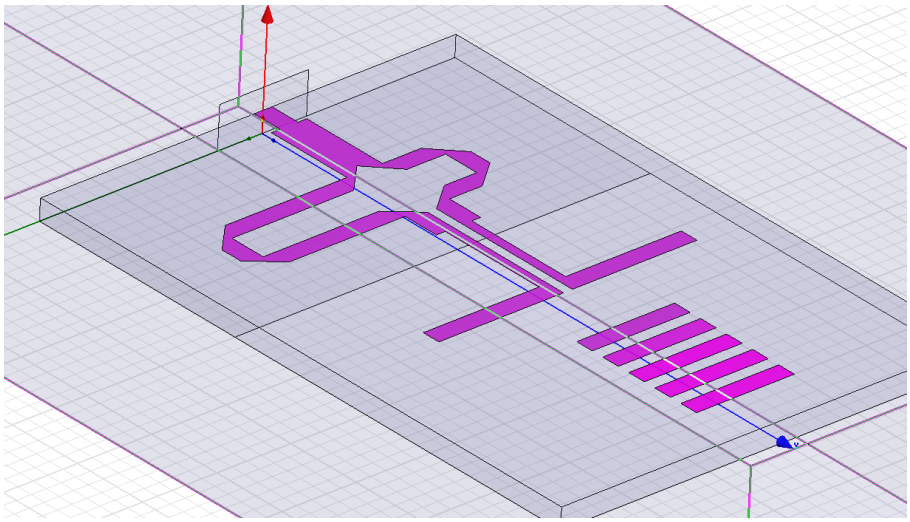

Figure 3.7. 3-D transparent view of the quasi-Yagi antenna model in HFSS

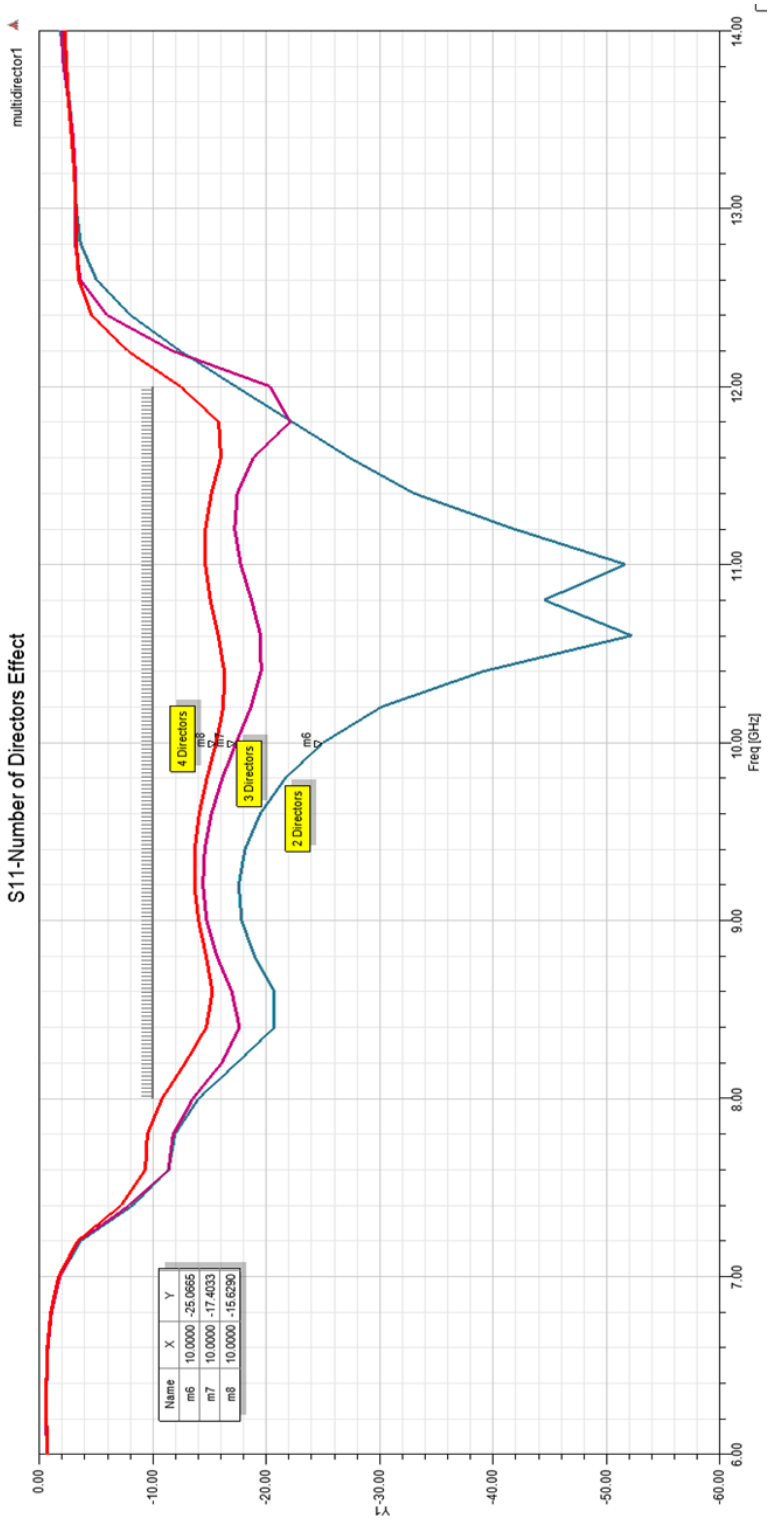

Figure 3.8. Effect of number of directors on return loss

The directors insertion improves the bandwidth of reference antenna, also the impedance match as can be seen in Figure 3.8. The resonance frequency about 8.1 GHz. As can be seen in Figure 3.8, is a significant difference between 2 and 3 directors bandwidth, about 200 MHz, but almost no difference at resonance frequency and range.

The antenna that has 4 directors, bandwidth decrease when compared with 2 and 3 directors results and its impedance matching at resonance frequency is also lower than the other antenna. In all antenna geometries, VSWR values are lower than 2.5 at frequency range, which guarantee at least 85% of entrance power will be radiated.

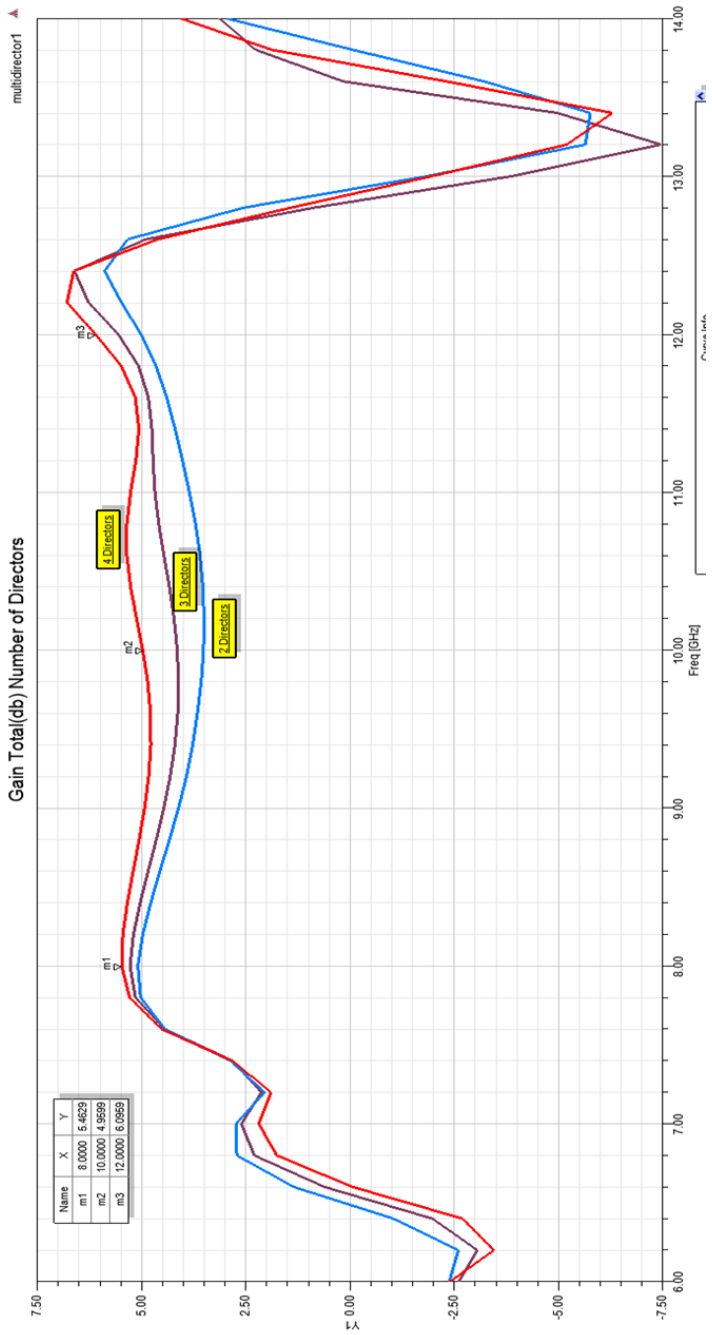

Figure 3.9. Effect of number of directors on antenna gain

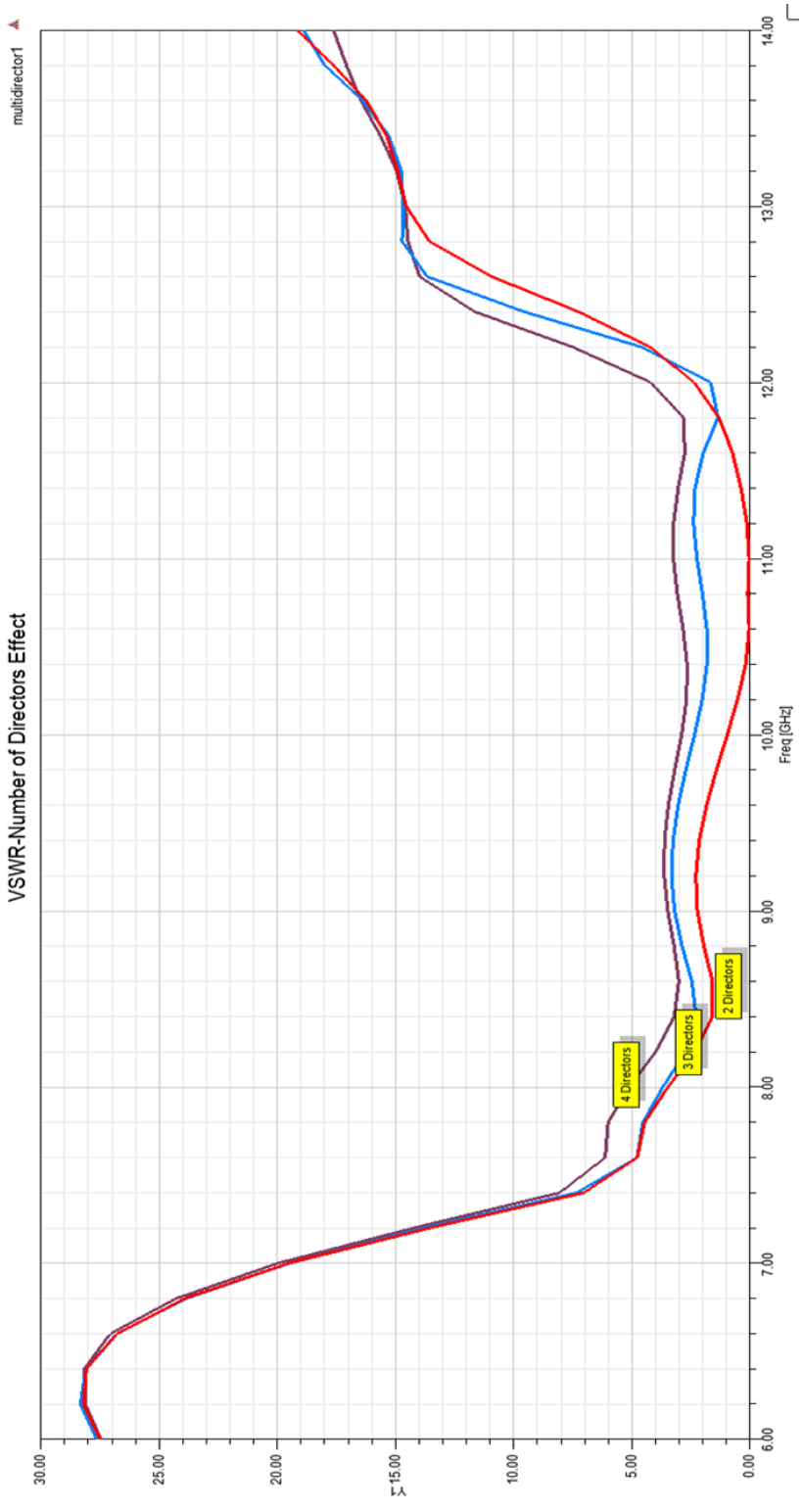

Figure 3.10. Effect of number of directors on antenna VSWR

3.2.2. Director Separation Effect

For reflection coefficient, better results are obtained with larger separations. This is obvious because the bigger distance the lesser coupling appears. About the radiation patterns, the E plane beam width seems to be insensitive to directors' distance. About H plane, the best directivity results are achieved with 2mm.

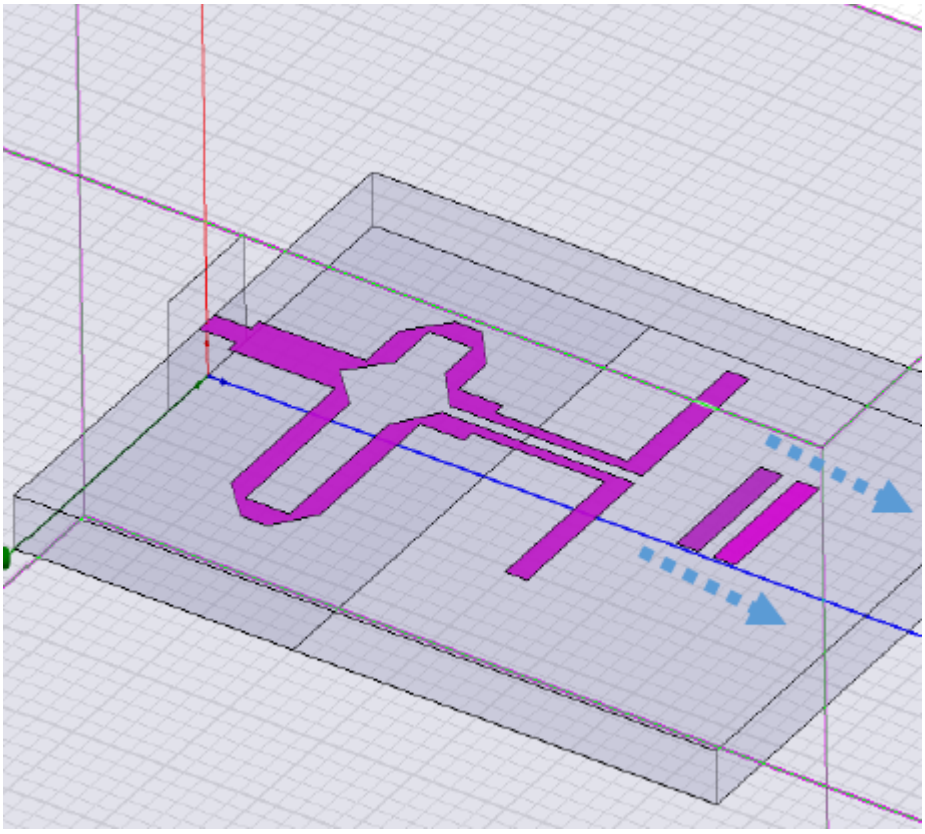

Figure 3.11. Directors separation view

The directors separation effect the reflections at the input due to coupling between the directors so the separation is a very important factor. If the design of directors separation is very close to each other the bandwidth decreases as seen in Figure 3.11. with blue arrows and also the gain decreases radically.

However if the distance between directors is too large, the losses will be too high. So the results were optimized with experimentally.

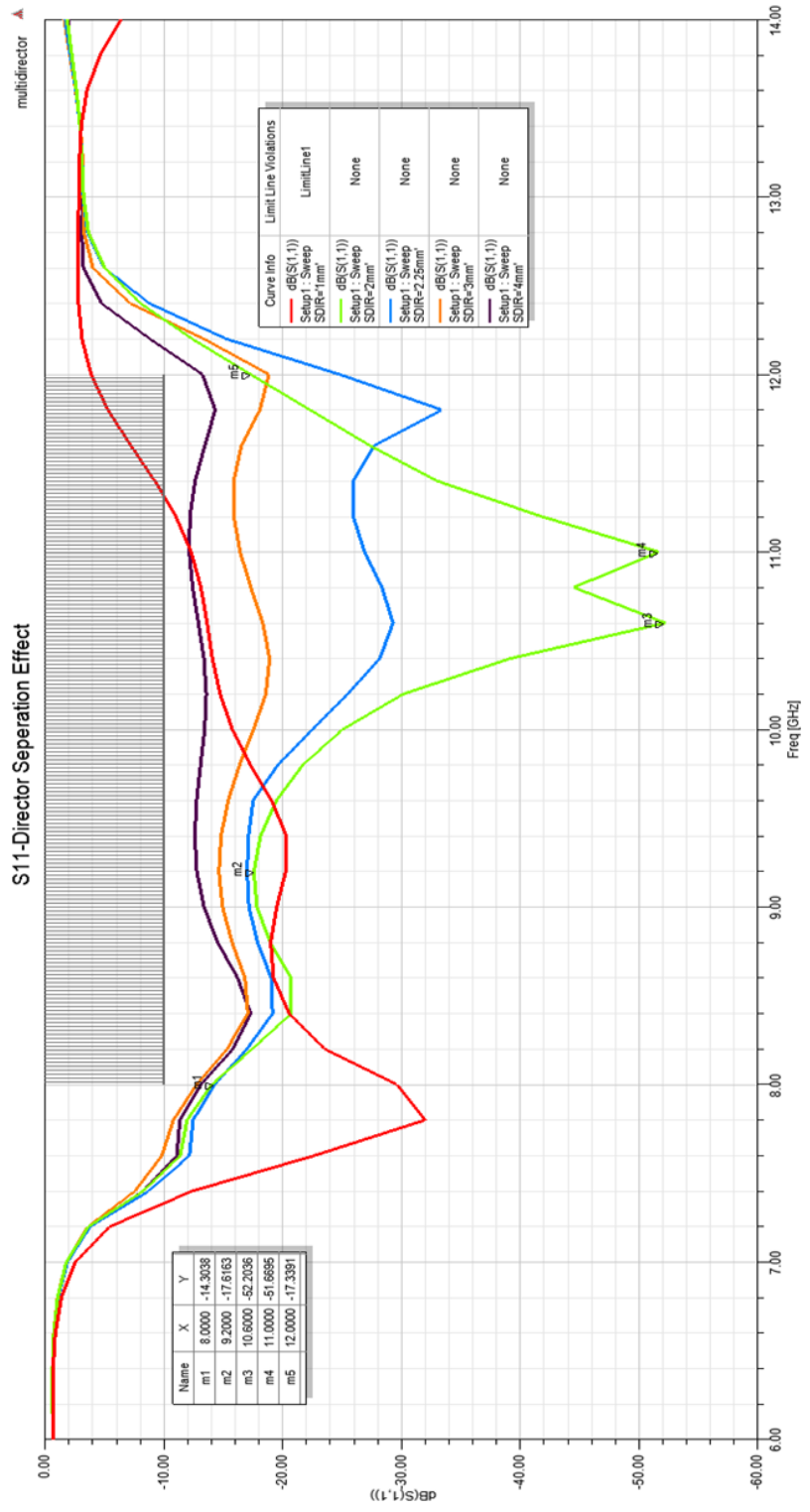

Figure 3.12. Effect of director separation (1, 2, 2.25, 3,4mm) on return losses

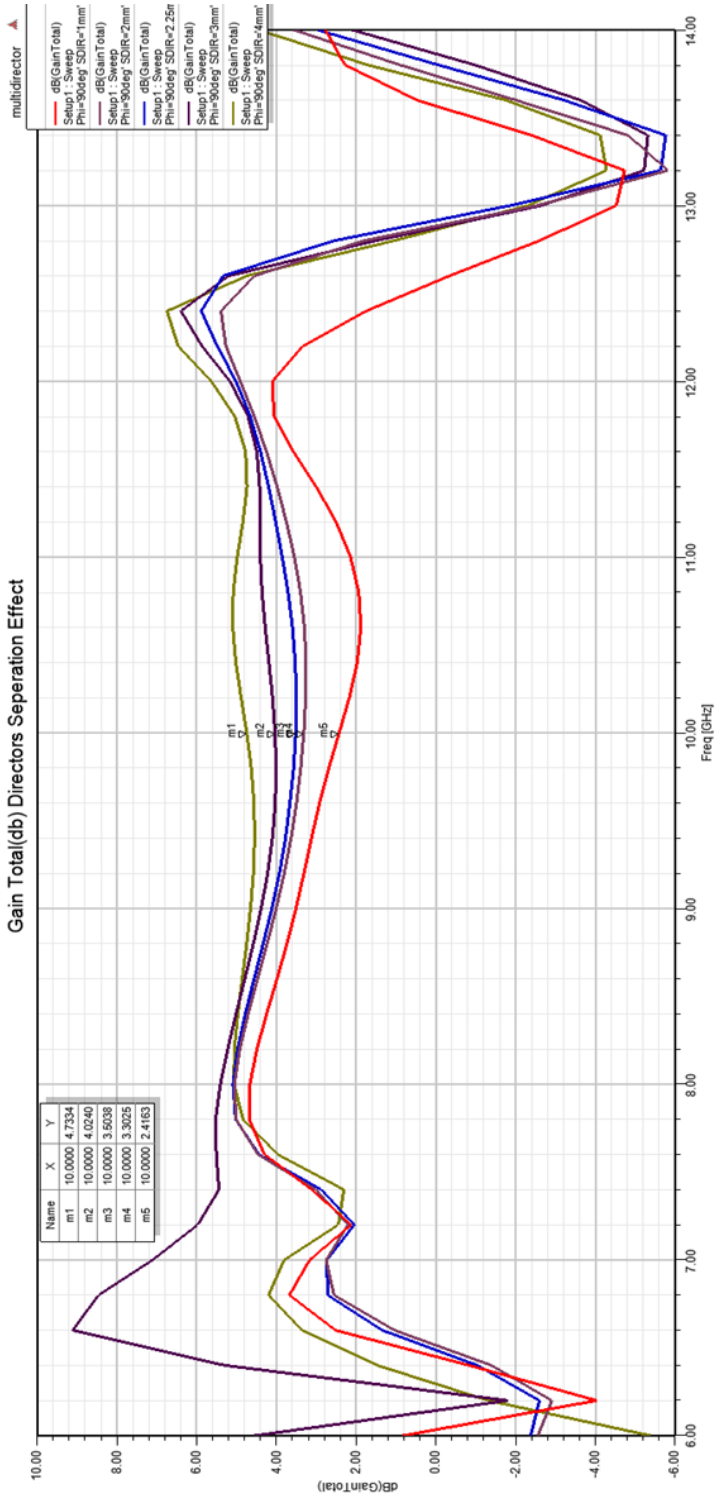

Figure 3.13. Effect of director separation (1, 2, 2.25, 3,4mm) on gain

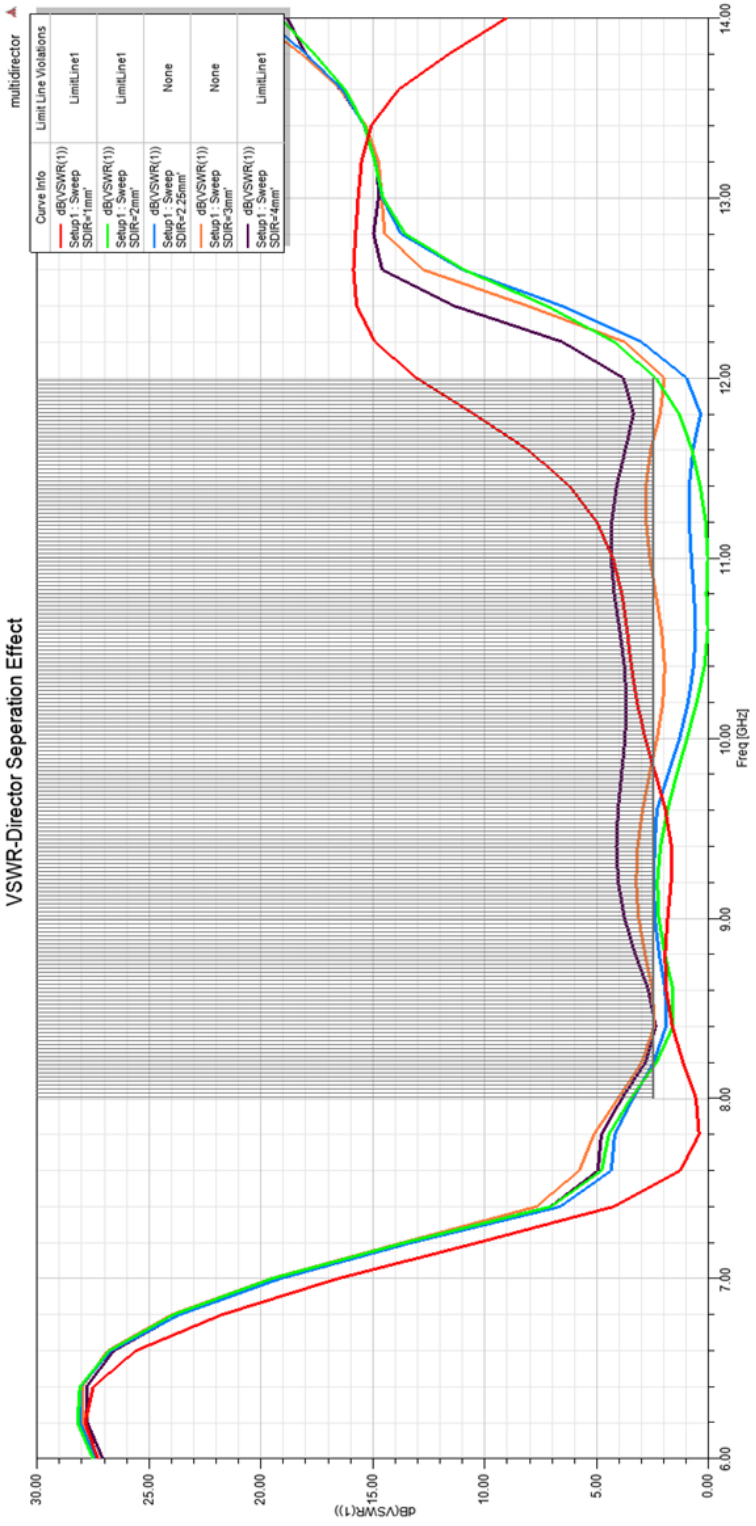

Figure 3.14. Effect of director separation (1, 2, 2.25, 3,4mm) on VSWR

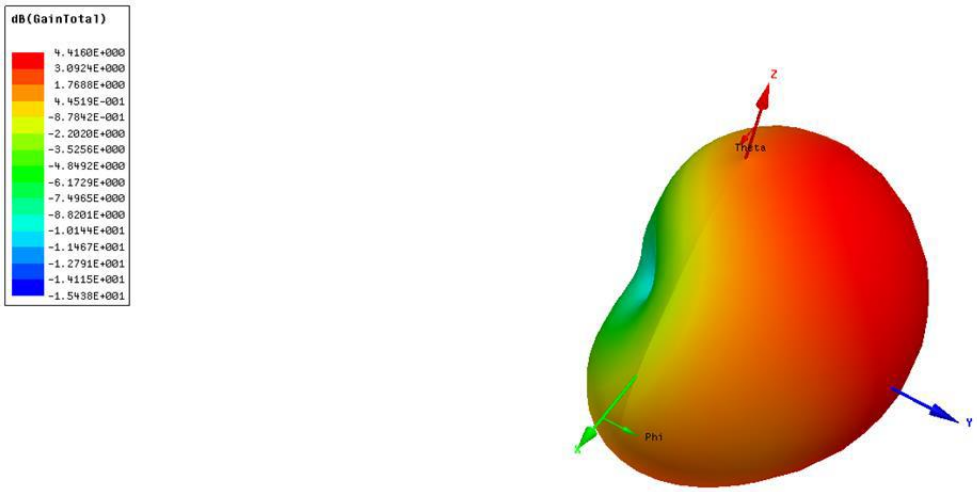

Figure 3.15. Total gain values on single element with polar form

Additionally, the compact size of the structure results in excellent mutual-coupling characteristics and allows great flexibility in array-element spacing in both directions. This enables the antenna to be used quite effectively in beamforming and phased arrays applications.

A few parameters are considered to be of great importance for satisfactory wideband performance: length of director and driver, distance between director and driver, distance between driver and reflector, length and width of CPS line.

To achieve dual polarization, two parallel horizontals and two parallel vertical quasi yagi elements is driven with equal phase and equal amplitude excitation in order to achieve an endfire pattern.

Determine the antenna width based on the array's spacing requirement: for a broadside array, the element spacing d must be less than λ at the highest frequency to avoid grating lobes; we choose element spacing equal to λ/2 to minimize array size; to feed these four elements with acceptable phase and magnitude imbalance the feeding network is designed.

In order to achieve good return loss and wide bandwidth, it is necessary for the length of the driver of quasi-Yagi element to be less than the guide wavelength, most preferably about $\lambda_g/10$ less than λ_g. In this work we used HFSS simulation software and optimized the antenna parameters for an X band prototype.

Table 3.3. *Number of Directors vs Gain*

Number of directors	**Average Gains (dbi)**
2	4.01
3	4.58
4	5.20

Only one director has been added to obtain a higher gain and better directivity of radiation pattern. There has a little difference between simulation and reality; the following reasons can be for these differences:

Feeding connecting type of SMA connector, coating type and production type. The connector type and z wedge bonding connection (2.9 mm SMA) as shown in Figure 5.24.

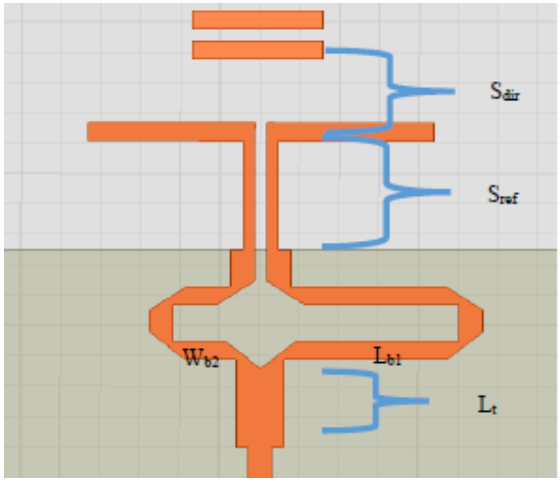

Figure 3.16. Characteristic properties descriptions

The length S_{dir} between radiation fold and director is important factor for the antenna performance and bandwidth. Director will improve the antenna's directivity. Figure 3.12. shows the relationship of frequency and reflection loss when S_{dir} changes.

Sref is also an impedance matching line with the length of $\lambda_g/4$, which is used to implement the impedance matching between the input port of CPS and radiation part.

L_{b1} is longer than W_{b2} about $\lambda g/4$, therefore the odd mode for this achieved for the radiation part.

In order to achieve the impedance matching at 50 Ω, L_t is added as an impedance matching line, the characteristic impedance of which is $Z_0=\sqrt{Z_1}\sqrt{Z_2}=\sqrt{50.25}=35.36$ Ω and the length is $\lambda_g/4$, where $\lambda_g = \lambda/\sqrt{\varepsilon_r}$. As the characteristic impedance of L_{b1} and W_{b2} are both 50 Ω, the equivalent input impedance from the top of L_t is 25 Ω.

The reflection is not a function of number of directors and the subsequent parasitic elements have not a significant influence on the antenna impedance. In addition, the beamwidth of E-plane and H-plane decrease with the increasing of the number of directors, as a result improving the directivity of the antenna.

3.2.3. Directors Length Effect

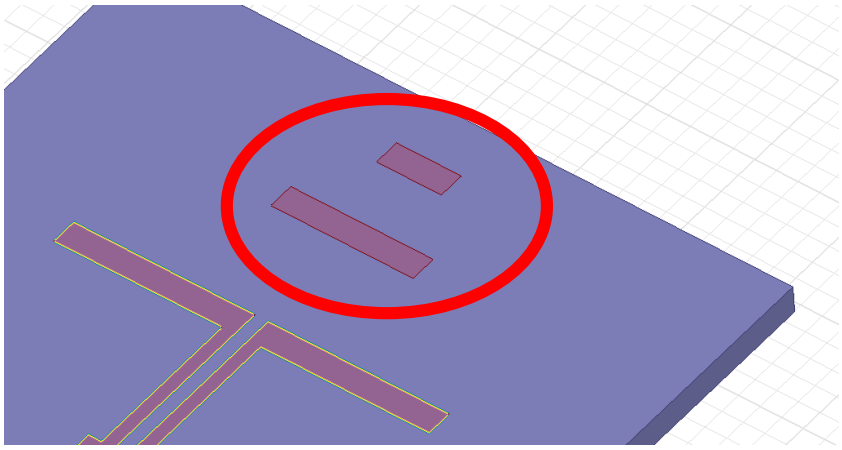

Figure 3.17. 3-D view of second director's length

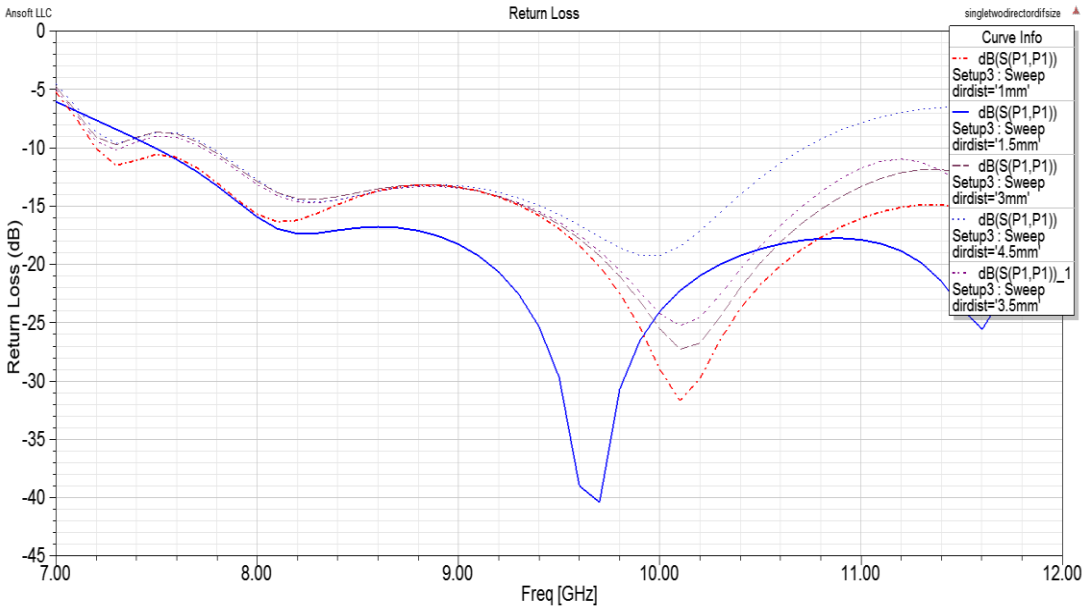

Figure 3.18. Different size of second director's return losses

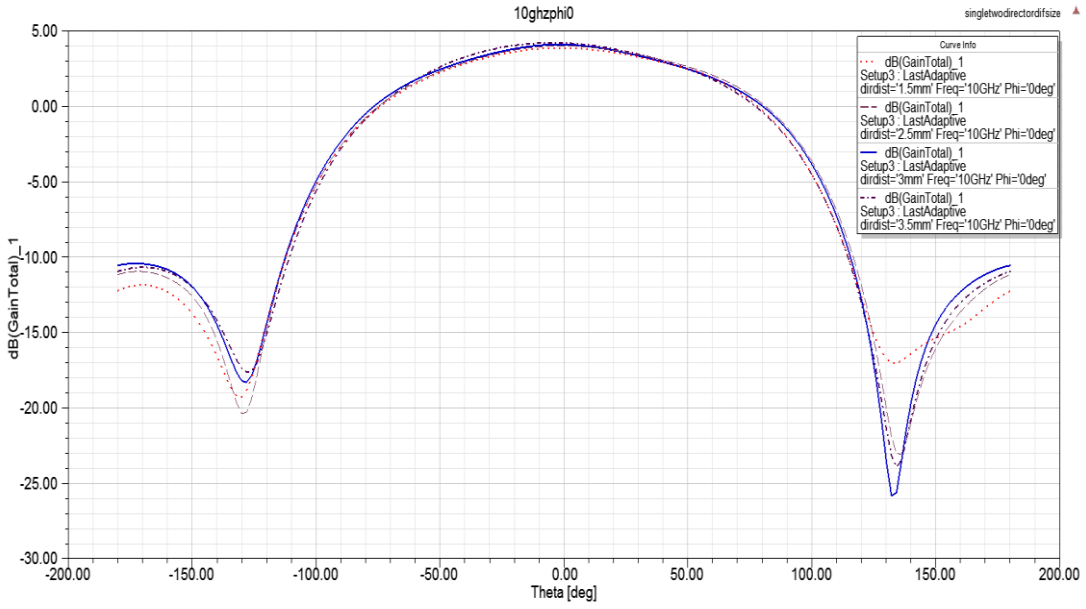

Figure 3.19. 10 GHz total gains of different size of second director(fi=0)

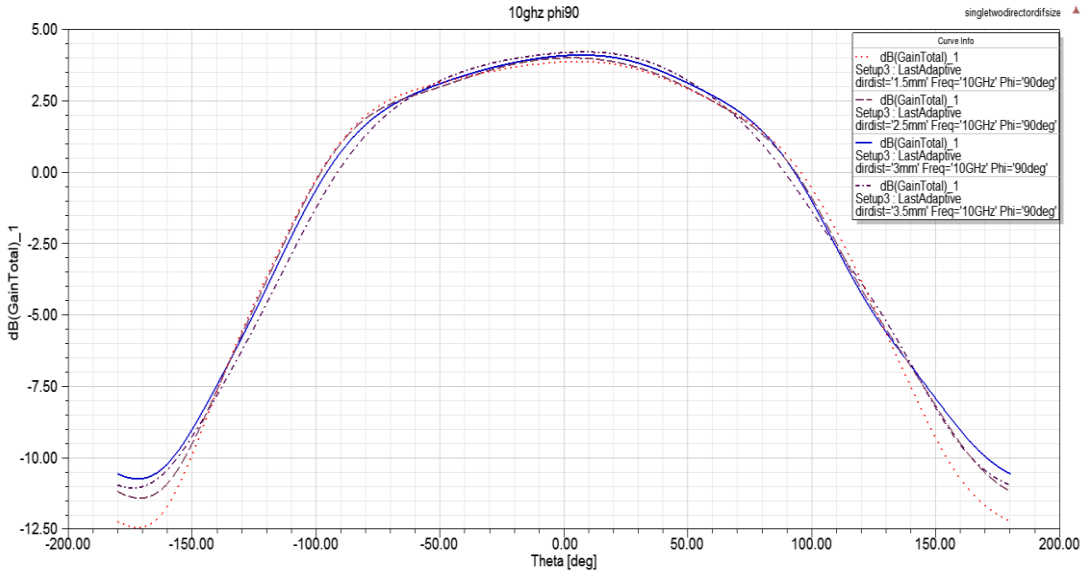

Figure 3.20. 10 GHz total gains of different size of second director(fi=90)

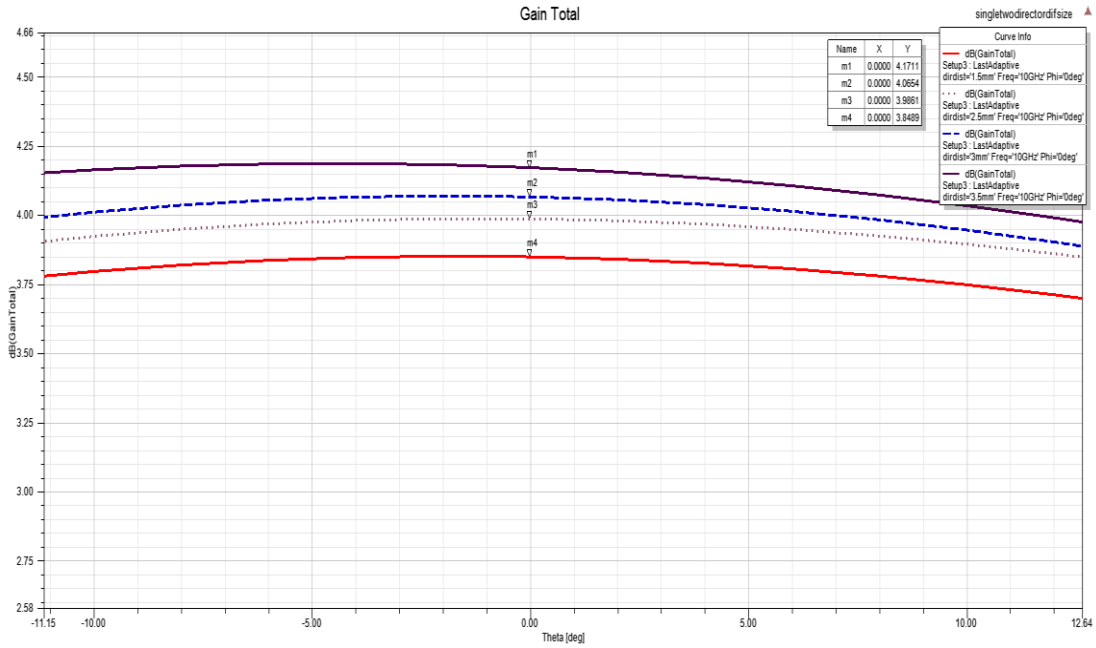

Figure 3.21. Different size of second director's total gains

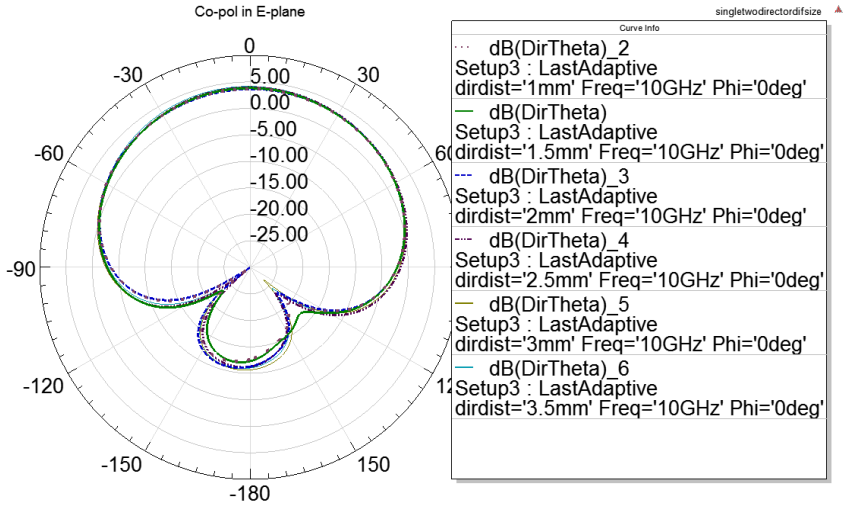

Figure 3.22. Co-pol in E plane at 10 GHz

Different size of directors is a kind of modification on the structure of quasi-Yagi antenna. Two configurations were chosen: the first one multi-director as the length of second director is about 3mm and a log-periodic director array as the lengths of second director are 1mm, 1.5mm, 2mm, 2,5mm, 3.5mm. In practice to simplify the structure the width of the elements are the same and it does not compromises the performance of the structure. The second simplification that is done to the structure is the use of equal distances between directors, this way, the log-proportionally is only applied to the lengths of the directors. The results show that the second configuration has the same bandwidth with same center frequency however there has a small differences in patterns such as side lobe levels are differnet with each other, back lobes levels are different. Finally, the total gain difference is about 0.1 dB so two configuration results are close to each other.

The antenna shows wide beam width in H plane, but its gain is too low, so we design a quasi-Yagi antenna array.

The size of director, the distance from radiator to director S_{dir} and the length of reflector W_{gro} has big influence on the return loss and L_{dir} has big influence on gain.

The structure parameters of single feed quasi-Yagi array are obtained at last and shown in Table 3.2.

The bandwidth is determined relative to the center frequency as a percentage given by

$$\frac{f_u}{f_l} 100=BW \qquad (3.8)$$

Where f_u and f_l are the upper and lower frequency limits where the input reflection loss amounts to S_{11}=-10 dB. The center frequency is given as

$$\frac{f_u+f_l}{2}=f_0 \qquad (3.9)$$

The quasi-Yagi radiator displayed a simulated BW of %50 and measured a significant BW of 52% as illustrated in Figure 3.23.

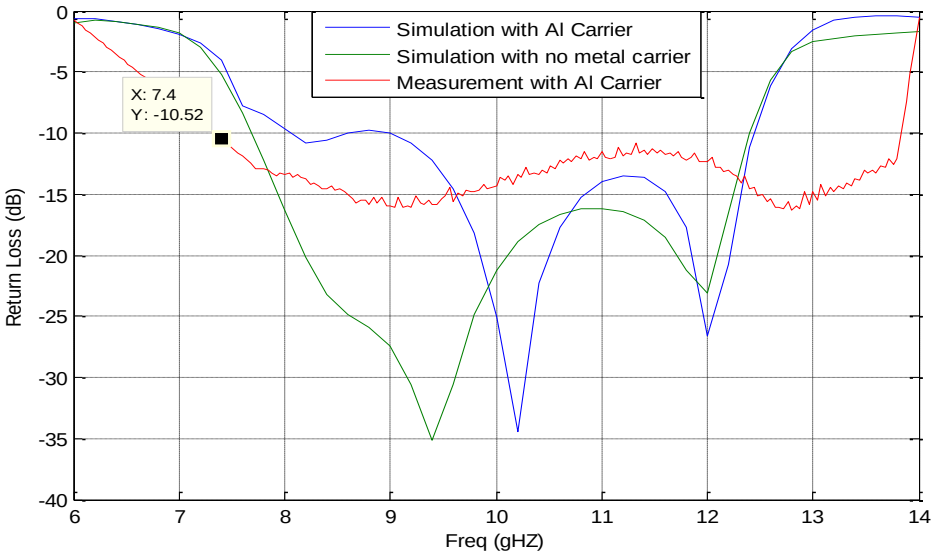

Figure 3.23. Return losses of single element antenna

CHAPTER 4

POWER DIVIDER DESIGN

4.1. Introduction

This section covers the beamforming network, which control the distrubution of energy across the elements of the array as well as the excitation phase of the feding currents feding the individual elements.The amplitude of the current feding the radiators is determined through controlling the impedance values of the microstrip feed lines.

The appropriate power divider solutions for our antenna are presented. There exists several possible power dividers, among which Wilkinson or T type dividers are the most common ones.

Three port network power dividers with one input and two outputs have a scattering matrix with the following nine independent elements:

$$[S]=\begin{bmatrix} S_{11} & S_{12} & S_{13} \\ S_{21} & S_{22} & S_{23} \\ S_{31} & S_{32} & S_{33} \end{bmatrix} \quad (4.1)$$

[S] matrix is symmetric for reciprocal networks and ($S_{ij}=S_{ji}$). Ideally, the network should be lossless and matched at all ports to avoid any loss of power. When first port is matched $S_{11}=0$ or second and third ports are matched $S_{22}=0$ and $S_{33}=0$ [22].

If an ideal network is assumed

$$[S]=\begin{bmatrix} 0 & S_{12} & S_{13} \\ S_{21} & 0 & S_{23} \\ S_{31} & S_{32} & 0 \end{bmatrix}$$

From the unitary matrix properties can be applied for the lossless structures. The unitary matrix formulations 4.1- 4.6 are shown below [23].

$$S_{12}S_{12}^{*}+S_{13}S_{13}^{*}=|S_{12}|^2 + |S_{13}|^2 =1 \quad (4.1)$$

$$S_{21}S_{21}^{*}+S_{23}S_{23}^{*}=|S_{21}|^2 + |S_{23}|^2 =1 \quad (4.2)$$

$$S_{12}S_{12}^{*}+S_{13}S_{13}^{*}=|S_{31}|^2 + |S_{32}|^2 =1 \quad (4.3)$$

$$S_{13}^{*} S_{23} = 0 \quad (4.4)$$

$$S_{23}^{*} S_{12} = 0 \quad (4.5)$$

$$S_{12}^{*} S_{13} = 0 \quad (4.6)$$

Which results in

$S_{12} \neq 0$

$S_{13} =0$, $S_{23} =0$,

As a result, $|S_{13}|^2 + |S_{23}|^2 =0$. If the network is reciprocal and matched at all ports, it is allowed to be lossy.

The resistive divider, Wilkinson divider and T junction dividers are commonly used in the systems. Each one has advantages and disadvantages these are shown in Table 4.1. [22]

Table 4.1. *Power divider types advantages and disadvantages*

Passive Power Divider	**Advantage**	**Disadvantage**
T-Junction	Lossless	- Not matched at all ports - No isolation between output ports
Resistive	Can be matched at all ports	- No isolation between output ports - Poor power handling limited by resistor tolerances - Lossy
Wilkinson	Lossless (if matched at all ports) High isolation	- Reflected power is dissipated through isolation resistor if mismatched

The main purpose of divider is designing an equal power split for each element. For higher frequencies the losses are very significant parameters for the antenna performances. To divide more efficiently the Wilkinson power divider type is selected.

4.2. Wilkinson Power Divider

The Wilkinson power divider is a three-port network that is lossless when the output ports are matched; where only reflected power is dissipated. Input power can be split into two or more in phase signals with the same amplitude. Usually, three-port networks cannot be matched without being lossy. The solution to this, in the Wilkinson power divider, is to add a resistor between the two outputs with the function to absorb energy if there is a mismatch between the outputs. For a two-way Wilkinson divider using $\lambda/4$ impedance transformers having a characteristics impedance of $\sqrt{2}\,Z_0$ and a lumped isolation resistor of $2Z_0$ with all three ports matched.

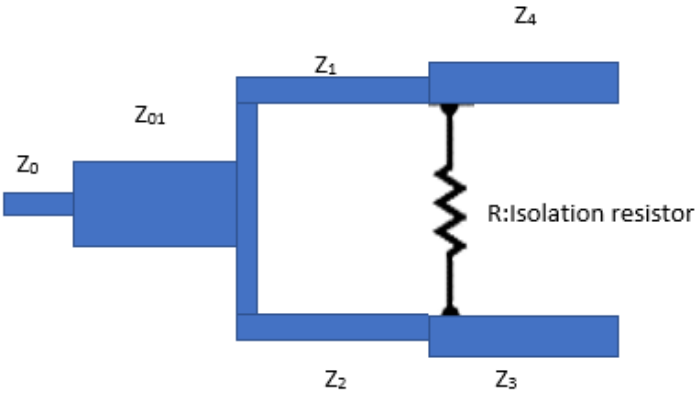

Figure 4.1. 2-Way one section Wilkinson power divider

Design for center frequency of 10 GHz and Z_0=50Ω requires the isolation resistor to be $2Z_0$=100Ω and the impedance of the quarter lambda transmission line split section to be $\sqrt{2}\ Z_0$=70.7Ω.

4.2.1. Derivation of Scattering Parameters

The S parameter matrix for the Wilkinson power divider can be found using even-odd mode analysis which uses circuit symmetry and superposition [22]. As a first step the circuit in Figure 4.2. is redrawn with all impedances normalized to the character impedance Z_0 and redrawn as shown in Figure 4.3.

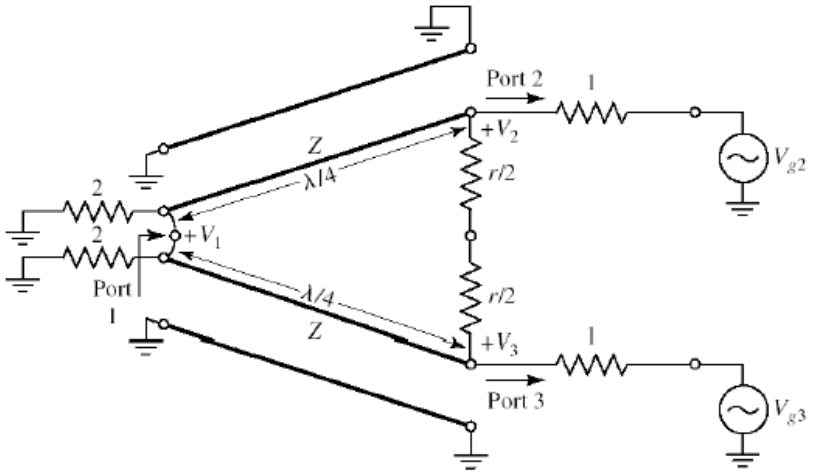

Figure 4.2. The Wilkinson power divider circuit [22] in normalized and symmetric form

There is no current flow between the r/2 resistors or the short circuit between the inputs of two transmission lines at port 1. Therefore, the circuit above can be bisected and separated into two systems, even and odd (Figure 4.3. (a) and (b) respectively). Each system can be then analyzed separately.

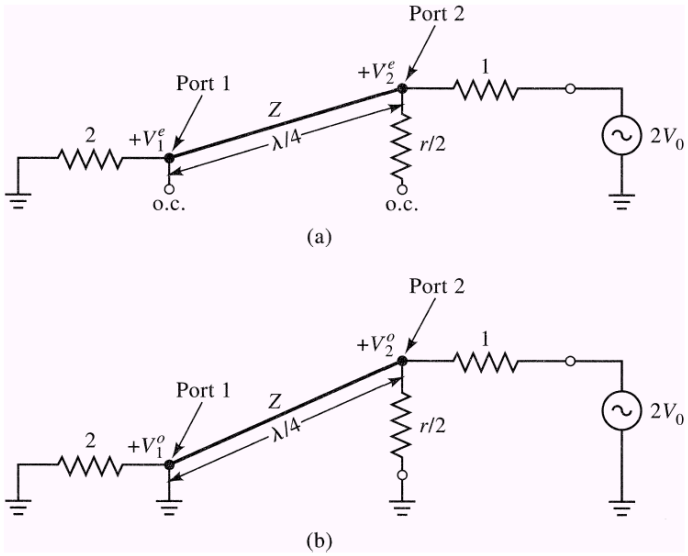

Figure 4.3. Bisection of the circuit of Figure 4.2. taken from [22]. (a)Even-mode excitation (b)Odd-mode excitation

4.2.1.1. Even Mode Analysis

First the input impedance at port 2 of the circuit in Fig.3 (a) is checked where $Z=\sqrt{2}$

$Z_{in}^{e}= \sqrt{2}^2/2 = 1$ (matched)

Then voltages at port 2 and port 1 are found

$$V_2^e = jV^+(1-\Gamma) = V_0 \quad (4.7)$$

$$V_1^e = V^+(1+\Gamma) = jV_0\frac{\Gamma+1}{\Gamma-1} \quad (4.8)$$

From Equation 4.7 and 4.8;

$$\Gamma=\frac{2-\sqrt{2}}{2+\sqrt{2}}$$

$V_1^e = -jV_0\sqrt{2}$

4.2.1.2. Odd Mode Analysis

Zin (input impedance) has to be found from Figure 4.3.(b)

$Z_{in} = \sqrt{2}^2/2 = 1$ (matched)

The voltages of port 1 and port 2;

$V_2^e = V_0$

$V_2^e = 0$ (ground)

The return loss at the input port in the circuit is shown below in Figure 4.4. (a) and its bisection (b) are used.

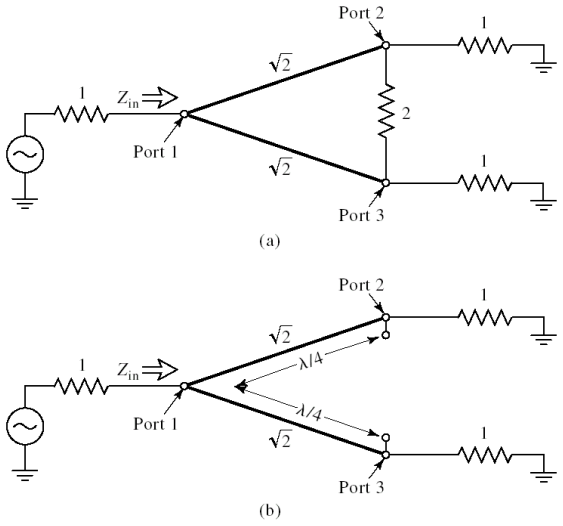

Figure 4.4. Input return loss of the Wilkinson divider (from [22] (a)Terminated Wilkinson divider (b)Bisection of the circuit in (a)

Matching the output ports are very significant for no current flow on the isolation resistor. If there is a mismatch at the output ports, the isolation resistor compensates this current flow and the reflections are diminished. The input port's impedance is:

$Z_{in} = \sqrt{2}^2/2 = 1$

As a result;

Input return loss $S_{11}=0$ when Zin =0 and output return losses $S_{22} = S_{33} =0$ when output matched. Insertion losses can be calculated with

$S_{12} = S_{21} = (V_1^e + V_1^o) / (V_2^e + V_2^o) = -j/\sqrt{2}$

$S_{13} = S_{31} = -j/\sqrt{2}$ $S_{23} = S_{32} =0$

The performance of the Wilkinson divider/coupler is commonly evaluated by the following figures of merit.

Table 4.2. *Parameters definitions for power divider*

Abbreviation	**Formulation**	**Definition**
RL_1[dB] and RL_2[dB]	-20log|S_{11}| and -20log|S_{22}|	return loss at ports 1 and 2
CP_{12}[dB]	-20log|S_{12}|	coupling between ports 1 and 2
IL_{23}[dB]	-20log|S_{23}|	isolation between ports 2 and 3

4.2.2. Microstrip Design Considerations

The significant factors of designing microstrip lines are size, higher-order modes, surface wave effects, dielectric loss, and power handling (such as dielectric strength and thermal conductivity).

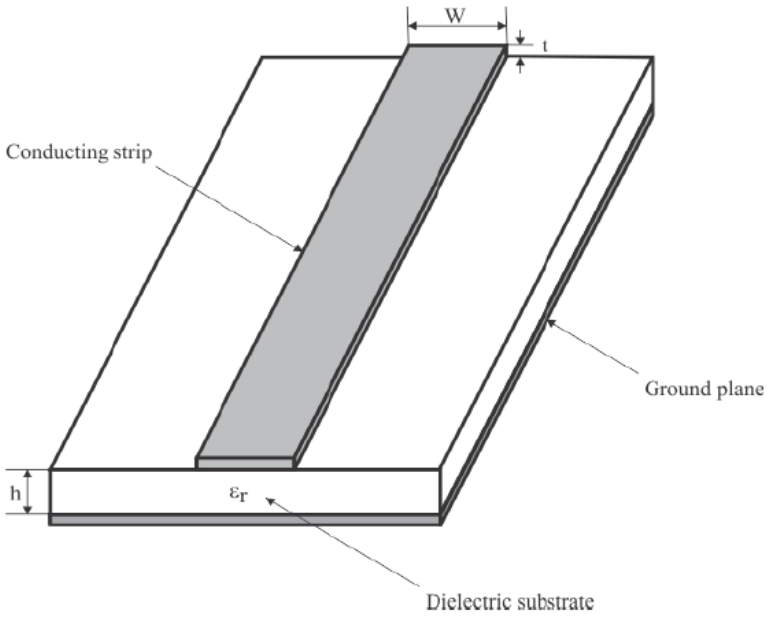

Figure 4.5. A microstrip line model

At lower frequencies, size can become more and more important as wavelength becomes large. Resulting in reduction for the design area which is critical in the final system design.

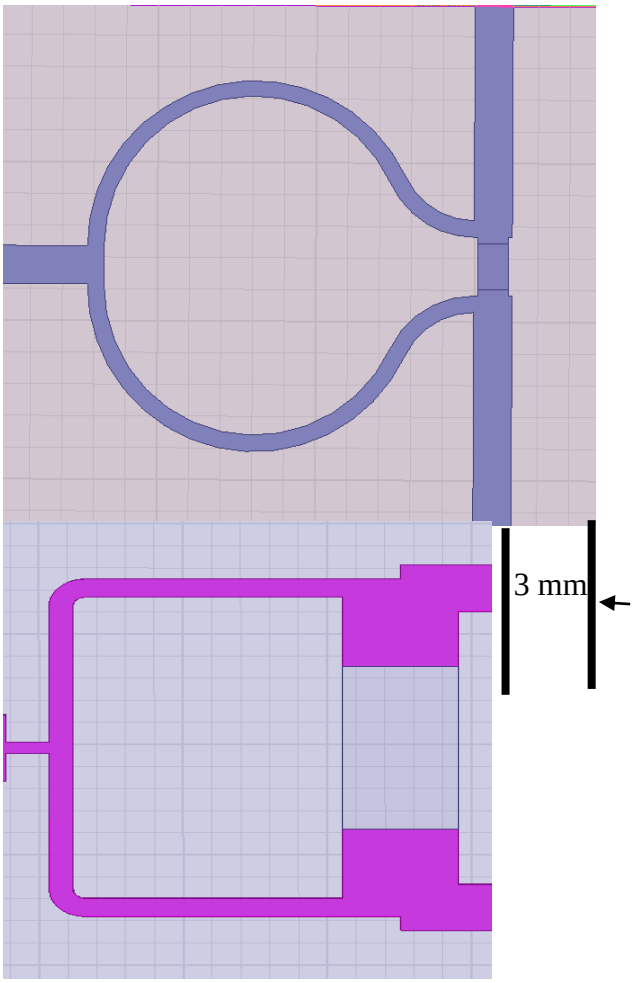

Figure 4.6. Two design topologies size difference by 3mm in length

In the design of the Wilkinson divider, two different topologies are compared which is circular split and rigid straight splits. Circular split can reduce the design area which is about 3mm as shown in Figure 4.6. However, the coupling between port 2 and port 3 is higher. Therefore, we used straight split design topology in the final design. To

save the area on the substrate, the circular split can be used however we used rigid straight topology. There are a few parameters such as higher order modes, power handling that has to be considered.

4.2.3. Single and Multi-Stage Divider Designs

The main purpose of this part of thesis is to improve the bandwidth capability of Wilkinson power divider. In the first step single section is applied but the bandwidth results are narrow so in the next two section power divider design is tried. As a result, for obtaining larger bandwidth multiple sections has to be used. The microstrip design was optimized for operation over the antenna bandwidth 4-16 GHz and utilized in a corporate feeding network for an antenna array. The designs were fabricated with thin film production high dielectric materials for having the capability for use in radom radar.

In the future master plan, the number of directors will be increased so that the total gain will be improved. Symmetric T-junction lines can be used in lower power modes effectively however when upper power levels equally power splitting is important for beamforming improvement of the structure.

Before starting with the design of Wilkinson on schematic, width and length of striplines were calculated. After we have applied into the software as shown in Figure 4.8. Resistances were optimized with optimizer. Because sheet resistance has to be obtained for producibility.

A single two section equal-split Wilkinson divider is then modeled and optimized using microstrip line models in MWO (Microwave Office Software). The variables optimized were the widths of the microstrip lines. The optimization is done for the S11<-20 dB over the frequency range 8 GHz to 12 GHz. However single stage power divider is not enough performance across the whole band, increase the operating bandwidth, increasing the stage numbers is necessary. During the second stage

designing the whole structure line widths and lengths have to be optimized at the same time. Bandwidth is not sufficient with one stage as seen in Figure 4.7.

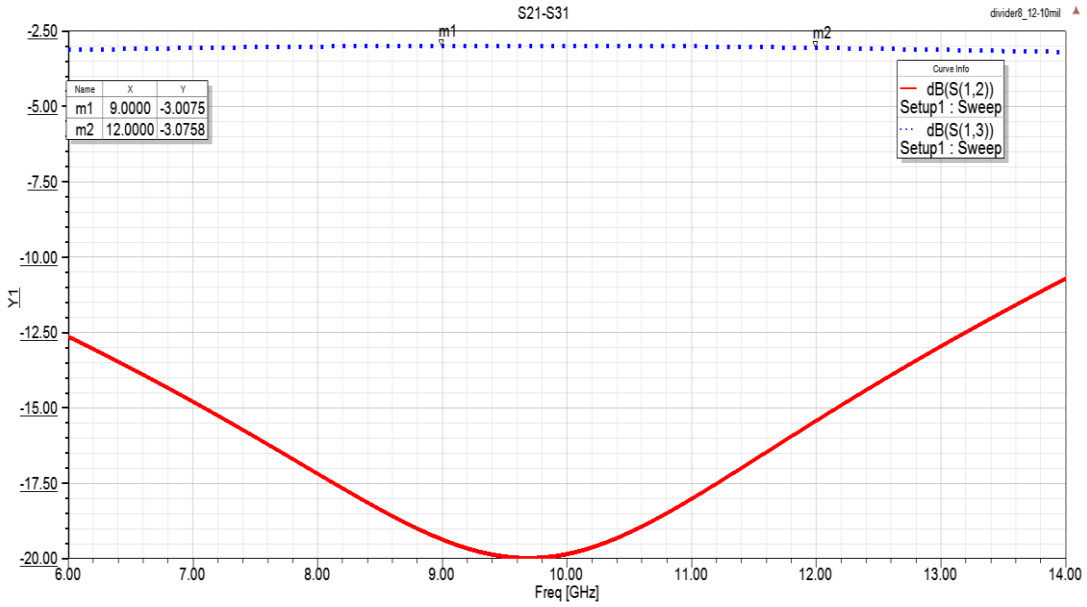

Figure 4.7. One stage Wilkinson divider return and insertion loss response

The design approach builds from two port network theory and derivation of scattering parameters of the Wilkinson divider and then investigates different microstrip topologies using Ansoft HFSS simulation software and AWR software for design optimization. Microstrip design considerations are also discussed especially in relation to the choice of an appropriate substrate for fabrication. The experimental results for the design prototype are also shown and discussed.

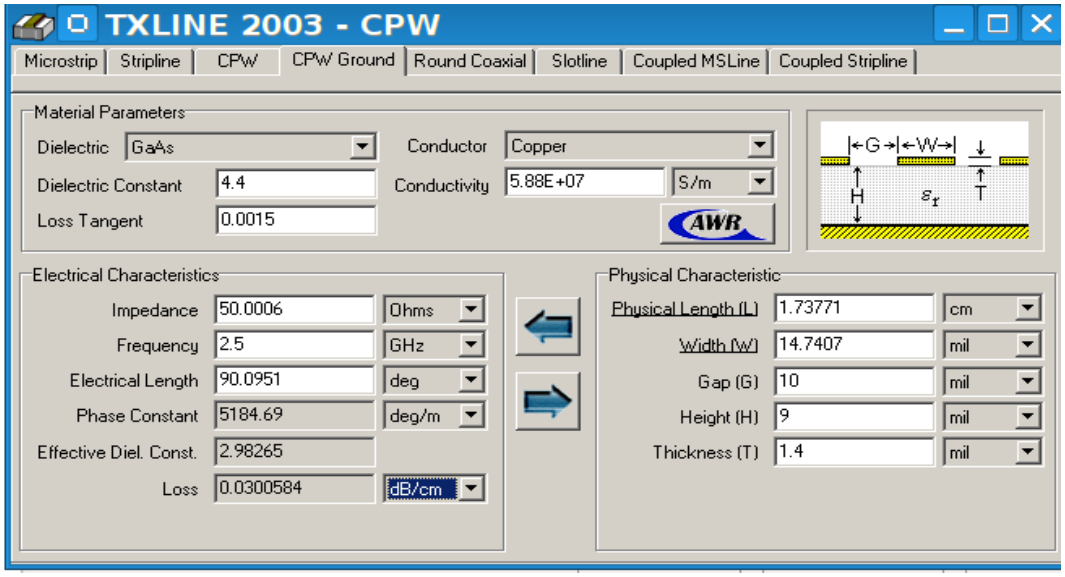

Figure 4.8. Length and width calculator in AWR Program

When having the lengths from input port to all output ports identical, the beam position is independent of frequency as well as the spacing between center to center of array elements. A center to center distance between each single antennas which is L_{dist} is defined. When the space between microstrip lines, that cause a mutual coupling. There is a tradeoff between grating lobes level and mutual coupling. Effect of the element spacing on grating lobes is investigated. Analyses are being done parametrically so that the effect on the characteristics in terms of return loss, radiation patterns and gain is investigated.

At the end of these analyses the final value L_{dist} =0.75λ_0=16mm is calculated to minimize the grating lobes levels. The dimensions defined for the feed network are summarized in Table 3.3. The simulated return loss response gains and radiation patterns of are given in Figure 5.11 through Figure 5.21.

The return loss, insertion loss, coupling and isolation between ports were evaluated to determine the optimized final design. A minimal return loss of -10 dB or better over band and isolation between output ports is a critical design requirement. Also -3dB coupling (half of the power) between input and output ports for each stage is anticipated. The frequency response of the 4:1 is expected to have a wider bandwidth

than seen in the 2:1 Wilkinson resulting from the use of additional cascaded 0,25 λ sections.

4.2.4. Divider Simulation Results

As a first step, we decided to analyze one stage Wilkinson divider with HFSS as shown in Figure 4.9. and the results shows one stage is not enough for wide bandwidth applications.

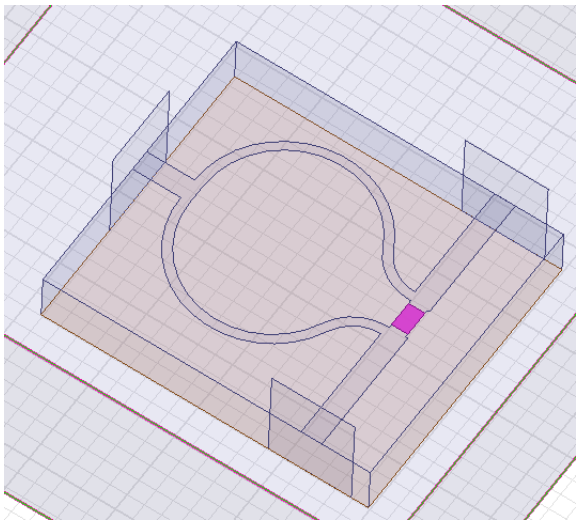

Figure 4.9. 3-D transparent view of the one stage Wilkinson divider in HFSS

The circular quarter wavelength split section 2:1 divider is being the conventional Wilkinson divider design was modeled first. After microstrip long lines were added the design and was optimized with AWR program. Figures 4.10. and Figure 4.14. show the 2:1 model in AWR and HFSS. Firstly, bandwidth is significant along the bandwidth. The bandwidth of the single antenna is wide so to achieve this power dividing has one more than section. If we increase the number of power dividing section, the operating frequency region will be enlarged. Impedance matching between the sections are more important.

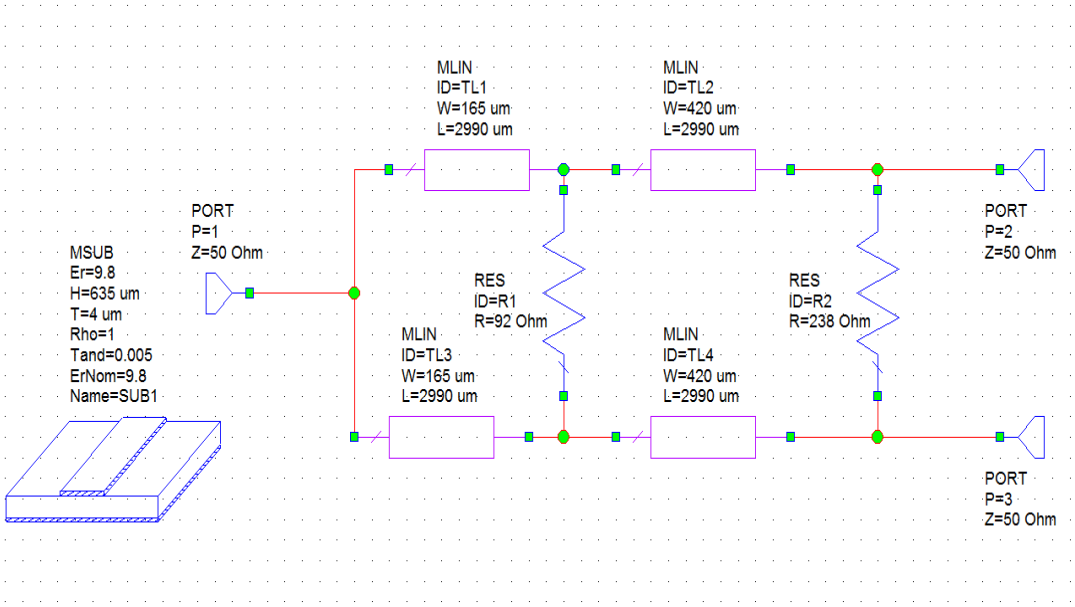

Figure 4.10. Equivalent circuit of 2:1 Wilkinson divider in AWR (straight quarter-lambda split section)

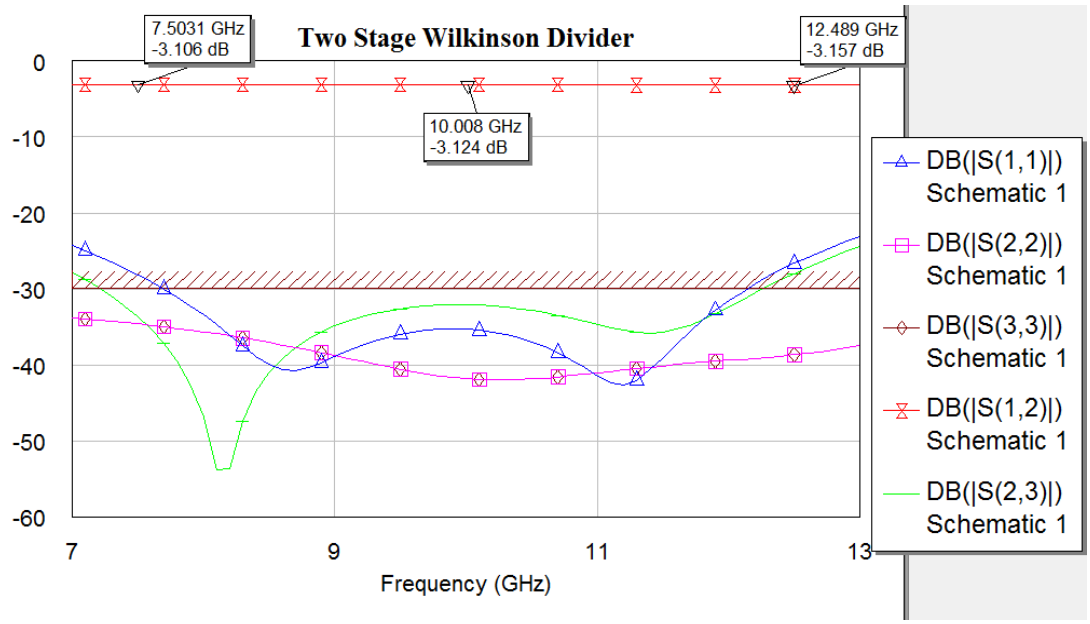

Figure 4.11. Simulated S parameters of 2:1 Wilkinson divider

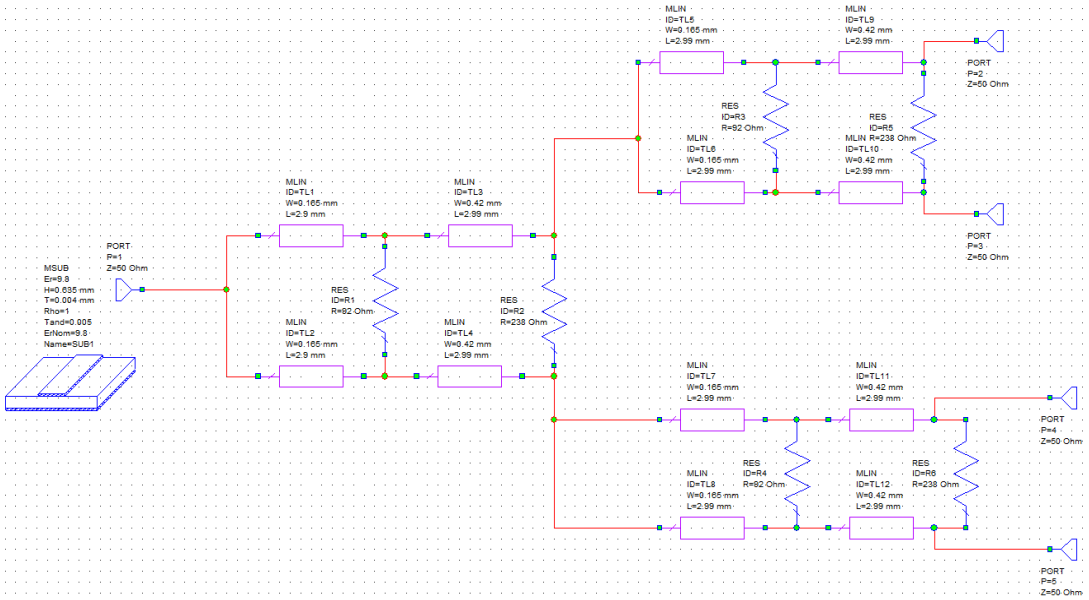

Figure 4.12. Equivalent circuit of 4:1 Wilkinson divider (straight quarter-lambda split section) in AWR

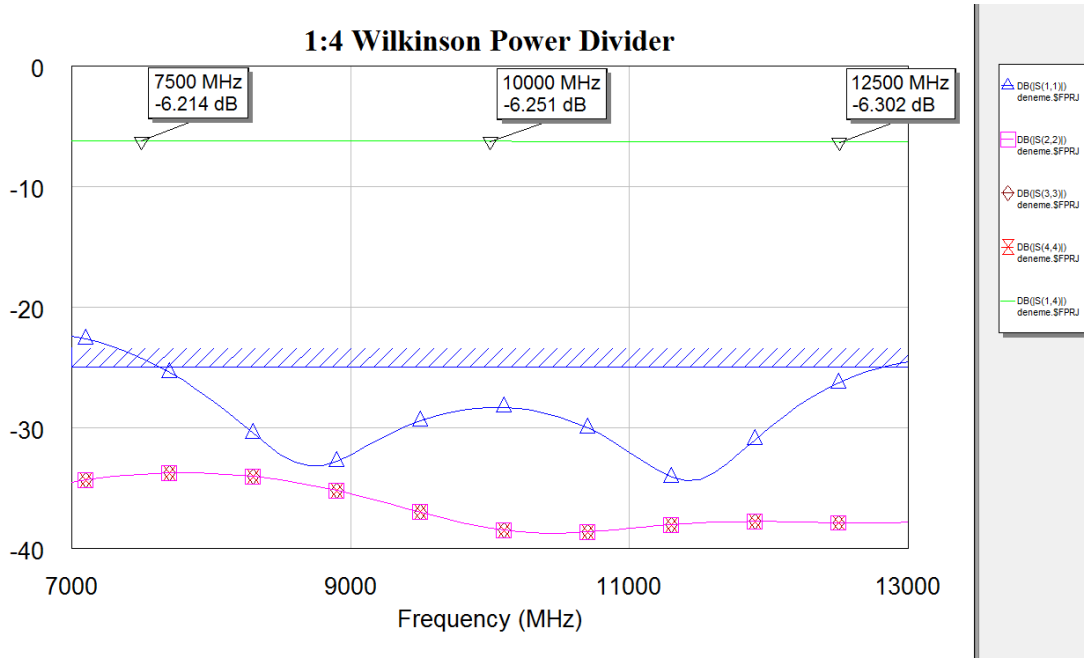

Figure 4.13. Simulated S parameters of 1:4 Wilkinson divider

The radiating characteristics of a single antenna are not adequate for some applications, such as if the antenna could not supply enough gain values or the requirements of radiation pattern geometry. In the design program we do not need any divider because we can divide all the power equally however in manufacturing, we have to design power dividers for splitting the total power equally. A single section equal-split Wilkinson power divider was designed and simulated. The analysis showed that such a design yields a narrow-band frequency response and did not achieve the BW required for a $|S_{11}|$<-20 dB. This is due to the quarter wave transformer arms of the divider ensuring only a matched condition at the design frequency 10 GHz. A multi section 3dB Wilkinson divider was then opted for, thus yielding a broader frequency response. The parameters were calculated with the power ratio K=1 using the following equations [15]:

$$Z_{01} = Z_0 \left(\frac{K}{1+K^2}\right)^{0.25} \quad (4.9)$$

Where Z_0 is the characteristic impedance, R is the isolation resistor which was omitted to ease the layout of the feed. The power ratio between port-1 and port-2 is $K_2=P_{n1}\backslash P_{n2}$ where n is an integer indicating power divider 1,2 and 3.

Then a single two section equal split Wilkinson divider is modelled and optimized using microstrip line models using AWR® and HFSS®.

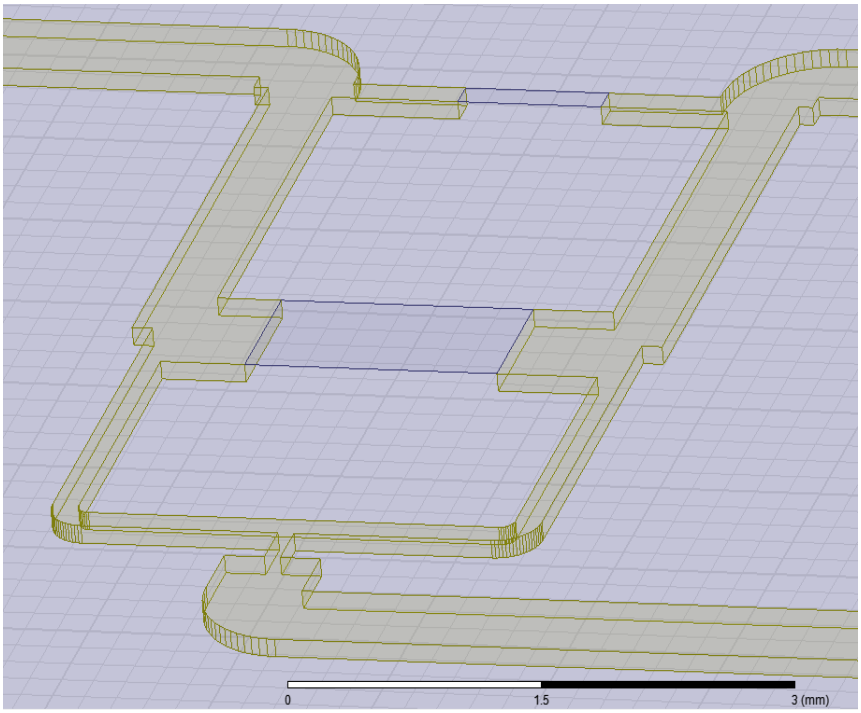

Figure 4.14. Simulated S parameters of 1:4 Wilkinson divider

Dividers which has smaller sizes present design issues are available. The results of input return loss is below -25 dB. Resistive layer which is between the coupled line is done with Tantalum Nitride thin film metallization. The resistivity value of this metallization is 100 ohm/sq in the HFSS program library. Finally, two different sections of Wilkinson divider are shown in Figure 4.14.

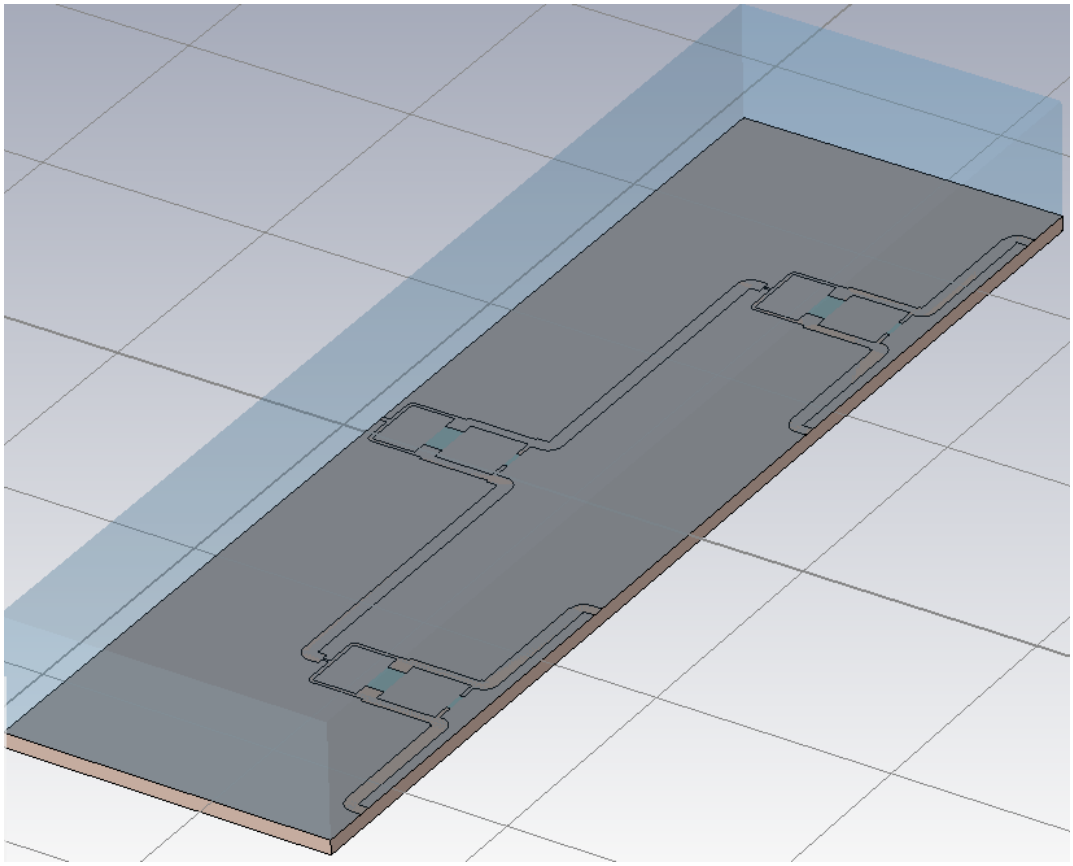

Figure 4.15. 3D View of 4 way Wilkinson power divider

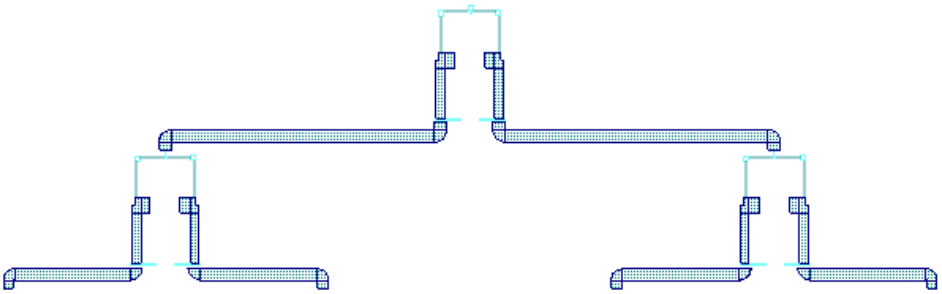

Figure 4.16. Lay out for the uniform beamforming network in AWR

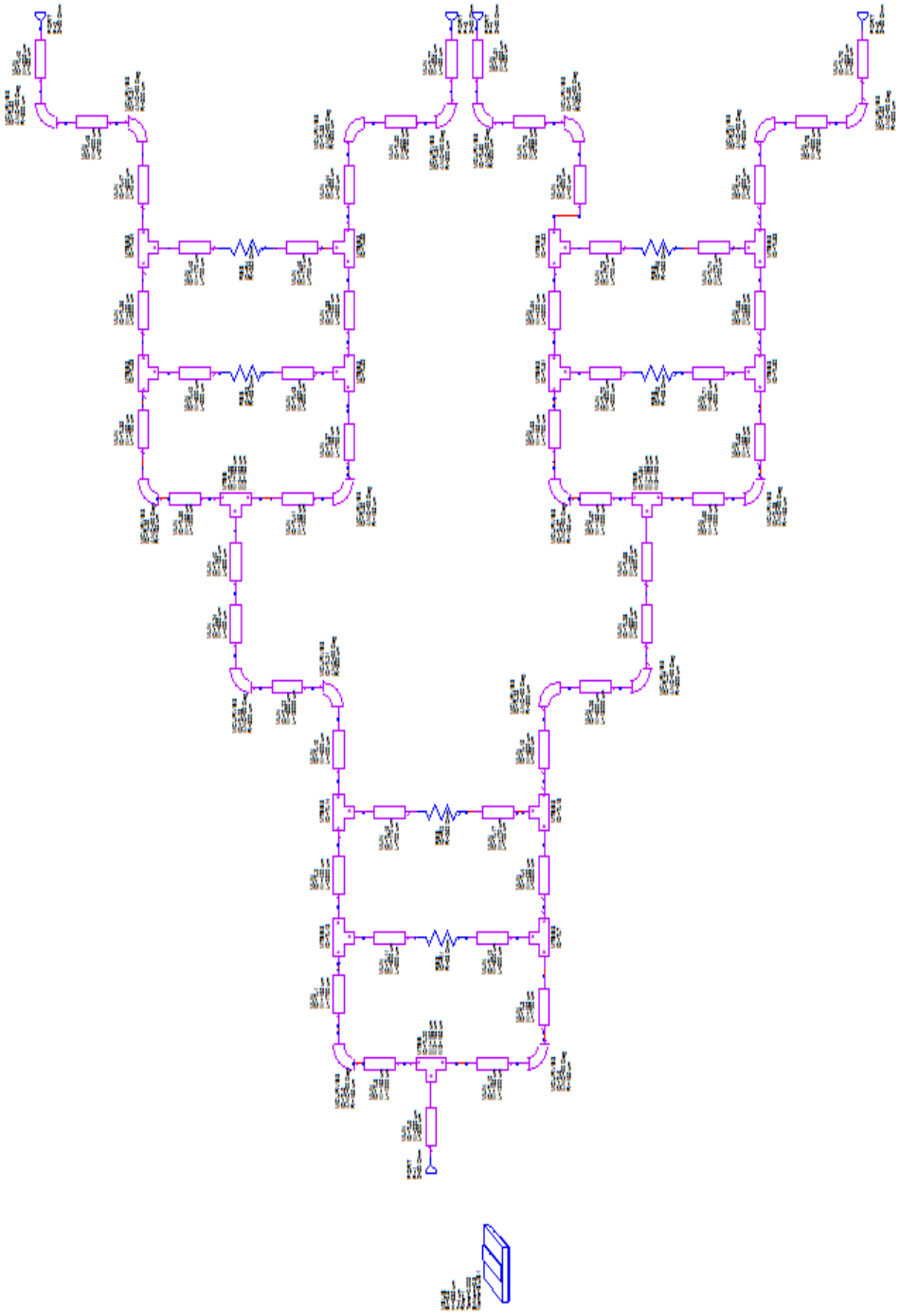

Figure 4.17. Microstrip model of uniform 1x4 beamforming network

When keeping the length from input port to all output ports identical, the beam position is independent of frequency as well as the spacing between the array elements. This condition contributes to a broadband array design [28]. The single 2-way divider was used back-to-back to form the 4-way equal Wilkinson power divider. To maintain the critical lengths of the quarter wave transformers in the power dividers as well as maintaining the element spacing, the radiators are fixed at the element spacing $\lambda_0/2$ and the line lengths of the lines with the characteristic impedance were optimized using the same simplex algorithm as was used with the single divider.

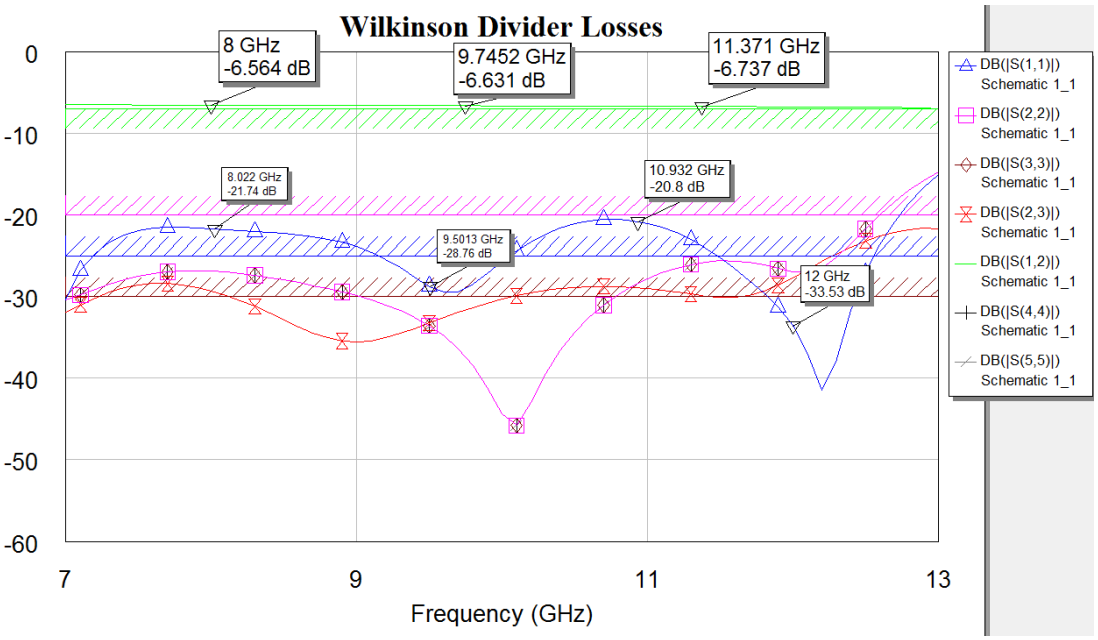

Figure 4.18. S-parameters for four-way Wilkinson divider

In addition, there are a few restrictions about the design such as the distance between the antennas, designing the divider onto the thick substrate.

The design of the 4-way equal divider, distances are 0.75λ is about 15 mm so in the final design we stretch the 50Ω lines to this distance. As a result, this will be caused more and more return losses at the ports.

Measuring the coupling to the output ports was done by placing port 2 of the network analyzer at the required output port of the beamforming network and terminating all other ports with 50 Ω broadband loads. A full 2 port measurement was performed. The coupling of only half the beamforming network is shown due to the symmetry of the network. The simulation results display an S_{21}, S_{31}, S_{41} and S_{51} of -10 dB across the band in Figure 4.17. The ripples in the measured transmission coefficient are due to mismatches in the beamforming network and the oscillation period being an indicator of the distance from input port to output ports.

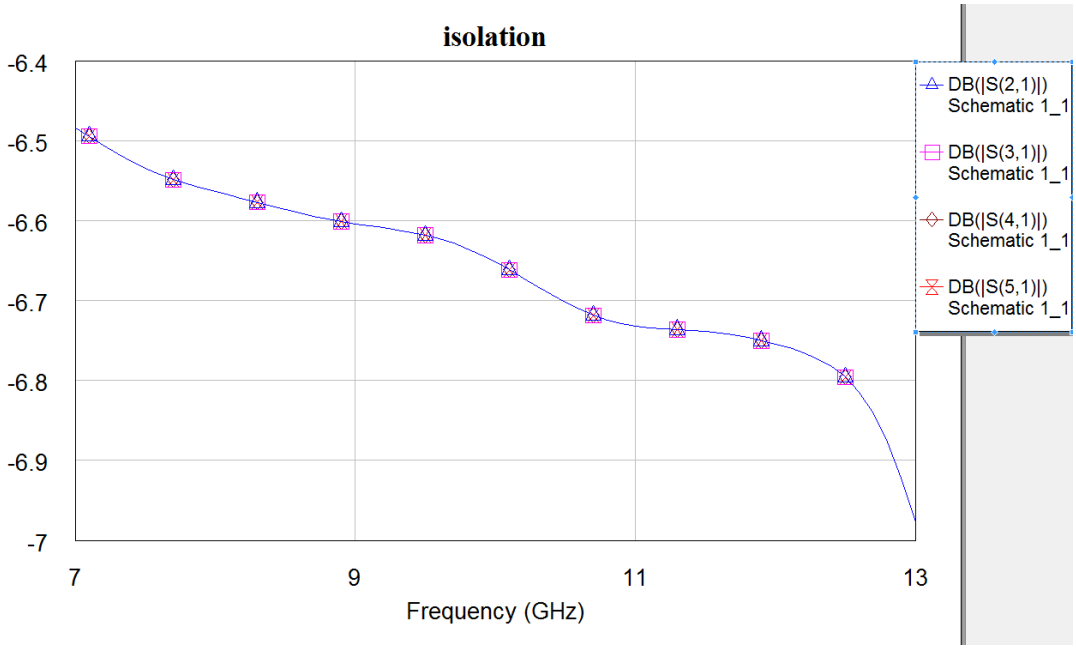

Figure 4.19. Simulated isolations for 4-way Wilkinson divider

4.3. Results

It is necessary to design two-way power divider since the uniform beamforming network comprises identical power dividers interconnected together. A single two section equal split Wilkinson divider was then modeled and optimized using microstrip line models in AWR microwave office software. The simplex optimization technique which is based on the "Nelder Meade optimizer" was employed. The widths and lengths of the microstrip lines variables were optimized. The optimization was done for the performance goal set as S11 <-25 dB over the frequency range 8 GHz to 12 GHz. But it is possible to achieve a Tschebyscheff frequency response for the input return loss by correctly choosing the parameters in Figure 4.2. The microstrip widths given in Table 4.2. were used as a starting point for optimization. TH optimized microstrip model with line widths and lengths for the single two section 3 dB Wilkinson divider and S parameters are shown in Figure 4.4. As we discussed the results, when we ignored some special corners and we equalize the same structure to the circular design we can have less return losses and more power insertion into the elements. For the second section we did the circular design for comparing with the straight design.

Table 4.3. *Calculated impedances for two-section equal power divider*

Parameters	**Impedance(Ω)**	**Width microstrip(mm)**	**Length λ**
Z0	50	0.6	N/A
Z01	44.7	0.74	1/4
Z1	70	0.25	1/4
Z2	70	0.25	1/4
Z3	54.25	0.49	1/4
Z4	54.25	0.49	1/4

CHAPTER 5

FABRICATIONS AND MEASUREMENTS OF A QUASI YAGI ANTENNA AND ARRAY ON THE CERAMIC SUBSTRATE

4.4. Fabrication Steps

To this point, quasi-Yagi antenna and array antenna designed with only one configuration. In order to compare and to prove the simulation results single antenna and four element linear array antenna are produced with thin film technology and measured. Final products are fabricated in the facilities of Aselsan Inc. The antenna designed only for one configuration and a few runs are done for clear results.

Thin film is a special technology for the fabrication that have too many advantages and also disadvantages. We used this technology that we have mentioned before. The material used as a substrate is Alumina Superstrate 99.6 quality, 4" square, 25 mil thick polycrystalline alumina (Al_2O_3) substrates are obtained from CoorsTek Inc. with a surface roughness is about 20 nm. Oxford Laser machine which is green wavelength 532nm laser for cutting process of final products.

Unsatisfactory adhesion between different materials is an important failure path in many packaging systems. When materials (metal-metal, metal-ceramic, metal-polymer, or polymer-ceramic) are bonded together, many problems arise such as cracking, formation of voids and delamination of the thin film. These type of adhesion problems are generally due to high residual stresses induced at the interface which is caused by the great variance of the thermo-mechanical properties between dissimilar materials [26]. ADS996 model is a double side polished wafer so the roughness of the wafer is very small, metallization adhesion problems that can be seen in the literature but we applied a new method for improving the adhesion quality because our design thickness is about 5um gold so the coating stress is very high.

In the first step, if we increased the roughness of the wafer with any method, to improve the adhesion. Thus we applied the “Ar(Argon)” gasses onto the alumina substrate for increasing the roughness to improve adhesion. An advanced ceramic such as alumina,
has the capability of operating at high power and high frequency applications. Its chemical inertness along with thermal and mechanical stability make alumina favorable as a commercial ceramic substrate for hybrid ICs, MCM and other thin film applications [25]

With higher adhesion strength, and smaller Coefficient of Thermal Expansion (CTE) mismatch between Au and alumina, the insertion of a TiW (Titanium Tungsten) adhesion layer with optimum substrate surface roughness and appropriate surface treatments could lead to better packaging [26].

Apart from heat and Ar (Argon) treatment, surface pre-treatments are realized inside wet bench at ambient cleanroom conditions (Class 1000). Solvent cleaning is performed by an initial application of acetone (ACE) followed by isopropyl alcohol (IPA) rinse on alumina surface. Acid etching, on the other hand, is performed by the application of piranha solution that is prepared by a careful mixture of sulfuric acid and hydrogen peroxide (3:1 ratio) on alumina surface. Ar plasma treatment conditioned at 70W for indicated durations. Heat treatments are carried out at a maximum of 150-170 C0 inside the magnetron sputter under vacuum.

Once related surface pre-treatment is applied, a thin layer of TiW is DC magnetron sputtered on substrate surfaces (Vaksis Magnetron Sputtering System). Before TiW deposition, the vacuum of the sputtering chamber needs to reach under 8x10^-7. As the right vacuum is satisfied, the substrates are sputtered with TiW at a power of 500 W, and under an Ar flow of 100 sccm at 3 mTorr pressure. During coating process, the horizontal movement of the substrate holder is maintained at a speed of 18 mm/s. Completed deposition process results in a TiW coating of ~80 nm.

During the production steps special via alignment marks are used which is the best way to align top metallization and truncated ground metallization. This step is very significant for the process steps and measurement results.

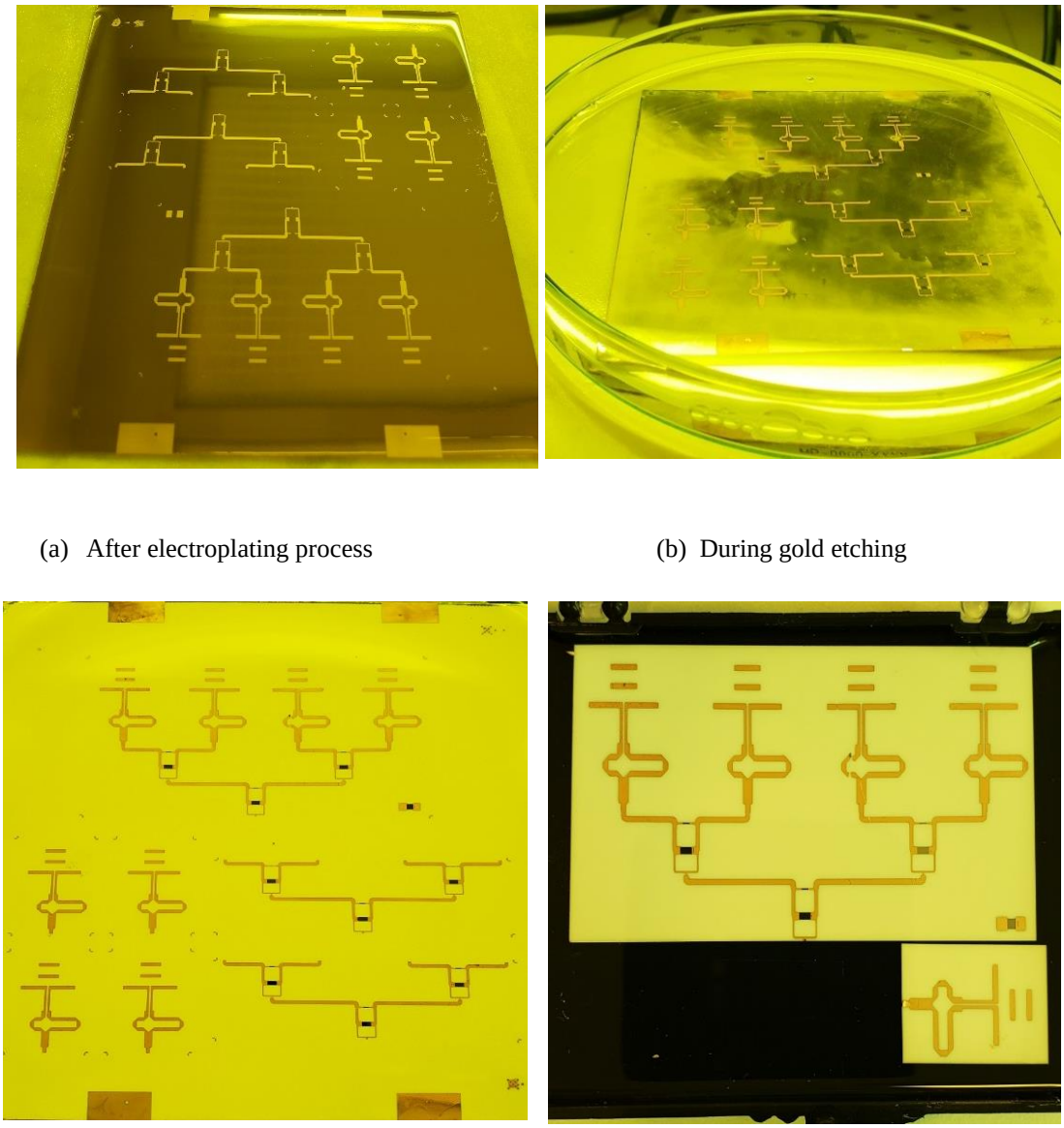

(a) After electroplating process (b) During gold etching

(c) After etching process (d) After cutting process

Figure 5.1. Fabrication Steps for the final structure (a)After electroplating coating (b) During gold etching (c) After etching process (d) After cutting process

4.5. Measurement of Fabricated Quasi Yagi Antenna and Array

Before the measurement processes, our design has truncated ground as a reflector element, so our grounding is important in generally, there need a mechanical test apparatus for antenna measurements. To have very close results, mechanical adaptors was designed additionally. To use SMA connectors for input, the designs are displayed in Figure 5.2.

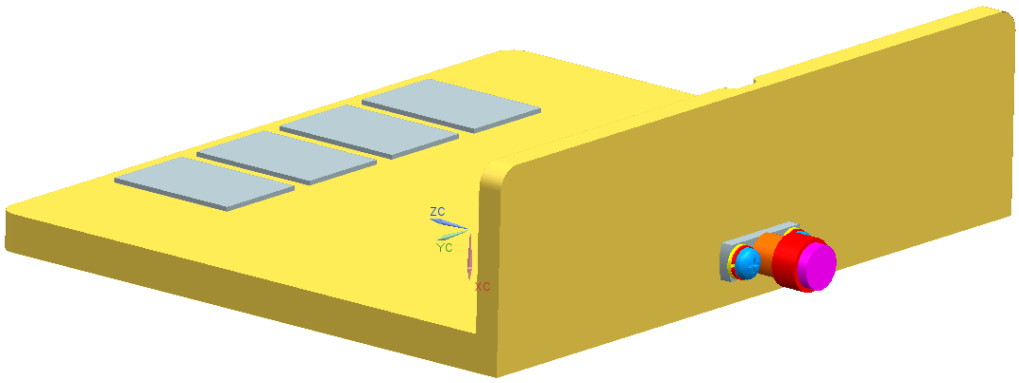

(a) From back corner view

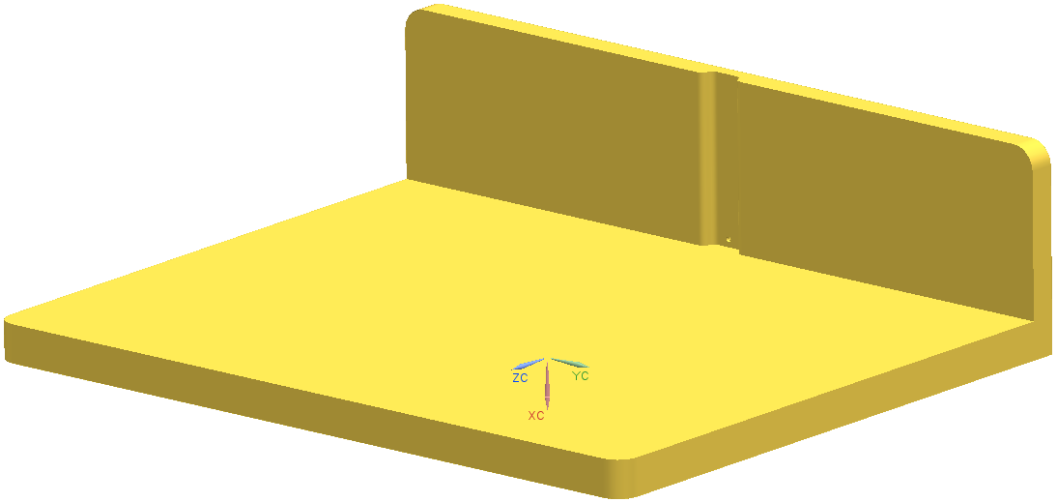

(b) From front side view

Figure 5.2. (a)Back appearance of mechanical test equipment of antenna array measurement (b) Front side appearance of mechanical test equipment

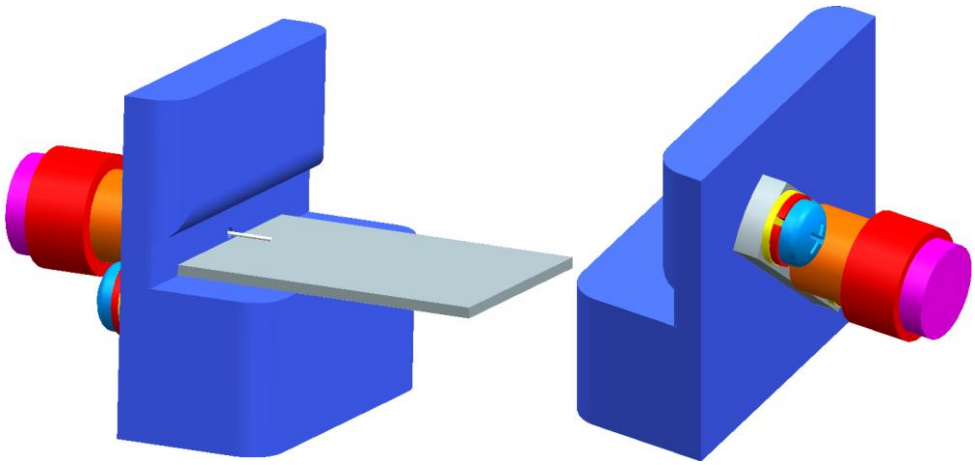

(a) Mechanical test equipment with antenna (b) Mechanical test equipment without antenna

Figure 5.3. (a)Mechanical test equipment of single element antenna (b)Test equipment without antenna

To start with to see the single element antenna performance, the antenna is pasted with conductive silver epoxy onto the metallic surface as shown in Figure 5.3. then it is fabricated and return losses measured. After the matching results are adequate for the system, for investigating results of the single element antenna, it is placed into the near field measurement chamber. In the second step single element antenna measurement results are compared with simulation results which are displayed respectively in Figure 5.6.

For the second part of thesis, four element array antennas with Wilkinson power divider are designed. All the return losses and VSWR measurements are done with N5242A PNA-X of Agilent Technologies network analyzer. Before the network analyzer measurements, input feeding RF cable calibrated with electronic calibration kit which is N4693D model. If the input feeding point is lossy, matching is not good that we say.

The total frequency response shifts about 200 MHz which is order of 1.5%.

The small differences between results of the single element dipole antenna which is seen from Figure 5.6. are agreed.

After the bandwidth requirements of the antenna are completed, radiation patterns and gain tests of the antenna are started with StarLab Spherical Near Field Measurement System of SATIMO that is shown in Figure 5.4.

The simulated gain and measured gains with frequency and theta in the 8 GHz, 10GHz, 12 GHz for the single element and four elements linear array antena. Differences between the measured and simulated gains of the single antenna that are shown in Figure 5.7., is within 2.5 dB. This difference between results may be from the measurement error in the measurement system.

Figure 5.4. Single element antenna measurement near field setup

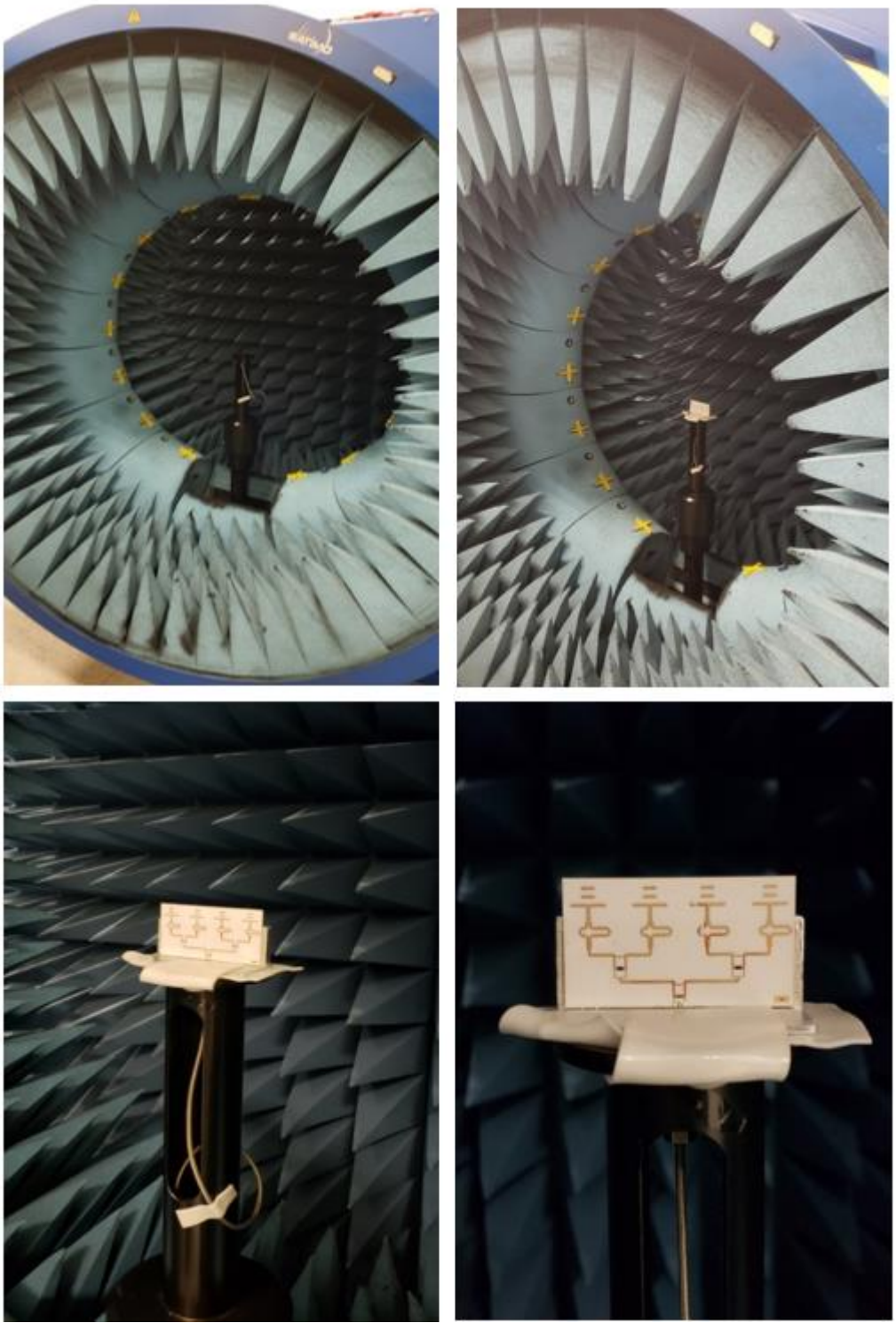

Figure 5.5. Four elements linear array antenna measurement setup

4.6. Comparison of Measurement and Simulation Results

In this section measured and simulated results of both single antenna and the array antenna are compared. Simulated results are generated using HFSS. The radiation patterns are simulated across the entire X-band and the E and H planes are shown in Figure 5.8. to Figure 5.23. respectively. The E and H planes are presented at 8 GHz, 10 GHz and 12 GHz through the X-band.

Mechanical test equipment is a compulsory factor for testing because gold metallization will not it let connect the SMA connectors. Using additional aluminum test equipment effects the return loss at the beginning of X-band frequencies as shown in Figure 5.6.

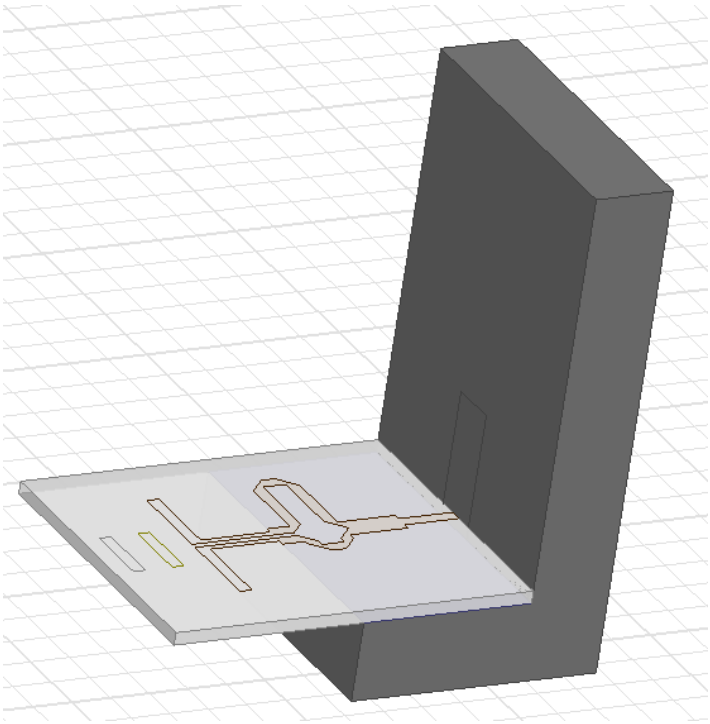

Figure 5.6. Single antenna with aluminium test equipment in HFSS

4.6.1. Single Element Antenna Results

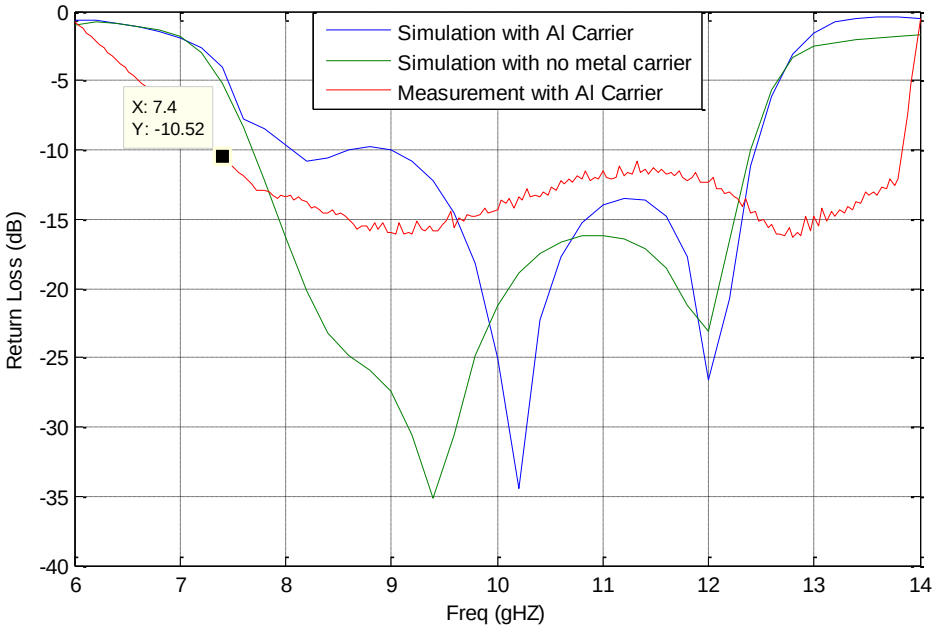

Figure 5.7. Measured and Simulated return losses of single element passive quasi-Yagi Antenna shown in Figure 5.4.

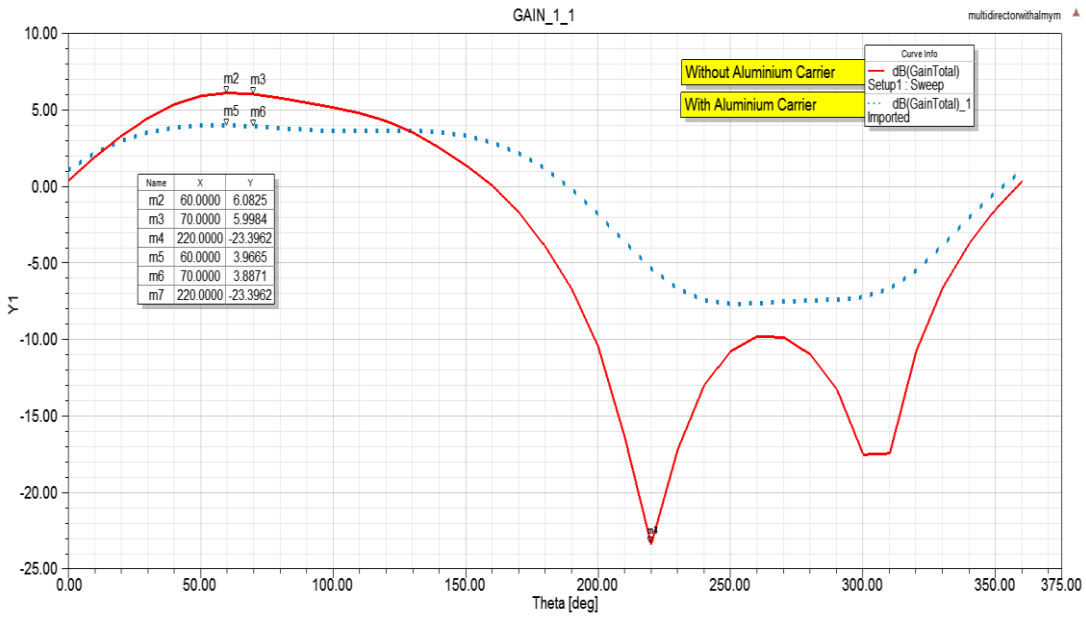

Figure 5.8. Gain of single element antenna with Aluminium carrier and without carrier

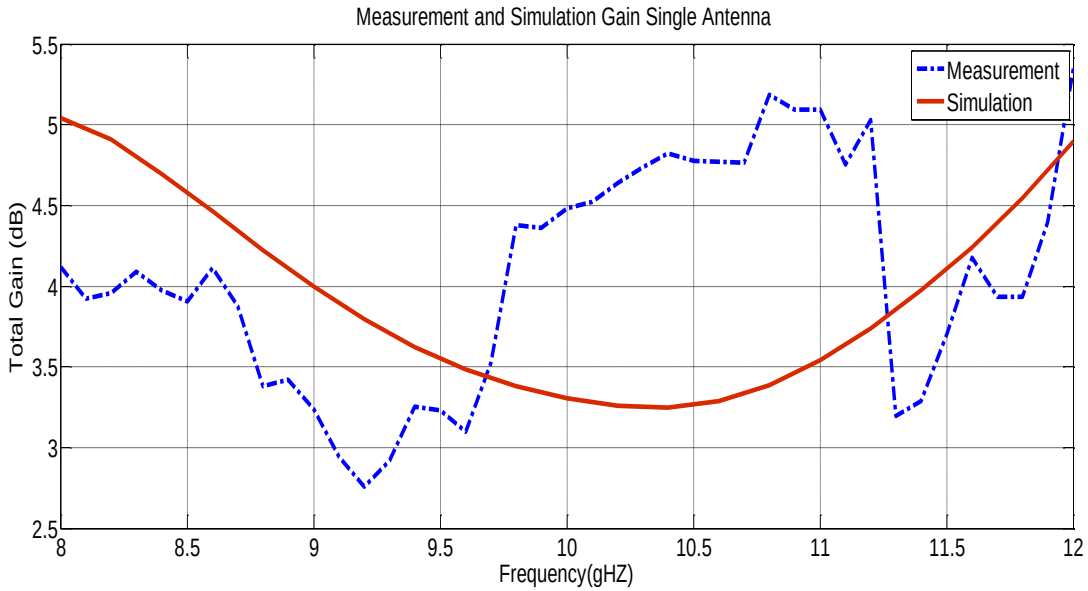

Figure 5.9. Measured and Simulated total gains of single element passive quasi-Yagi Antenna of Figure 5.4.

All the measurements are done with aluminum carrier with compulsory factors of feeding point so all the simulation results are given with Aluminum carrier as shown in Figure 5.6.

The distance from the reflector and the length of the driver are very sensitive parameters since they affect the impedance BW and design frequency. To shift the impedance BW of the quasi-Yagi radiator to cover the higher frequency range, it is thus necessary to shorten the driver or reduce the distance of the driver from the reflector or both.

The measured gains illustrate a minimum gain of 2.9 dB across the band (see Figure 5.8.). The gain agrees well with reported gain of 3 dB to 5 dB by Kaneda. The simulated gain for the quasi-Yagi radiator, with balun at 8 GHz, 10 GHz and 12 GHz are 4.1 dB, 4.5 dB and 5 dB respectively. The measured gain ranges from 5 dB, 3.4 dB, 4 dB corresponding to the gain at 8 GHz, 10 GHz and 12 GHz.

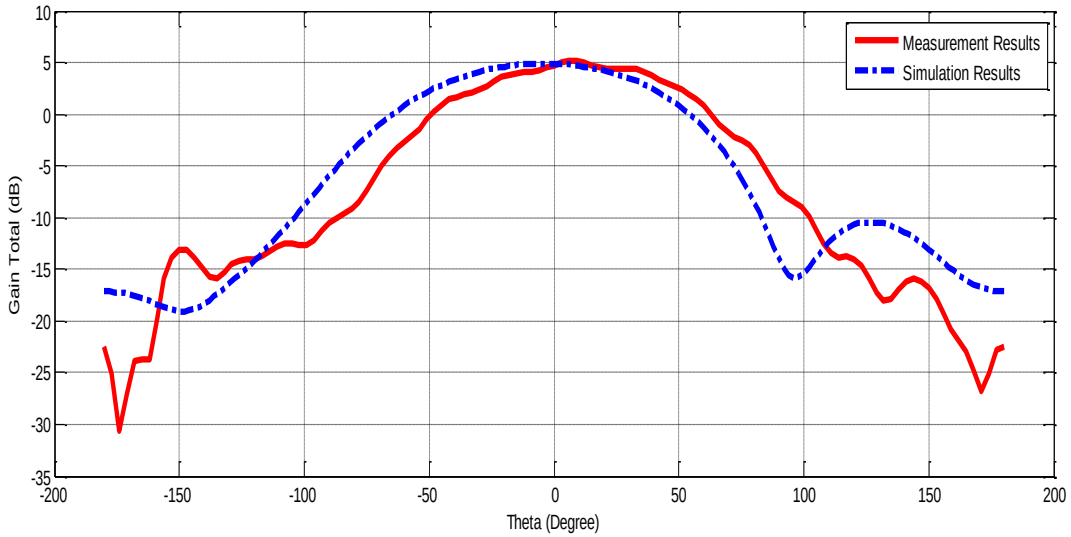

Figure 5.10. Single Element Antenna 8GHz Total Gain Measurement and Simulation (fi=0 degree)

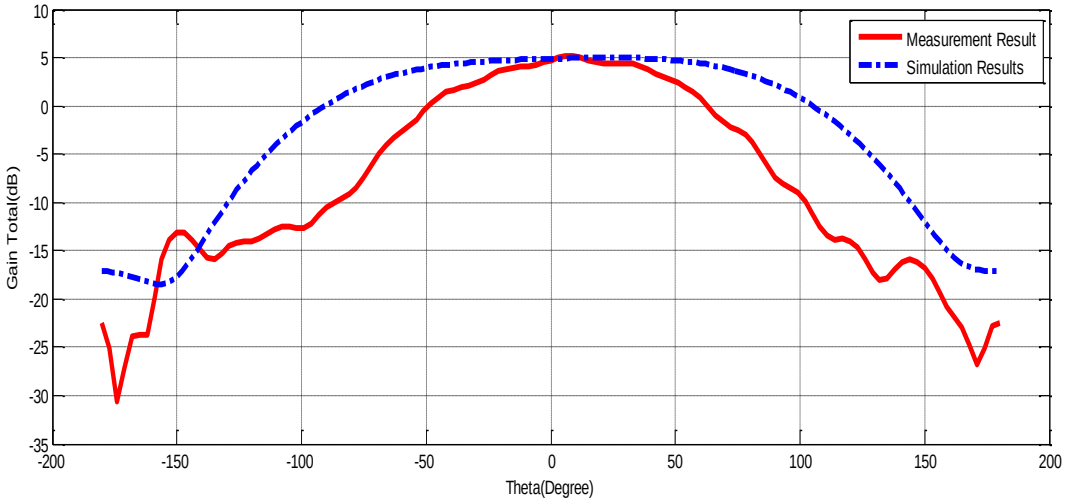

Figure 5.11. Single Element Antenna 8GHz Total Gain Measurement and Simulation (fi=90 degree)

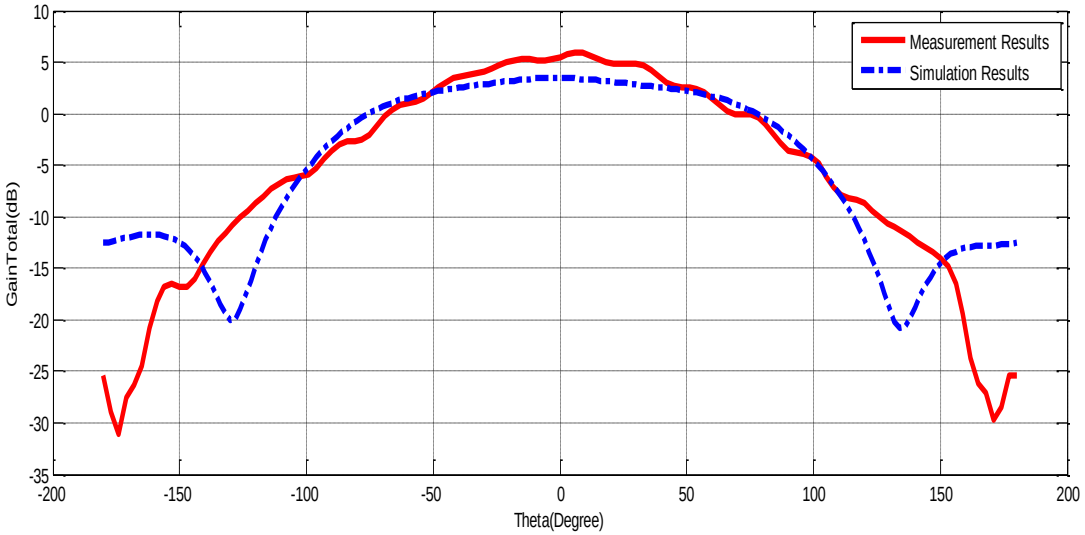

Figure 5.12. Single Element Antenna 10GHz Total Gain Measurement and Simulation (fi=0 degree)

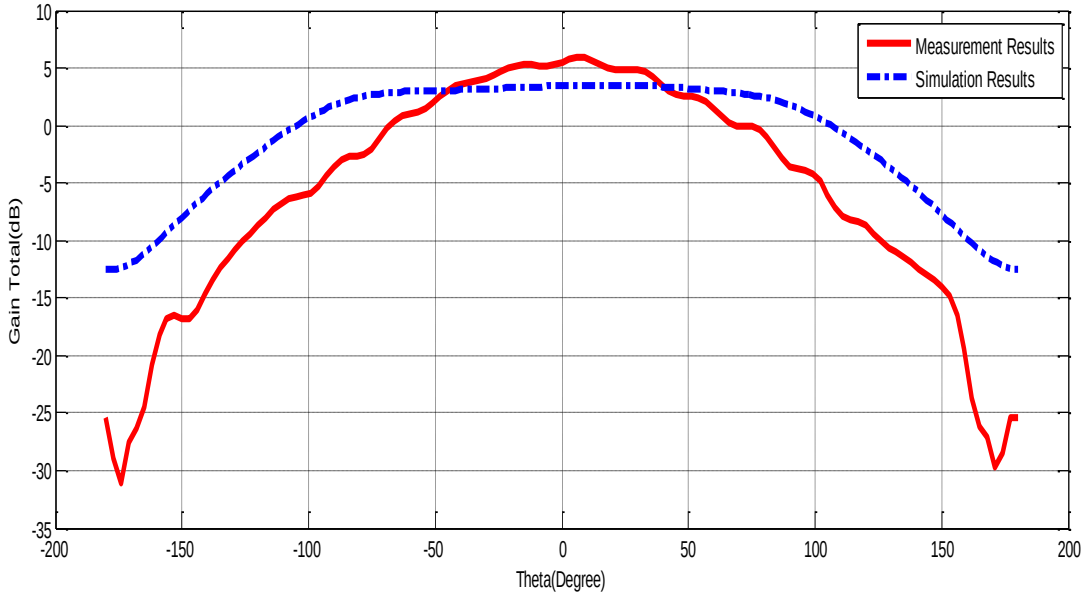

Figure 5.13. Single Element Antenna 10GHz Total Gain Measurement and Simulation(fi=90 degree)

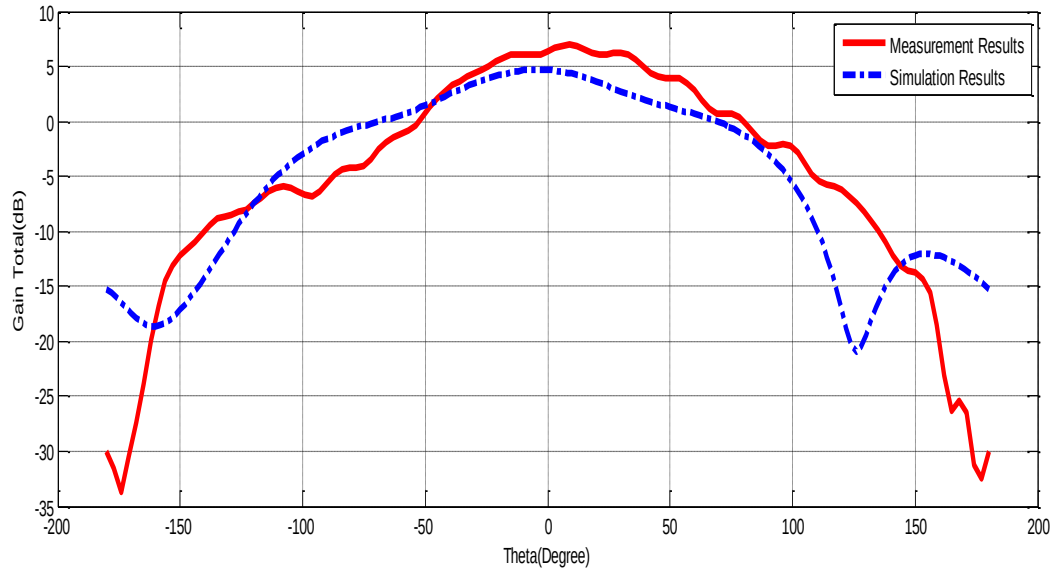

Figure 5.14. Single Element Antenna 12GHz Total Gain Measurement and Simulation (fi=0 degree)

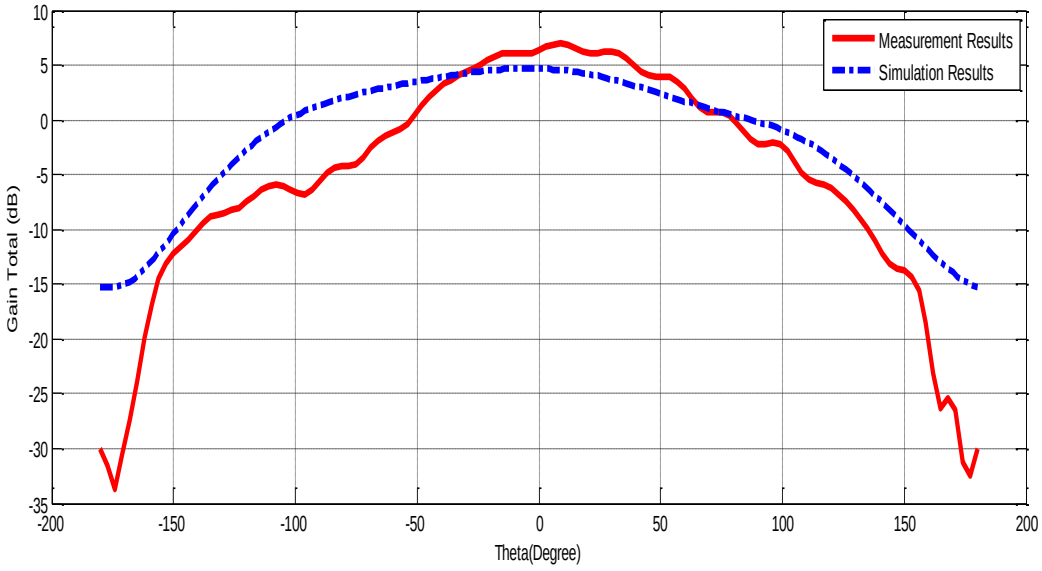

Figure 5.15. Single Element Antenna 12GHz Total Gain Measurement and Simulation (fi=90 degree)

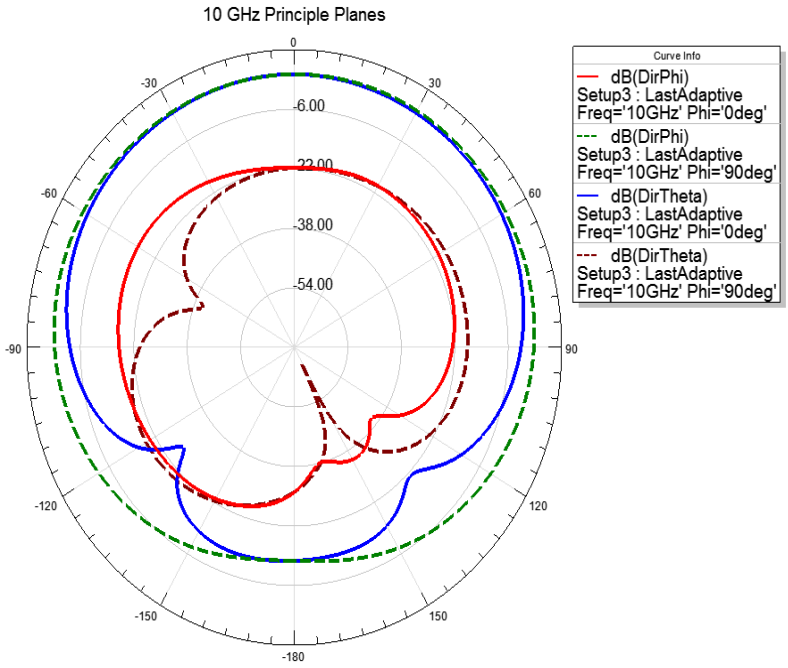

Figure 5.16. Single Element Antenna 10 GHz Cut-planes Radiation Patterns

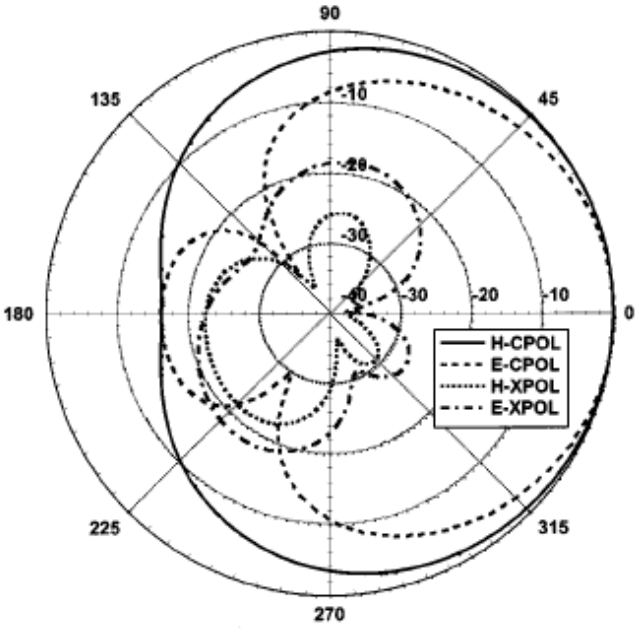

Figure 5.17. Single Element Antenna 10 GHz Literature Radiation Patterns[6]

Figure 5.15. shows well-defined end-fire radiation patterns displayed by the quasi-Yagi radiator with a simulated front –to-back ratio better than 12 dB and a measured front-to-back ratio better than 15 dB. The quasi-Yagi radiator yields a simulated HPBW(Half Power Beamwidth) at 8 GHz,10 GHz and 12 GHz amounts to 126^0, 148^0 ,98^0, where the measured HPBW corresponds to 98^0,127^0,122^0 respectively. The difference between the simulation and measurement is believed to be due to measurement errors as well as the SMA coax to microstrip transition.

An H-plane cut is also presented in Figure 5.10 to 5.22 below. It is noticed that the measured radiation patterns do not correlate and amplitude ripples are present, most probably due to the measurement setup and reflections within the test range.

To find out the production limits of antennas some additional simulations are done. Director's length and driver lengths are the most important parameters for working properly. The length of the director's has been swept from 1.3 mm to 5.3 mm. The results are presented in Figure 5.18. displays the S_{11} parameter and also the driver length has been swept from 1.9 mm to 5.9 mm. The results are presented in Figure 5.19. displays the S_{11} parameter. The antenna cannot operate if the director's length is bigger than 5 mm. For bigger sizes, the directors display a reflector character and the back lobes get more important. On the other hand, although bandwidth is independent with director's length, the reflection coefficient response starts to get worse. The total dipole length or the driver length is very significant factor for operating as shown in Figure 5.20. As a result, the driver length must be between 3 mm to 4 mm for operating.

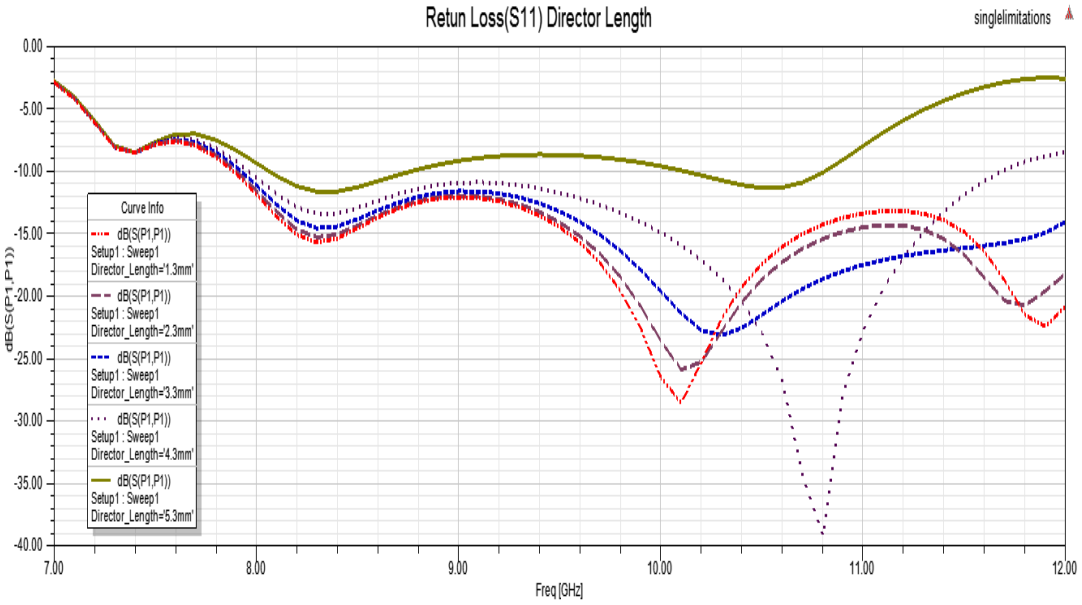

Figure 5.18. Director Length variation of antenna characteristics to find out the operating limitations

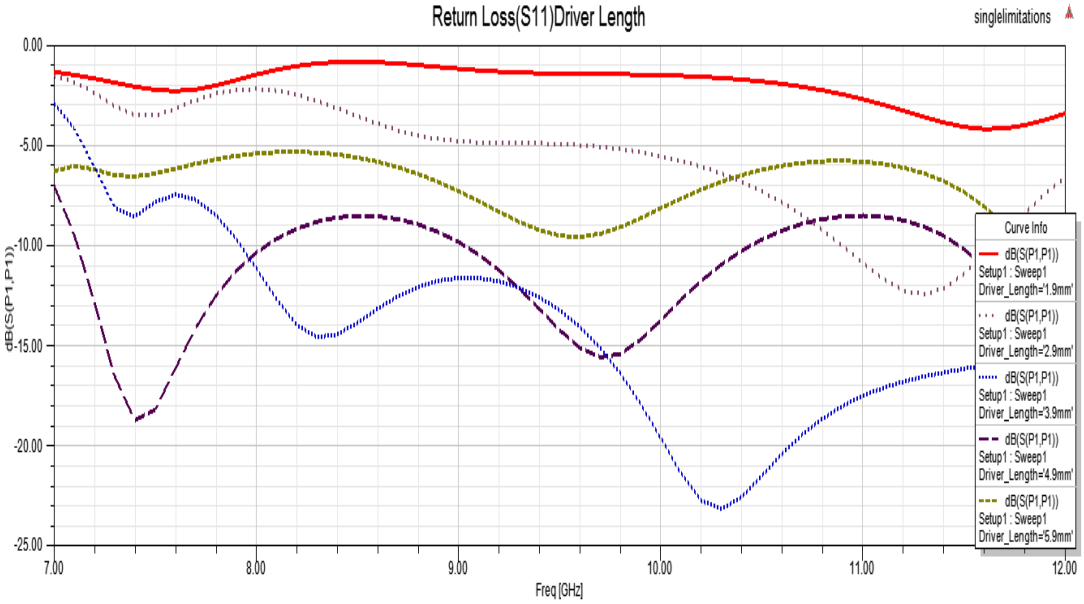

Figure 5.19. Driver length variation of antenna characteristics to find out the operating limitations

4.6.2. Four Elements Antenna Results

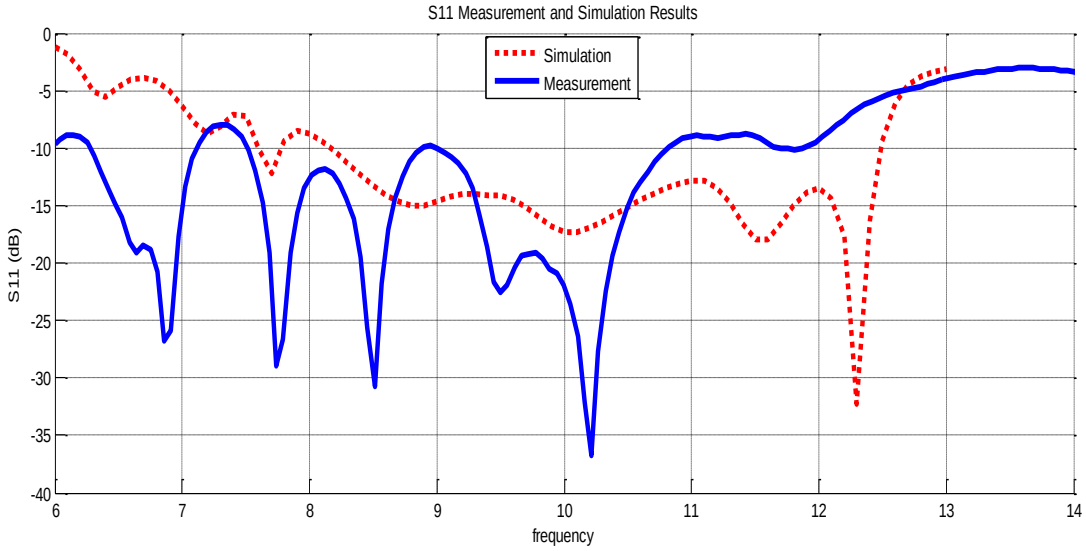

Figure 5.20. S11 Return Loss Measurement and Simulation Results of Four Element Array

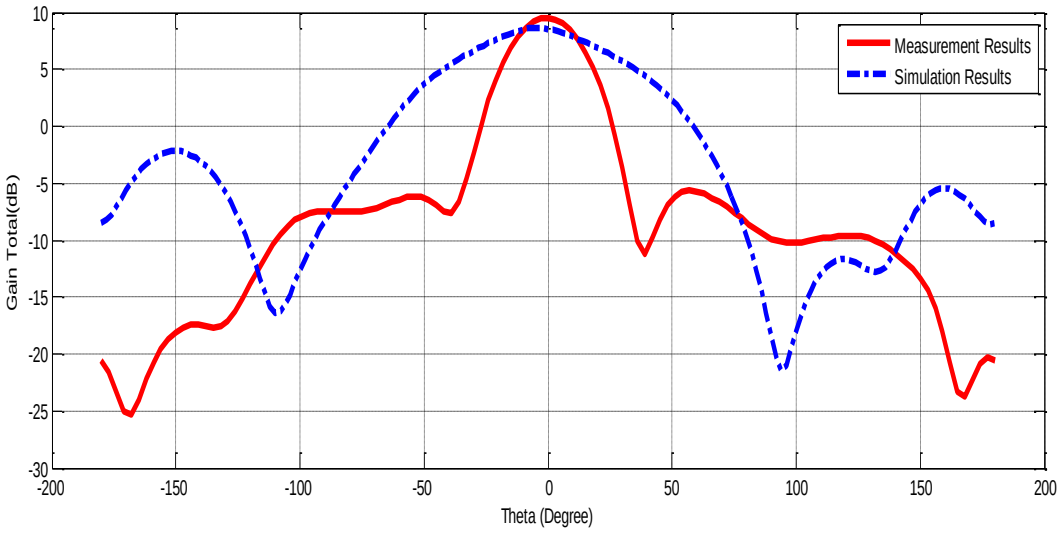

Figure 5.21. 8GHz Total Gain Measurement Whole Theta Values of Array Antenna (fi=0 degree)

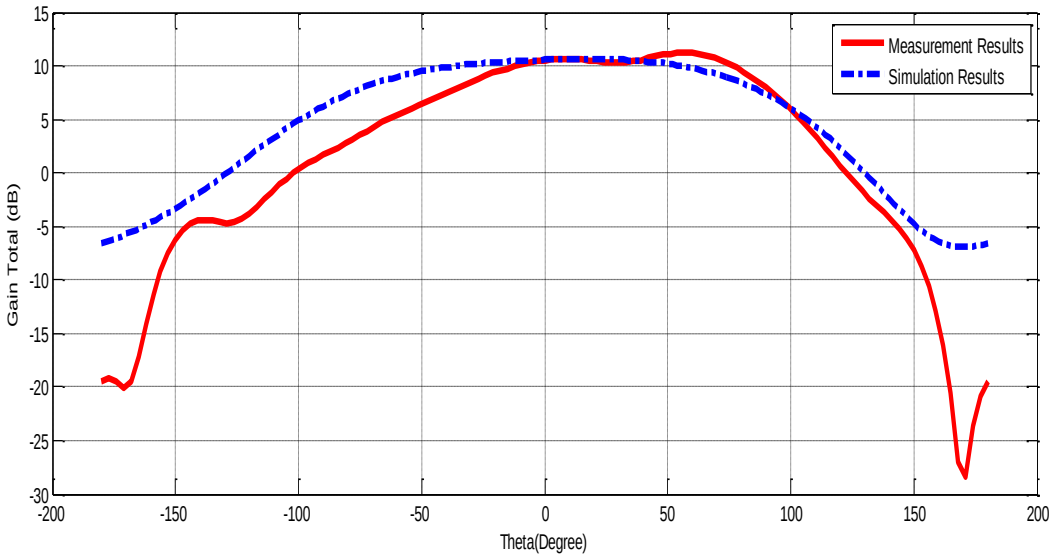

Figure 5.22. 8GHz Total Gain Measurement and Simulation of Array Antenna (fi=90 degree)

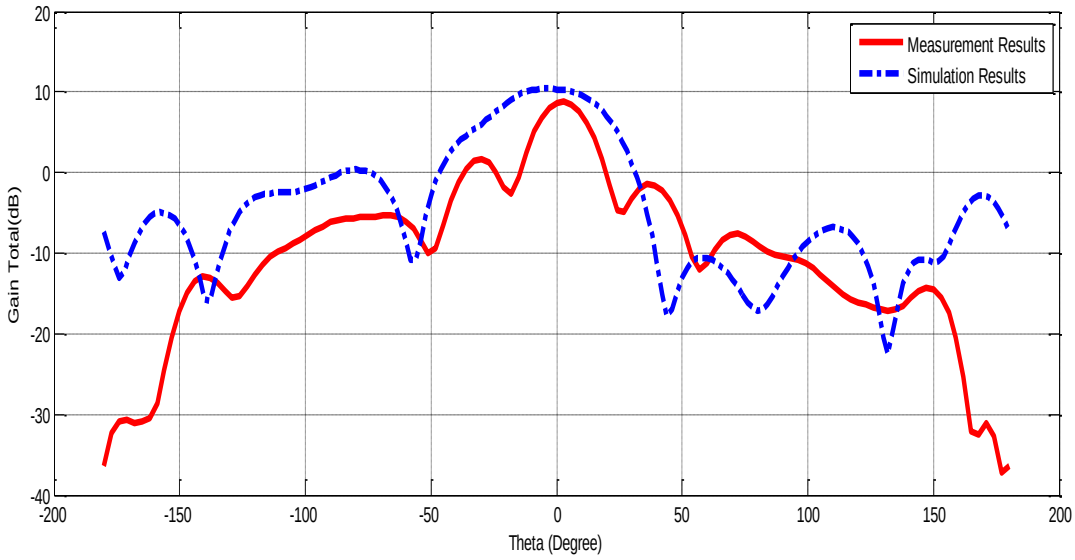

Figure 5.23. 12GHz Total Gain Measurement and Simulation of Array Antenna (fi=0 degree)

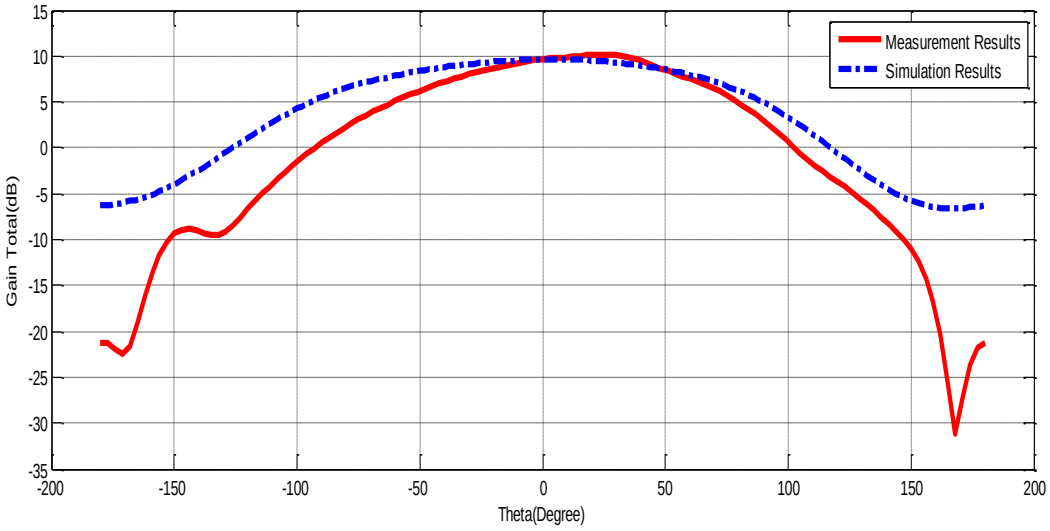

Figure 5.24. 12GHz Total Gain Measurement Whole Theta Values of Array Antenna (fi=90 degree)

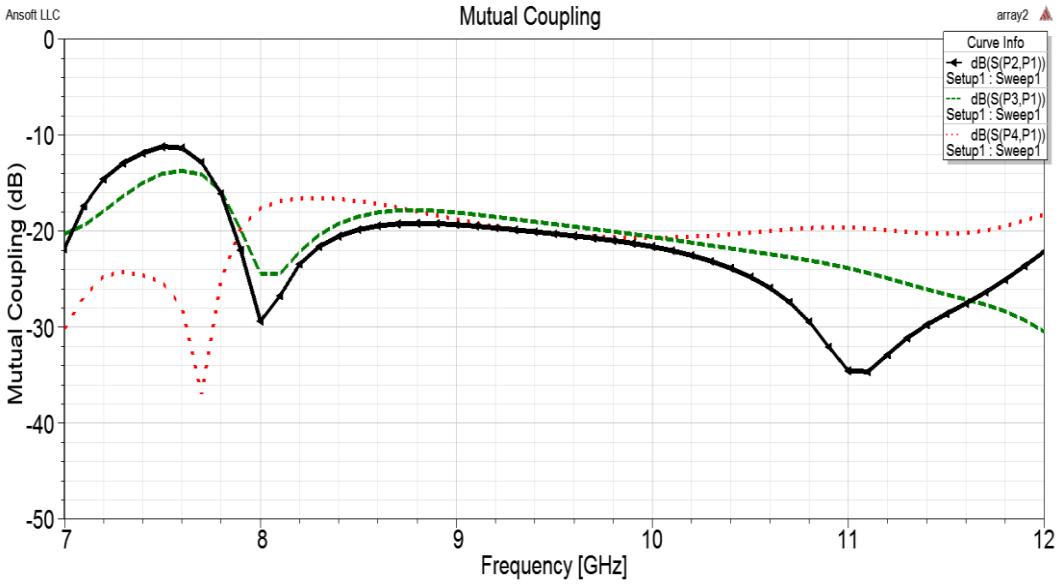

Figure 5.25. Mutual coupling between antennas

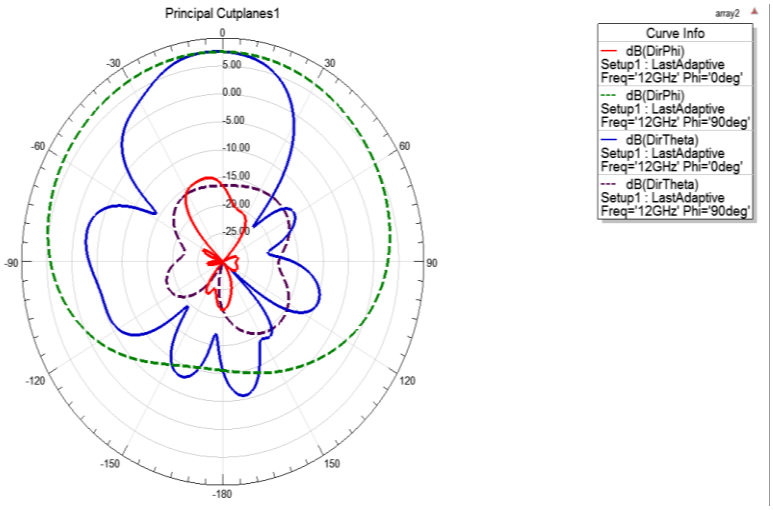

Figure 5.26. 12 GHz cut-planes radiation patterns

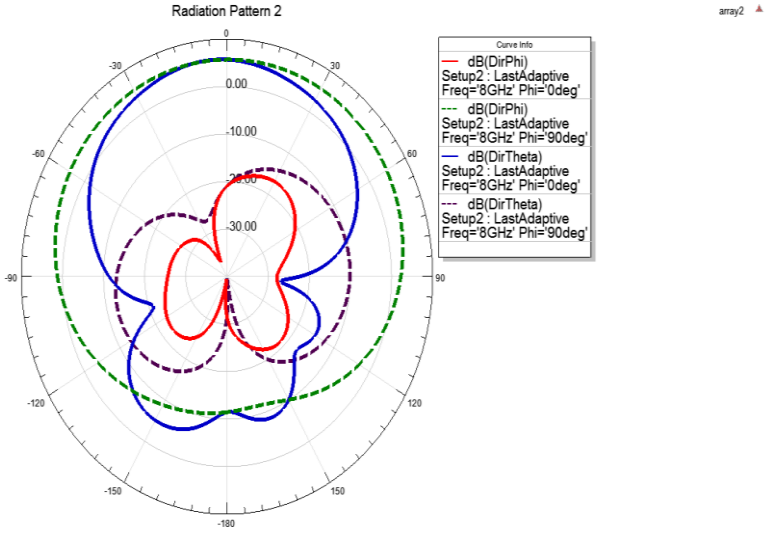

Figure 5.27. 8 GHz cut-planes radiation patterns

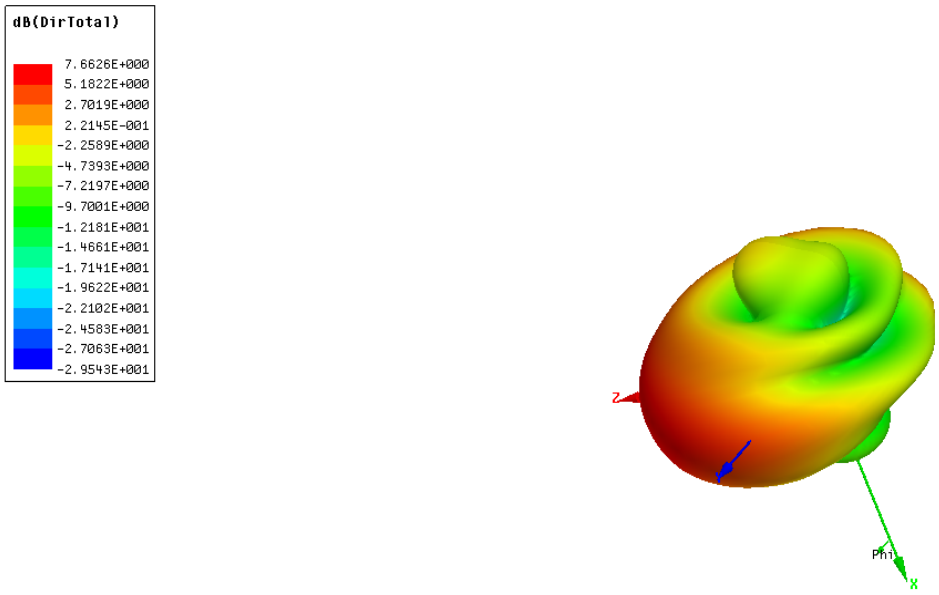

Figure 5.28. 10 GHz 3D Polar Directivity

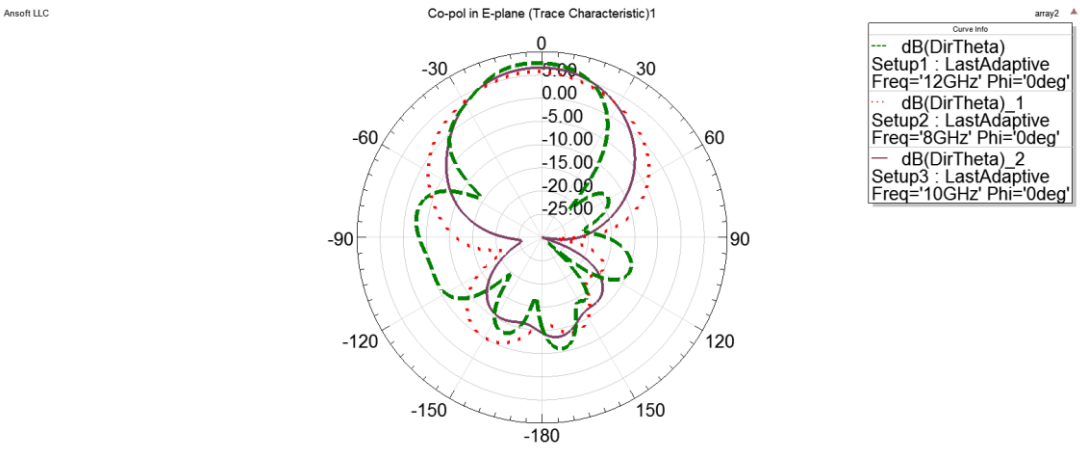

Figure 5.29. Co-Pol in E-Plane in 8 GHz, 10 GHz, 12 GHz

In addition, as seen from Figure 5.29. there are differences in pattern responses between different operating frequencies of the antenna.

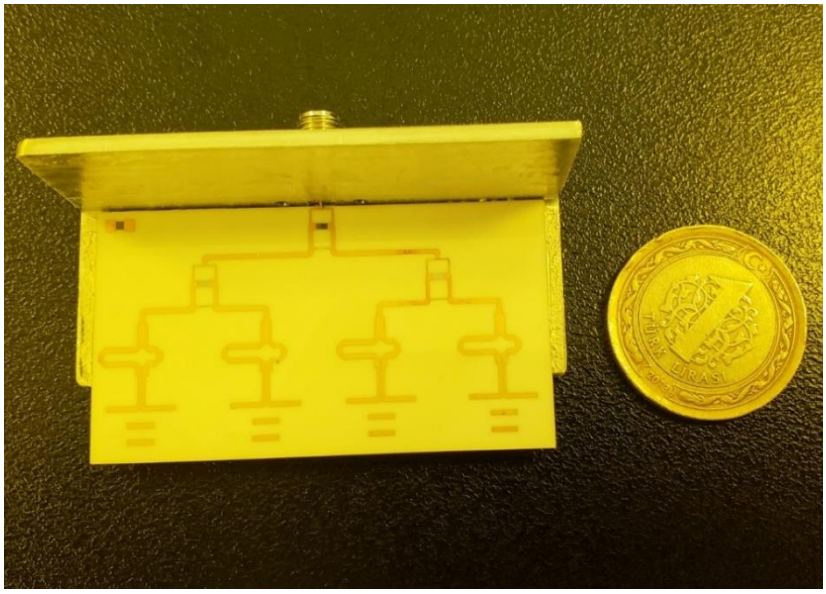

Figure 5.30. 2-D Quasi-Yagi array antenna fabricated

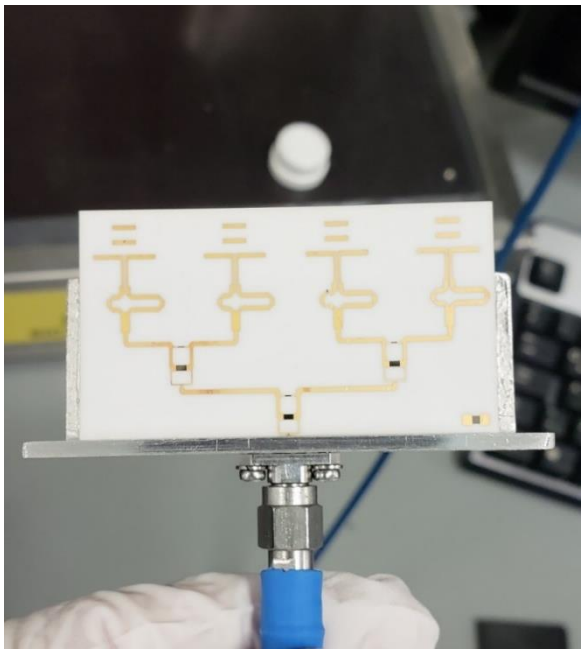

Figure 5.31. Return losses measurement setup with Network Analyzer

The total results of the array antennas and single element antenna are almost acceptable. Because copper or silver metallization are not used on the coating for conductivity, we used gold, so it is not solderable for this reason our input connection is done with “z” gold wedge bonding as seen in the Figure 5.24. This connection type has some advantages also have disadvantages.

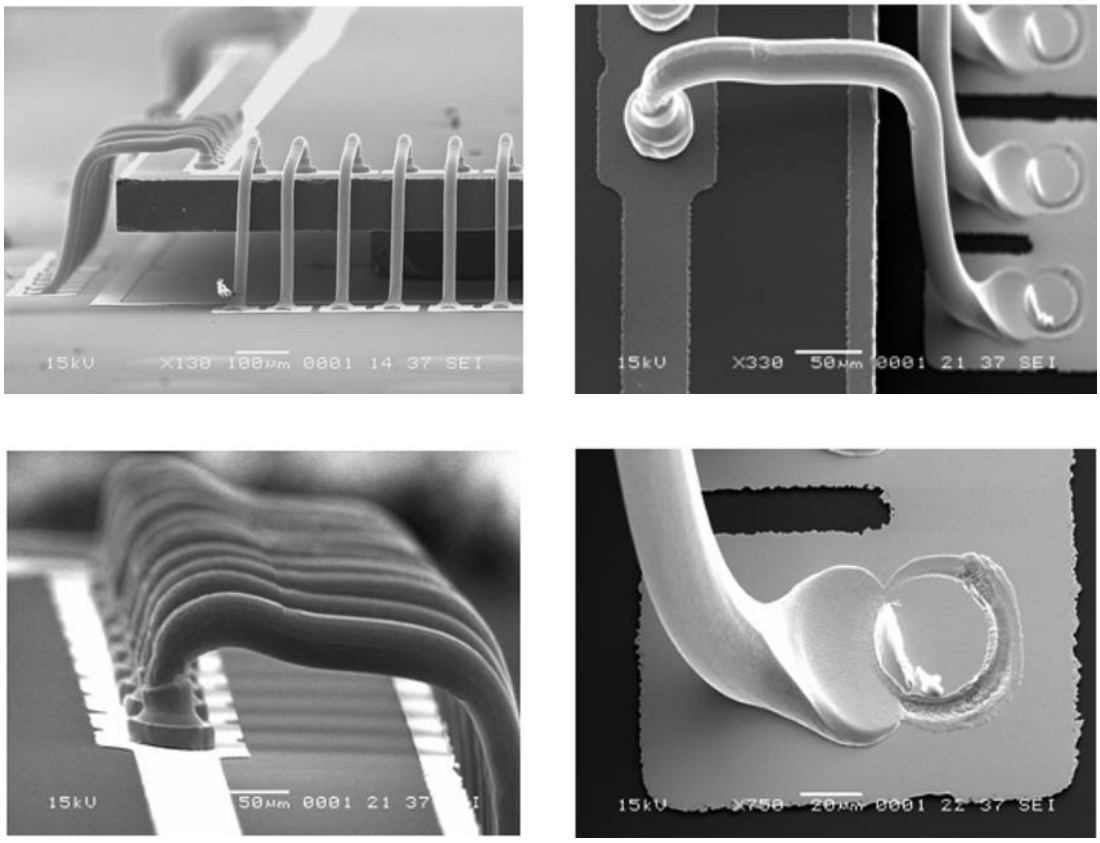

Figure 5.32. “z” gold wedge bonding samples

One important parameter in this context is the mutual coupling between elements within an array system which may not only complicate the array design, but also causes the scan blindness problem in many planar antenna arrays [19]. We chose horizontal center to center spacing was extremely close 14 mm, which corresponds to 0.6 λ_0 at the center frequency of the antenna, coupling will be below -22 dB.

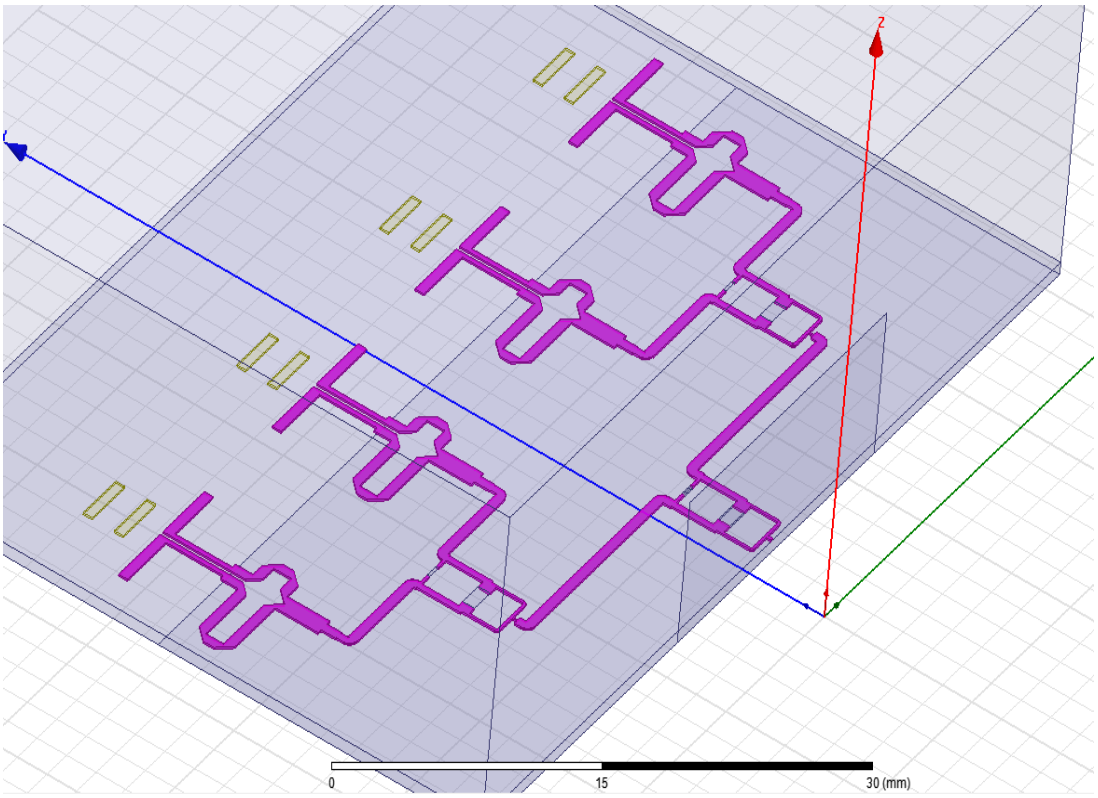

Figure 5.33. 3-D View of final design of 1x4 quasi-Yagi antenna in HFSS

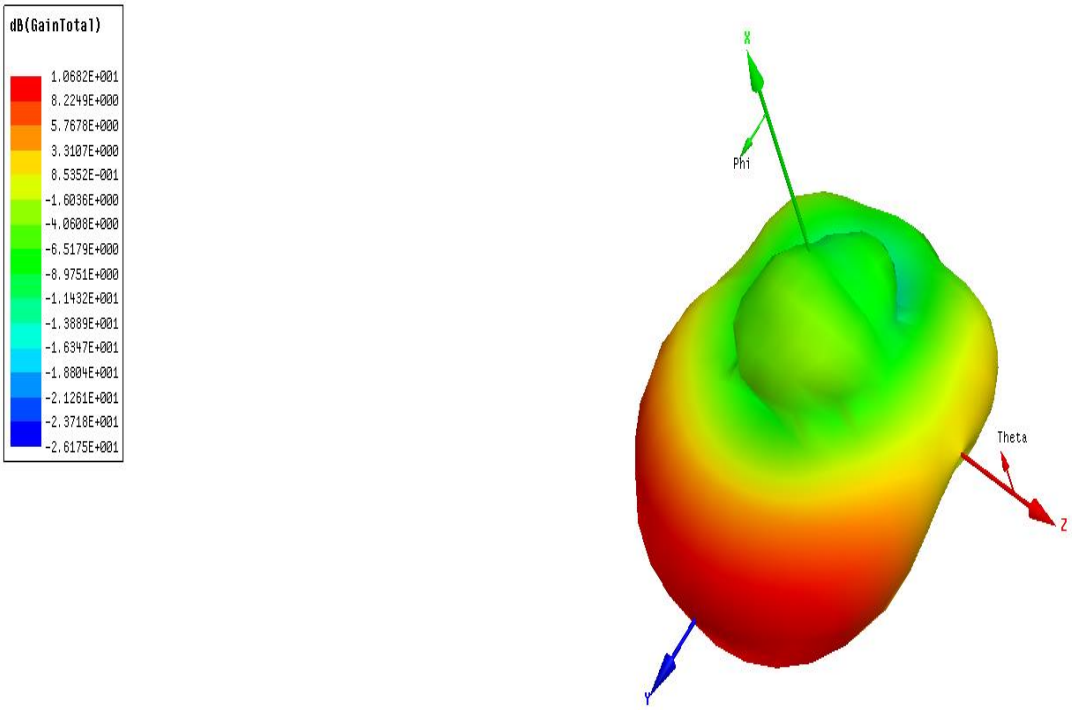

Figure 5.34. Final design of 1x4 element quasi-Yagi antenna 3-D total gain results

CHAPTER 6

CONCLUSIONS

Quasi-yagi antenna array which is printed on a ceramic substrate is investigated, designed and manufactured. Most of previous researches done on broadband antennas has always been focusing on designing an antenna with low dielectric constant substrate materials. Not much research had been done on building antennas using a high dielectric constant substrate. The reason for using low dielectric constant material is that better radiation efficiency and larger bandwidth can be obtained. However, for this thesis, a high dielectric constant ceramic material has been chosen.

At the beginning of project, the requirements are determined. The optimized antenna is proposed by simulation that has not only wide beamwidth but also high gain. The final size of the antenna 70mm X 30 mm with the thickness is about 0.635 mm and the characteristic of minimization is obtained. A portion of the non-reflected power gets dissipated as heat or as thermal loss in the antenna. Thermal loss is due to the dielectric loss in the Al_2O_3 ceramic substrate and the conductor loss in the gold trace. For a small-form-factor Al_2O_3, the heat loss is minimal. The final design will use in package system so the minimal heating loss will give the advantage.

The antenna can be made by a both side printed circuit with the simple structure. The ground layer at the bottom side is extremely important in RF design. The return path for the RF signal is in the ground plane beneath the RF trace. For good RF performance, the return path should be uninterrupted and as wide as possible. If the ground plane is interrupted, return currents will find the next smallest path around the interruption. This forms a current loop, adding undesired inductance, affecting the impedance match between the radio and antenna, and attenuating the RF signal significantly. If the ground plane beneath the RF trace is narrow, it does not behave like a microstrip and may have more signal leakage. The design is truncated ground plane so the distance between feeding point and metal coating thickness is the important factors for the designing.

From the above simulation results which presented in Chapter 3 and Chapter 5, it can be observed that the return loss degrades when the length of the director is increased. When the length of the director is set at 5.8 mm, both the design frequency and the return loss are affected greatly. However, when the length of the director is set at 3.8mm, the simulated results showed an acceptable return loss of –17.5 dB at the desired design frequency of 10 GHz. Hence, it can be deduced that the return loss of the antenna is sensitive to variations of this parameter, as it affects the impedance bandwidth as well as the design frequency.

Based on the results obtained, it is observed that although all plots produce a reasonable S_{11} return loss, the best result achieved would be when S_{dir} is set to be 2 mm. At S_{dir}=2mm, the antenna achieved a good return loss of –17.5 dB at the desired frequency of 10 GHz. Therefore, it can be deduced that the impedance bandwidth and the design frequency are also slightly affected with variations of the distance between the director and driver of the antenna.

After analyzing the results, it can be assumed that the return loss would degrade with increasing distance between the coupled microstrip lines. When the length of the gap between the coupled microstrip lines which W_{cps} set to be 0.7mm, the return loss achieved is only –9 dB at 11 GHz. However, when W_{cps} is set at 0.3mm, the antenna obtained a very good return loss of –21 dB at 10.5 GHz. Although the center frequency is not achieved at the desired frequency of 10 GHz, variations to other parameters should be able to solve this problem. Therefore, it can be deduced that the return loss would be most desirable when the distance between the coupled microstrip lines is set at 0.3 mm.

The directivity of printed quasi-Yagi antennas can be notably improved by adding parasitic elements. A careful design of these elements has not a significant effect on the impedance properties of the antennas. Simulation and the measurements results are very close to each other so this array structure can be used in the wideband radar systems. In addition to this type of antenna has a balanced behavior between all the necessary characteristics for a very good planar antenna.

As a future work, delay lines can be added to each element of the array. Delay lines will be used as proof of concept for the implementation of a phased array antenna employing electronic phase shifters. Beam scanning will be illustrated by delaying the excitation currents to each element by some phase angles. At the end of this work it can be operated in a missile, satellite or aircraft radar in the future.

The production cost can be reduced with large scale manufacture. Also, the performance of antenna is good, the volume is smaller compared with traditional antenna therefore it is highly recommended for implementation in many antenna applications and can meet the requirements of industry.

REFERENCES

[1] Y. S H Khraisat, Design of 4 Elements Rectangular Microstrip Patch Antenna with High Gain for 2.4 GHz Applications modern applied science vol.6 No.1 January 2012

[2] R. Garg, P. Bhartia, I. Bahl and A. Ittipoon, Microstrip Antenna Design Handbook, Artech House, Boston, London, 2001.

[3] C. A. Balanis, Antenna Theory - Analysis and Design, John Wiley & Sons, Inc. Third Edition, New York, 2005.

[4] R. Garg, P. Bhartia, I. Bahl and A. Ittipiboon, "Microstrip Antenna Design Handbook" , Artech House, Boston, London, 2001.

[5] K. S. Yngvesson, T. L. Korzeniowski, Y. Kim, E. L. Kollbuerg and J. F. Johansson, The Tapered Slot Antenna – A New Integrated Element For MillimeterWave Applications, IEEE Transactions on Microwave Theory and Techniques, Vol. 37, pp. 365-374, February 1989.

[6] Y. Qian and T. Itoh, "A Broadband Uniplanar Microstrip-to-CPS Transition," Proc. Asia Pacific Microwave Conf., Vol. 2, City University of Hong Kong, Dept. of Electronic Eng., Hong Kong, PRC, 1997, pp.609-612.

[7] J.R James and P.S. Hall, "Handbook of Microstrip Antennas", Peter Peregrinus Ltd., London, 1989.

[8] K. H. Han, B. Lacroix, J. Papapolymerou and M. Swaminathan, New Microstrip-to-CPS Transition for Millimeter-Wave Application, Electronic Components and Technology Conference (ECTC), 2011 IEEE 61st, pp. 1052-1057, June 2011.

[9] I. J. Bahl and P. Bhartia, "Microstrip Antennas," Artech House, Massachusetts, 1980.

[10] H. J. Song, M. E. Bialkowski and P.Kabacik, “Parameter Study of a Broadband

[11] Kaneda, N., Y. Qian, and T. Itoh, “A novel Yagi-Uda dipole array fed by a microstripto-CPS transition,” Asia Pacific Microwave.

[12] Y. Qian and T. Itoh, “A Broadband Uniplanar Microstrip-to-CPS Transition,” *Proc. Asia Pacific Microwave Conf.*, Vol. 2, City University of Hong Kong, Dept. of Electronic Eng., Hong Kong, PRC, 1997, pp.609-612.

[13] E. A´ vila-Navarro, J. A. Carrasco, and C. Reig, “Printed dipole antennas for personal communication systems,” ,IETE Technical Review, vol. 27, no. 4, pp. 286–292, 2010.

[14] E. J. Wilkinson, "An n-Way Hybrid Power Divider", IRE Trans. Microwave Theory Tech., Vol. 8, January 1960, pp. 116–118.

[15] L. I. Parad and R. L. Moynihan, "Split-Tee Power Divider", IRE Trans. Microwave Theory Tech., Vol. 8, January 1965, pp. 91–95.

[16] S. B. Cohn, "A Class of Broadband Three-Port TEM-Mode Hybrids", IRE Trans. Microwave Theory Tech., Vol. 16, February 1968, pp. 110–116.

[17] R. B. Ekinge, "A New Method of Synthesizing Matched Broad-Band TEM-Mode Three-Ports", IEEE Trans. Microwave Theory Tech., Vol. 19, January 1971, pp. 81–88.

[18] D. M. Pozar and D. H. Schaubert, “Scan blindness in infinite phased arrays of printed dipoles,” *IEEE Trans. Antennas Propagat*, vol. AP-32, pp. 602–610, June 1984. K. Elissa, “Title of paper if known,” unpublished.

[19] H. Wang and G. Yang, “ Design of 4×4 Microstrip Quasi-Yagi Beam-steering Antenna Array Operation at 3.5GHz for Future 5G Vehicle Applications”, 2017

International Workshop on Antenna Technology: Small Antennas, Innovative Structures, and Applications (iWAT)

[20] E.H.Fooks, R.A.Zakarevicius, ” Microwave Engineering Using Microdtrip Circuits “ , Prentice Hall, 1989.

[21] Collin, R. E., *Foundations for Microwave Engineering*, John Wiley & Sons, Inc., 2001, pp.442-443.

[22] Pozar, D. M., *Microwave Engineering*, John Wiley & Sons, Inc., 2005, third ed., pp. 318- 324.

[23] Tang, X., Mouthaan, K., *Analysis and design of compact two-way Wilkinson power dividers using coupled lines*. APMC, Singapore (2009), 1319–1322.

[24] Ralf Riedel, I.-W. C., Ceramics Science and Technology, Volume 1, Structures, Wiley, February 2008.

[25] V.K. Khanna, "Adhesion–delamination phenomena at the surfaces and interfaces in microelectronics and MEMS structures and packaged devices." Journal of Physics D: Applied Physics 44(3): 034004, 2011.

[26] Hong, J. S., Lancaster, M. J., *Microstrip Filters for RF/Microwave Applications*, John Wiley & Sons, Inc., 2001, p. 84.

[27] Pozar, D. M., Schaubert, D., *Microstrip antennas: the analysis and design of microstrip antennas and arrays*, John Wiley & Sons, Inc., 1995, p. 19.

[28] Gupta, K. C., Garg, R., Bahl, I. J., Bhartia, P., *Microstrip Lines and Slotlines*, Artech House, 1996, second ed., pp. 94

APPENDICES

A. Alumina Coorstek %99.5-99.6 Data Sheet

PROPERTIES*		UNITS	TEST	AD-85 Nom. 85% Al_2O_3	AD-90 Nom. 90% Al_2O_3	AD-94 Nom. 94% Al_2O_3	AD-96 Nom. 96% Al_2O_3	FG-995 Nom. 98.5% Al_2O_3	AD-995 Nom. 99.5% Al_2O_3	PLASMAPURE™ AD-998 Min. 99.8% Al_2O_3	PLASMAPURE-UC™ ALUMINA Min. 99.9% Al_2O_3
Density		g/cm^3	ASTM-C20	3.42	3.60	3.70	3.72	3.80	3.90	3.92	3.92
Crystal Size	Average	MICRONS	ASTM-E112	6	4	8	6	6	6	6	3
Water Absorption		%	ASTM-373	0	0	0	0	0	0	0	0
Gas Permeability		-	-	0	0	0	0	0	0	0	0
Color		-	-	WHITE	WHITE	WHITE	WHITE	WHITE	IVORY	IVORY	IVORY
Flexural Strength (MOR)	20° C	MPa (psi x 10^3)	ASTM-F417	296 (43)	338 (49)	352 (51)	358 (52)	375 (54)	379 (55)	390 (57)	400 (58)
Elastic Modulus	20° C	GPa (psi x 10^6)	ASTM-C848	221 (32)	276 (40)	303 (44)	303 (44)	350 (51)	370 (54)	380 (55)	386(56)
Poisson's Ratio	20° C	-	ASTM-C848	0.22	0.22	0.21	0.21	0.22	0.22	0.22	0.22
Compressive Strength	20° C	MPa (psi x 10^3)	ASTM-C773	1930 (280)	2482 (360)	2103 (305)	2068 (300)	2500 (363)	2600 (377)	2650 (384)	2700 (392)
Hardness		R45N	ROCKWELL 45 N	73	75	78	78	82	83	83	86
		GPa (kg/mm^2)	KNOOP 1000 gm	9.4 (960)	10.4 (1058)	11.5 (1175)	11.5 (1175)	13.7 (1400)	14.1 (1440)	14.1 (1440)	14.5 (1480)
Tensile Strength	25° C	MPa (psi x 10^3)	ACMA TEST #4	155 (22)	221 (32)	193 (28)	221 (32)	248 (36)	262 (38)	272 (39)	283 (41)
Fracture Toughness	K(I c)	MPa $m^{1/2}$	NOTCHED BEAM	3 - 4	3 - 4	4 - 5	4 - 5	4 - 5	4 - 5	4 - 5	4 - 5
Thermal Conductivity	20° C	W/m K	ASTM-C408	16.0	16.7	22.4	24.7	27.5	30.0	31.0	33.0
Coefficient of Thermal Expansion	25-1000° C	1X 10^{-6}/°C	ASTM-C372	7.2	8.1	8.2	8.2	8.2	8.2	8.2	8.2
Specific Heat	100° C	J/kg°K	ASTM-E1269	920	920	880	880	880	880	880	870
Thermal Shock Resistance	Δ Tc	°C	❶	300	250	250	250	200	200	200	200
Dielectric Strength	6.35mm	ac-kV/mm (ac V/mil)	ASTM-D116	9.4 (240)	8.3 (210)	8.3 (210)	8.3 (210)	8.7 (220)	8.7 (220)	8.7 (220)	8.7 (220)
Dielectric Constant	1 MHz	25° C	ASTM-D150	8.2	8.8	9.1	9.0	9.6	9.7	9.8	9.8
Dielectric Loss (tan delta)	1 MHz	25° C	ASTM-D150	0.0009	0.0004	0.0004	0.0002	0.0002	0.0001	< 0.0001	<0.0001
Volume Resistivity	25° C	ohm-cm	ASTM-D1829	> 10^{14}	> 10^{14}	> 10^{14}	> 10^{14}	> 10^{14}	> 10^{14}	> 10^{14}	> 10^{15}
	500° C	ohm-cm	ASTM-D1829	4 x 10^8	4 x 10^8	4 x 10^9	4 x 10^9	2 x 10^{10}	2 x 10^{10}	2 x 10^{11}	1 x 10^{12}